A STUDY OF THE INFLUENCE OF HETEROGENEOUS NUCLEATION ON THE FOAMABILITY OF A POLYMER CLAY NANOCOMPOSITE

A STUDY OF THE INFLUENCE OF HETEROGENEOUS NUCLEATION ON THE FOAMABILITY OF A POLYMER CLAY NANOCOMPOSITE

by

KAREN K. YEUNG

A Thesis
Submitted to the School of Graduate Studies
in Partial Fulfillment of the Requirements
for the Degree
Masters of Applied Science

McMaster University

MASTERS OF APPLIED SCIENCE (2005) McMaster University
(Chemical Engineering) Hamilton, Ontario, Canada

TITLE:	A Study of the Influence of Heterogeneous Nucleation on the Foamability of a Polymer Clay Nanocomposite
AUTHOR:	Karen K. Yeung
	B.A.Sc. (University of Waterloo, Canada)
SUPERVISORS:	Dr. Michael Thompson
NUMBER OF PAGES:	xix, 115

ABSTRACT

Polymer composites are fast becoming a material in the manufacturing of automotive interior and exterior parts such as facias and dashboard components. Production of rigid structural foams are ideal because they reduce the overall weight as well as reduce the amount of material used to manufacture the part. Polymer-clay nanocomposites are a classification of materials containing a blend of polymer and a small weight percentage of nanoclay. These materials are currently of interest to automotive part manufacturers because they are known to deliver improved mechanical properties and increase foamability of a polymer.

The current study investigates the changes in material properties and the foamability of a thermoplastic polyolefin (TPO)-clay nanocomposite as the degree of intercalation was varied. The TPO-clay nanocomposite was produced by melt blending TPO, nanoclay and maleic anhydride grafted polypropylene (MAHgPP) in a co-rotating twin screw extruder. The material was subjected to a multi-pass process to vary the degree of intercalation. Degree of intercalation was tracked by rheology, XRD and TEM micrographs. Part density, cell density and flexural modulus measurements were performed on foamed and non-foamed injection molded bars to observe changes in the foamability of the material. Material was also processed without clay and analyzed in the same manner.

Through TEM and XRD analysis it was found that the degree of intercalation and delamination was varied with increasing number of passes. Rheological measurements showed that the TPO-clay nanocomposite underwent β-scission and intercalation simultaneously. The changes in intercalation had a positive effect on the foamability of the TPO-clay nanocomposite. As well, the TPO-clay nanocomposite experienced an increase in flexural properties for both unfoamed and foamed parts compared to the TPO-PPgMAH blend; TPO-clay nanocomposite experienced a 44% and 23% increase

in the flexural modulus for unfoamed and foamed parts respectively. Data also showed that there was a limit to the number of times the TPO-clay nanocomposite can be recycled before the foamability of the material begins to decrease, which was attributed to material degradation.

ACKNOWLEDGEMENTS

First and foremost I would like to thank Dr. Michael Thompson for his support and guidance throughout this project.

I would like to thank Elizabeth Takacs for sharing her expertise on equipment operation and knowledge of polymer rheology, Dr. Gianluigi Botton and Mr. Fred Pearson from the McMaster Department of Material Science for their knowledge and operation of the TEM microscopes, Dr. Jim Britten for his assistance on XRD data, Dr. Neil McManus from the University of Waterloo for help on FT-IR data and Mr. Rob Lemmon for help on flexural data.

I would also like to thank Dr. Andy Hrymak and the staff, colleagues and friends from the Department of Chemical Engineering for their support over the past two years.

Last but not least, I would like to thank and dedicate this thesis to my parents, Kathy and Jimmy for their love and support.

Table of Contents

List of Figures

List of Tables

Nomenclature

ΔP	Pressure drop
ΔS	Entropy change
$\dot{\gamma}$	Shear rate
σ	Interfacial tension
θ	Wetting angle
α	Thermal diffusivity
$\chi(t)$	Fraction of intercalated clay particles at time t
η	Viscosity
η^*	Dynamic viscosity
λ	Wavelength
ν_g	Gas volume fraction
ω	Frequency
ω_c	Crossover frequency
ρ	Density

ρ_c Density of polymer matrix

ρ_{fc} Density of foam

ρ_g Density of gas

τ Relaxation time

θ Angle of incidence

θ Temperature difference

θ_i Difference between T_i and T_∞

θ_o Difference between T_o and T_∞

D Average cell size

c_{pc} Heat capacity of clay

c_{pPP} Heat capacity of polypropylene

d D-spacing

k_c Thermal conductivity coefficient of clay

k_{PP} Thermal conductivity coefficient of polypropylene

b Half the depth of injection molded part

b Width of sample for flexural testing

C_1 Concentration of heterogeneous nucleation sites

c_p Heat capacity

d Depth of sample for flexural testing

d Depth of tactoid

E_B	Tangent modulus of elasticity MPa
f_1	Frequency factor of the gas molecules joining the nucleus
G^*_{het}	Nucleation energy
G'	Storage dynamic modulus
G"	Loss dynamic modulus
H	Height
h	Heat transfer coefficient
$I_i(\infty)$	Diffraction peak for a completely intercalated sample
$I_i(t)$	Intensity of the diffraction peak at 2θ measured at time t
k	Boltzmann constant
k	Thermal conductivity
L	Length of clay tactoid
L	Support span width for flexural testing
m	Initial slope of compression load (N) vs. compression extension (mm)
M_n	Number average molecular weight
M_w	Weight average molecular weight
N	Number of cells per cubic centimeters
n	Number of cells counted in a given area
n	Power law index
N_1	Rate of heterogeneous nucleation

PI	Polydispersity index
Q	Volumetric flowrate
R	Radius
R	Unitless scaling factor in cell density calculations
T	Temperature
T_∞	Temperature of mold
T_i	Melt temperature
T_{max}	Temperature including viscous dissipation
T_o	Crystallization temperature
v	Flow velocity
W	Width

Chapter 1

Introduction

1.1 Polymer Clay Nanocomposites

The automotive industry is constantly striving to research and develop better materials for building automobiles. Materials that have good mechanical properties to withstand the impact of collisions, are light weight to improve fuel efficiency and predictable properties are favored. Over the past few decades, automotive manufacturers have been shifting towards the use of polymeric materials for various components in automobiles, such as interior dashboard components and fascias. Polymer materials, compared to metallic materials, have a lower density, are easily molded and consist of better impact and flexure properties. Currently, polyurethane, polyethylene, polystyrene and polypropylene are the main polymeric materials used in automotive manufacturing. However, recently automotive part makers have grown interested in producing parts with themoplastic polyolefins (TPO) due to their improvement in impact properties compared to polymers that are currently being used. Automotive-grade TPO tend to be a polypropylene based material containing ethylene propylene rubber (EPR); the rubber domains give TPO exceptional impact properties.

A large problem that arises when dealing with automotive polymeric materials is that they have the inability to participate in in-process recycling. Remainder of this thesis will refer to recyclability in the context of in-process recycling only. Subjecting the materials to multiple processing passes can have a negative effect on the mechanical properties. Polymeric materials are known to undergo degradation when exposed to high temperatures for a long period of time. Using recyclable materials can help reduce the amount of scrap material generated from processed parts that do not meet specifications.

As mentioned previously, the automotive manufacturers are constantly striving to use materials that will reduce the overall weight of the automobile. A common way to reduce the weight without sacrificing the size of the part is through foaming. Not only do foams reduce the overall weight of the car, but require less material to make a part, which leads to cost savings in the manufacturing a part. However, with foaming, the mechanical properties have a tendency to decrease. The most common foam used in the production of exterior automotive parts are structural foams. Structural foams consist of a foam core sandwiched between unfoamed layers (also known as the skin layer). The skin layer allows structural foams to offer better mechanical properties compared to fully foamed parts.

TPOs are generally difficult to foam because it contains rubber; it is difficult to dissolve gas into a rubber. In addition, due to the polypropylene content, exposure to high temperatures during processing can lead to degradation reactions. Polypropylene undergoes β-scission at normal melt processing conditions, which lowers the already poor melt strength of the polymer. Low melt strength means that foaming of the material is generally difficult, which can affect the overall structure and mechanical properties of the foamed part. Ideally, automotive parts should be manufactured with a material that has good foamability and mechanical properties, and can maintain these properties even after being recycled.

A research group from Toyota observed that the addition of a small weight percentage of nanoclay substantially improved the mechanical properties of the a polyamide [Fukushima *et al.*, 1988]. This finding launched the area of research in polymer-clay nanocomposites. Since then, studies have been conducted on making various polymer-clay nanocomposite systems including polystyrene [Vaia *et al.*, 1995], polyamide [Incarnato *et al.*, 2004; Chandra *et al.*, 2004] and polypropylene [Wong and Chen, 2002; Solomon *et al.*, 2001]. Depending on the compatibility of the polymeric material with the surface chemistry of the clay platelets, polymer-clay nanocomposites can exhibit different morphological configurations that are dependent on the dispersion and orientation of clay tactoids and platelets. There are three basic morphologies, which include tactoid (clay particle that consists of two or more clay platelets), intercalated (separation of clay platelets in a tactoid) and exfoliated (clay platelets with random orientation) [Sinha Ray and Okamoto, 2003].

There are various ways to produce polymer-clay nanocomposites. This includes in-situ polymerization, solution dispersion and melt blending. In-situ polymerization involves coating the surface of the clay platelets with initiator. Then the clay is swollen with monomer, which begins to polymerize within the clay galleries. In the solution dispersion method, clay is added to a solvent causing the clay galleries to swell. Polymer is then dissolved into the solvent, whereby the polymeric chains replace the solvent molecules situated between the clay layers. The solvent is evaporated off, leaving a polymer-clay nanocomposite. Melt blending involves adding and mixing clay into molten polymer. This method is more practical in a manufacturing environment because it uses conventional processing equipment such as extruders and injection molding machines. It is also more cost effective than in-situ polymerization and more environmentally friendly than solution dispersion methods.

It has been found that the addition of clay into various polymeric materials improves tensile and flexural properties [Wong and Chen, 2002], thermal stability [Zanetti *et al.*,

2004], flame retardant properties [Tidjani, 2005] and gas permeability [Yano *et al.*, 1993]. Exfoliated polymer-clay nanocomposites are hypothesized to show the most improvement in these properties. To date, fully exfoliated polyolefin-clay nanocomposites have not been made though a melt blending process.

Dennis *et al.* [2001] has shown that an increase in the degree of intercalation and delamination (large clay tactoids peeling apart to form individual platelet structures or smaller clay tactoids) can be achieved by applying shear to the material and increasing the residence time. Lew *et al.* [2004a] has also shown that subjecting the material to multiple extrusions can improve the degree of intercalation for polyamide-clay nanocomposites. In their study, mechanical properties remained the same even after multiple passes. This suggests that polymer-clay nanocomposites may be a recyclable material.

It is well known that imperfections and impurities in a polymeric materials can act as heterogeneous nucleating agents. The addition of filler materials introduce heterogeneous nucleation sites into the polymeric material, which have been shown to improve the foamability of the material. Nanoclay has been shown to be an effective heterogeneous nucleating agent due to its high aspect ratio. With polymer-clay nancomposites, intercalation and delamination of clay platelets increase the aspect ratio of the clay, therefore increasing the total surface area for the nucleation sites for bubbles.

1.2 Objectives

In general, it appears that polymer-clay nanocomposites has the ability to increase foamability, improve flexural properties and able to be in-process recycled. It appears to be recyclable, as well as has the ability to maintain mechanical properties when it

is recycled. Moreover, the improvement in intercalation, as mentioned previously, can improve the foamability of the material. In this study, a TPO grade that is currently being used to manufacture automotive parts will be subjected to multi-pass extrusion using a twin screw extruder. Observations on the foamability, mechanical properties and rheology will take throughout the recycling process. The objectives of this study is as follows:

- To increase the level of intercalation and delamination by subjecting the material though a multi-pass extrusion process.
- Determine the effects of degradation on intercalation, and to hypothesize the mode of intercalation.
- To study the foamability of a polymer-clay nanocomposite as the level of intercalation and delamination is varied.
- To increase specific mechanical properties of the polymer (property per weight basis) and to determine the changes of mechanical properties after multi-pass extrusion process.

1.3 Outline

In Chapter 1, the reader is introduced to the concept of polymer-clay nanocomposites and how this research may be beneficial to automotive manufacturing. An introduction to the terminology specific to polymer-clay nanocomposites, as well as analytical techniques such as transmission electron microscopy (TEM) and x-ray diffraction (XRD) will be presented in Chapter 2. Also, this chapter will discuss the literature on polymer-clay nanocomposites that is relevant to the current study presented in this publication. This includes studies on intercalation, rheology, degradation,

foaming and flexural properties. Chapter 3 will go through the materials, type of experiments and experimental parameters used in obtaining results presented in this publication. The results from these experiments will be presented in two separate chapters. Chapter 4 will focus on the results and discussion of TPO-clay nanocomposites, which include TEM, XRD, rheological measurements, flexural modulus and FT-IR measurements. Chapter 5 will focus on the results and discussion of cell density, degradation and flexural modulus of TPO-clay nanocomposite foams. Finally, Chapter 6 will summarize the findings of this study, along with recommendations on the future work of this project.

Chapter 2

Literature Review

2.1 Introduction

The addition of clay into a polymeric material has been shown to increase certain properties in the material such as mechanical properties as well as improve foamability of the material. These improvements are dependent on the orientation of the clay platelets in the polymeric material with respect to each other. Orientation has been shown to be affected by the compatibility between the clay surface modifiers and the polymeric material, processing conditions, and degradation. The following sections contain a review of concepts and previous research on polymer clay nanocomposites that pertain to the current study.

2.2 Thermoplastic Polyolefins

Thermoplastic polyolefin (TPO) is a polypropylene based material that contains a mixture of various polyethylene copolymer, polyethylene polypropylene copolymer

and EPDM or EPR rubbers. TPOs are a difficult material to study because the composition for each TPO is different for each plastic material manufacturer; classification of materials is usually kept a trade secret. This makes each study of TPOs unique to the particular material used in experimentation. Bacci *et al.* [2004] has done a study on a reactor grade of TPO produced by Basel Polyolefins, which is the same manufacturer that produces the material used in this study. According to their research, the TPO is a heterophasic EPR (ethylene propylene rubber) consisting of a minor component phase polypropylene homopolymer and a major component phase of EPR rubber with a undisclosed level of ethylene content. This thesis will assume these are the contents of the TPO studied.

2.3 Nanoclay

Materials such as wood, clay and carbon black are popular organic materials that are used to make polymer nanocomposites. Clay is especially popular because it is layered, meaning it has a high aspect ratio and a high plane of strength and stiffness.

Clay is a natural occurring material. One particle of clay, called a gallery, consists of sheet-like structures, also referred to as platelets, which are stacked together and weakly interact with one another. These platelets are made up of alumina octahedral (AlO_6) and silica tetrahedral (SiO_4) in different ratios to each other. In polymer-clay nanocomposites, smectite clays are most commonly used, mainly montmorillonite. Each layer consists of a 2:1 ratio of SiO_4 and AlO_6, with a thickness of approximately 0.96nm per layer. This means each clay layer contains a layer of AlO_6 sandwiched between two layers of SiO_4. Each clay layer carries a negative charge on the surface of the clay, making it hydrophilic, meaning it is incompatible with polymeric material. To make montmorillonite compatible with polymeric materials, it is modified through an ion exchange with a catonic surfactant, making the clay organophilic. Modifying

the surface of the clay lowers the interfacial free energy, allowing the polymer chains to affix to the clay surface [Pinnavaia and Beall, 2000]. This process will not only make the clay more compatible with the polymer, it also helps slightly to separate the clay layers, which facilitates the intercalation mechanism. Intercalation will be discussed further in Section 2.5.

2.4 Morphology

There are three main classifications of polymer clay nanaocomposites, depending on the orientation of the clay layers within the polymer matrix: tactoid, intercalated and exfoliated. In tactoid polymer clay nanocomposites, the polymer surrounds the galleries. In this configuration, the clay merely acts as a filler and provides little to no improvement in mechanical or physical properties. Intercalated clays involve the diffusion of polymeric material between the clay layers. Some researchers define that clay is exfoliated when the distance between the clay layers is greater than or equal to the effective radius of gyration of the polymer chain [Galgali *et al.*, 2001]. Others state that to achieve exfoliation, the clay layers must be disoriented and non-parallel to the tactoid clay particle [Sinha Ray and Okamoto, 2003], as shown in Figure 2.1. In this work, exfoliation will be defined as the latter. A polymer clay nanocomposite can also contain aggregates, which are tactoids that exhibit associative interactions. Aggregates are present with insufficient mixing of the polymer and the clay during processing, and can lead to stress concentrators in the material.

2.5 Intercalation

During processing, a clay particle can stay as an aggregate, break off into tactoids, have its layers separate by intercalation, or have the layers delaminate from the tac-

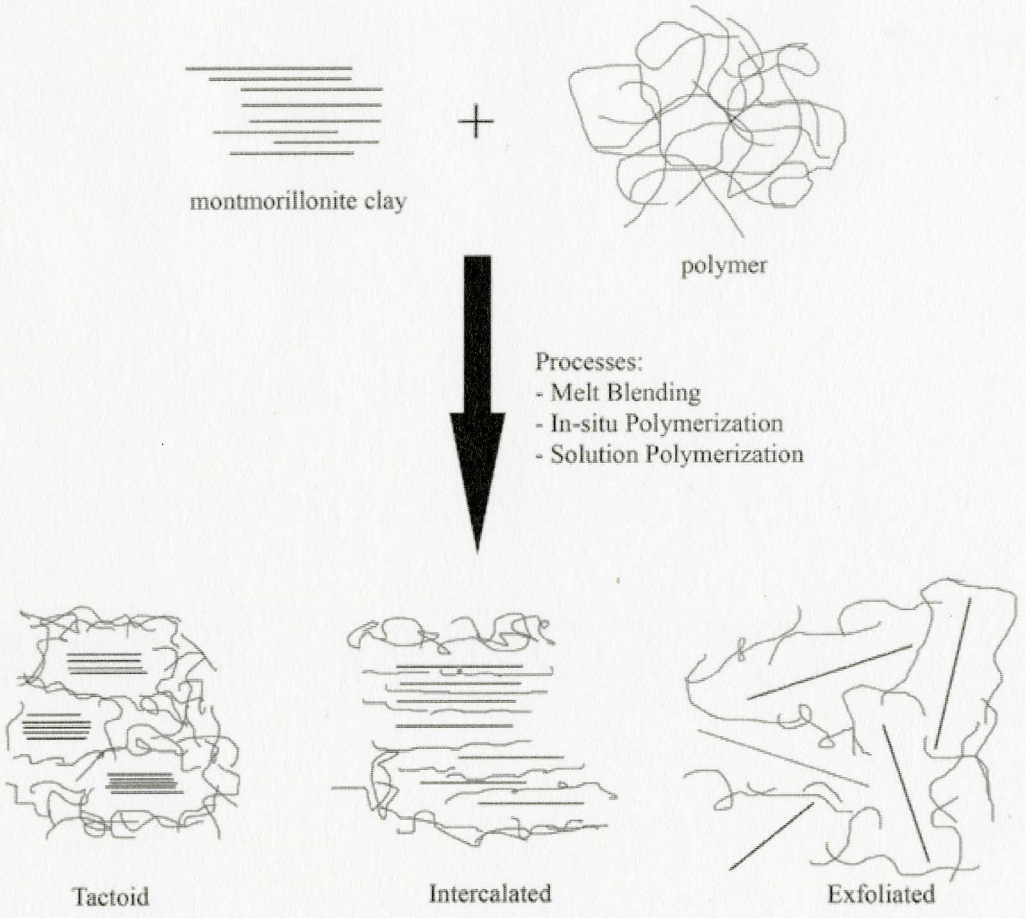

Figure 2.1: Polymer clay nanocomposite morphological classifications

toid. These various mechanisms are brought upon by different aspects of the process.

Intercalation is a thermodynamic process which is dependent on the interactions between the polymer and clay. The degree of intercalation is dependant on the how well the polarity of the clay matches that of the polymer [LeBaron *et al.*, 1999]. As the polymer intercalates, ΔS decreases, but as the spacing between the clay layers increase, ΔS increases. This suggests that the degree of intercalation is determined by the optimization of the conformational freedom of chains upon intercalation [Vaia *et al.*, 1996]. Intercalation, although a thermodynamic process, is affected by physical aspects of the material and clay, and processing conditions. It has been shown that improvements in intercalation can be directly related to the type of clay modifying agents, addition of compatibilizers, mixing residence time and shear during processing [Dennis *et al.*, 2001; Wang *et al.*, 2004]. Clay modifying agents such as quaternary ammonium ions and the addition of compatibilizers improves intercalation, but this chemical modification method will only help to achieve partial intercalation. Furthermore, an increase in the residence time in an extruder has also been proven to increase the degree of intercalation [Dennis *et al.*, 2001; Lew *et al.*, 2004a]. Studies have suggested that introducing some degree of shearing can help improve the dispersion of clay particles [Wang *et al.*, 2004]. In a process that involves shear, clay particles are forced apart by shear, causing aggregates to breakdown into clay tactoid particles.

Dennis *et al.* [2001] hypothesized two stages of intercalation when the system is introduced to shear forces. The first stage involves the larger tactoid particles sliding apart to form smaller tactoid particles. The tactoids can continue to slide apart or enter the second stage of intercalation. In the second stage of intercalation, the polymer diffuses to the edge of the tactoid, causing the end of the particles to intercalate first. As the polymer continues to diffuse into the clay layer, the shear forces from the process begin to bend the clay platelet away from the aggregate. This initiates

the peeling effect, or delamination. The outer layers tend to separate, or peel off first, forming a heterogeneous microstructure consisting of larger clay layer spacings towards the exterior of the particle. This is because there are steric and electrostatic forces that keep together the layers located in the interior of the particle [Vaia *et al.*, 1996]. If adequate mixing is involved in the process, it is possible to overcome these forces and have these layers separate completely from the clay particle and become dispersed into the polymer matrix [Lee and Kim, 2004].

The degree of intercalation can also be affected by the chain structure of the polymer. The molecular weight of a polymer can affect the rate of intercalation but does not determine the final distance between the layers [Vaia *et al.*, 1996]. Clay platelet spacing can be dependent on the location and amount of functional groups that exist on the main polymer chain. If the functional groups are located on the ends of the polymer chain, the clay platelets will be able to separate, and possibly delaminate and form exfoliated structures. If the polymer chain contains multiple functionalities, this may restrict the platelet's ability to separate completely from the gallery [Wang *et al.*, 2003]. The distance between the layers would be related to the shortest distance between two functionalizations along the polymer chain. In this case, the platelets tend to align themselves parallel to one another. However, if adequate shear is applied, the bond between the functional group and the clay surface can be broken to allow for exfoliation or delamination to occur [Lee and Kim, 2004].

Since TPOs consist of polypropylene and an EPR rubber phase, the ability of these components to participate in intercalation is important. For polypropylene, intercalation will occur with the addition of a compatibilizer. Since polypropylene does not contain any polar groups, it has the inability to form a bond with the charged clay surface. Maleic anhydride is most commonly used as a compatiblizer in polypropylene-clay nanocomposites because it contains functional groups and has good miscibility with polypropylene. The polar groups facilitate intercalation by

forming hydrogen bonds to the oxygen groups in the silicate layers [Kato and Usuki, 2000]. Wang *et al.* [2004] has shown that the addition of MAH improves the degree of intercalation. Hasegawa *et al.* [2004] found that EPR rubbers formed a similar polymer-clay nanostructure to that of a polypropylene-MAH system with the addition of MAH. These findings may suggest that intercalation of TPO-MAH is similar to that of polypropylene-MAH.

2.6 Determination of Layer Spacings

It is difficult to fully establish the morphology of a polymer-clay nanocomposite. However, there are some methods that can suggest which morphology the material falls under. The difficulty lies in the fact that these methods highly depend on the orientation of the clay particles. These will be further discussed in the sections describing these methods. There are two methods that are commonly used to characterize polymer clay nanocomposites: transmission electron microscopy (TEM) and X-ray diffraction (XRD).

2.6.1 Transmission Electron Microscopy (TEM)

Transmission electron microscopy give a visual examination of the placement and orientation of the clay platelets on a nanoscale. TEM involves shooting a highly concentrated electron beam onto a thinly sliced sample. TEM micrographs gives a qualitative view on the morphology of the polymer-clay nanocomposite, and gives a quantitative outlook on the degree of intercalation and delamination. It can also provide insight on the orientation of the clay particles with respect to each other and preferred orientation of the particles.

The major disadvantage to TEM is that it is dependent on particle orientation. Since

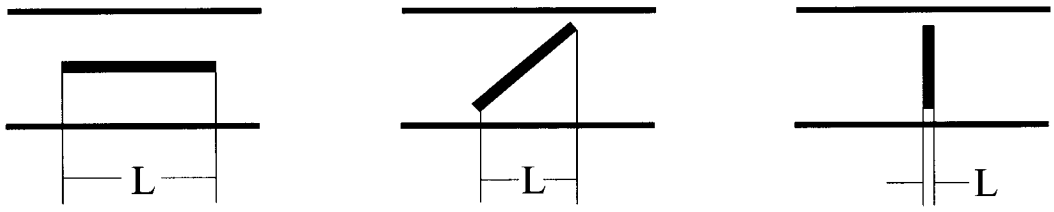

Figure 2.2: Particle orientation effect on length measurements for TEM micrographs)

clay particles are not spherical, the orientation with respect to the electron beam will affect the way the particle appears on the micrograph. If the particles are not aligned directly perpendicular to the electron beam, the measured length of the particle will be less than the actual length of the particle, as shown in Figure 2.2. This means that any estimates of particle size distribution using TEM micrographs will be at best an approximate estimate of the actual values.

2.6.2 X-Ray Diffraction

X-ray diffraction is another method that is commonly used to determine the spacings between the clay layers. It consists of studying the Bragg diffracted beam patterns created by the clay layers when the sample is subjected to an X-ray beam. The measured value in this case the angle between the incident X-ray beam and the diffracted beam. The distance between the clay layers can be calculated using Bragg's Law (Equation 2.1), where λ is the wavelength of the monochromatic X-ray beam, d is the spacing between the clay layers (d-spacing) and θ is the angle of incidence.

$$n\lambda = 2dsin\theta \tag{2.1}$$

Intercalation is determined by the change in the location of the diffraction peak. In most cases, the diffraction peak of the original nanoclay material is compared to that of the nanocomposite material diffraction peak. As the degree of intercalation of the material increases, then according to Equation 2.1, the diffraction peak should shift to a lower value of 2θ. Complete delamination of the clay platelets would show the disappearance of the diffraction peak altogether.

Further analysis of the diffraction patterns can provide insight into the physical nature of the material. Peak intensities can be related to the fraction of clay particles that are intercalated [Vaia *et al.*, 1995]. The fraction of intercalated clay particles can be calculated using Equation 2.2, where $\chi(t)$ is the fraction of intercalated clay particles at time t, $I_i(t)$ is the intensity of the diffraction peak at 2θ measured at time t, and $I_i(\infty)$ is the diffraction peak for a completely intercalated sample.

$$\chi(t) = \frac{I_i(t)}{I_i(\infty)} \tag{2.2}$$

Peak intensities can also determine whether the particles have a preferred orientation [Eckel *et al.*, 2004]. This can be done by obtaining cross-sections along different axis of the same material and observing any changes in the diffraction peak. The breath of the diffraction peak can also provide information about the nanocomposite. Sinha Ray *et al.* [2003] claim that it is related to the average size of the particles.

Like the TEM micrographs, X-ray diffraction can be misleading because it is dependent on the orientation of the clay layers. If the layers are perfectly parallel to each other, then the diffraction angle should give a good estimate of the actual layer spacing. If the layers are not parallel to each other, the diffraction angle will not represent the actual layer spacing.

2.7 Rheology

The flow characteristics of filled polymers are usually different than the flow characteristics of an unfilled polymer due to interactions between the filler material itself and the filler material with the polymer. The rheological study of polymer-clay nanocomposites can be separated into two sections: linear viscoelastic and non-linear viscoelastic properties.

2.7.1 Linear Viscoelastic Properties

Solomon *et al.* [2001] indicated that the low frequency ($0.1s^{-1}$ to $1s^{-1}$) storage dynamic modulus (G') for a polymer clay nanocomposite was greater than that of the neat polymeric material, and that G' and G" displayed non-terminal behaviour at low frequencies. This means that that polymer-clay nanocomposites experience incomplete relaxation [Li *et al.*, 2003; Incarnato *et al.*, 2004; Galgali *et al.*, 2001]. This non-terminal behaviour is caused by the presence of a percolation network [Krishnamoorti and Silva, 2000]. A percolation network is a three-dimensional network which is formed by clay tactoids and platelets with a random orientation that are held together by hydrogen bonding due to presence the of hydroxyl groups on the clay surface [Lee and Kim, 2004]. As the clay intercalates, more clay tactoids and platelets are introduced into the percolation network, which means there is more resistance to flow. Using this information, Li *et al.* [2003] presented a rheological approach to tracking the degree of intercalation. It was discovered that the G' and G" increased monotonically with increasing degree of intercalation. The dynamic viscosities (η^*) at low frequencies are also known to be higher than neat polymeric materials [Incarnato *et al.*, 2004], and also increase monotonically as the degree of intercalation increases [Li *et al.*, 2003; Galgali *et al.*, 2001].

2.7.2 Non-Linear Viscoelastic Properties

Orientation of the clay tactoids and platelets can affect the flow characteristics of the material, and thus affects the overall rheological properties. Clay particles that are aligned along the direction of flow would apply less resistance to flow than non-aligned particles, therefore rheological properties (η^*, G' and G") should be larger for materials containing non-aligned particles [Ren *et al.*, 2003; Krishnamoorti and Silva, 2000]. The Cox-Merz rule does not apply for polymer-clay nanocomposites because shear rheological measurements yield aligned particles while dynamic rheological measurements yield non-aligned particles [Di *et al.*, 2002; Ren *et al.*, 2003]. Under high shear, there is a break-down in the percolation network, allowing clay particles to align along the direction of flow [Krishnamoorti and Silva, 2000]. Polymer-clay nanocomposites are also known to have a shear-thinning behaviour at low shear rates, which is indicated by the lack of a Newtonian plateau at low shear rates in the viscosity curves [Krishnamoorti *et al.*, 1996].

2.8 Degradation

To attain a finished polymeric product, the polymer must be subjected to some degree of processing. The extruder is an intricate part of the polymer processing industry. It consists of one or two rotating screws used for mixing and compounding. These screws contain various mixing elements to compress, stretch and convey polymer. Injection molding is another way that polymeric materials can be processed. It consists of injecting molten polymer into a mold, where the shape of the mold is the final shape the polymer material. In each of these processing methods, the material is subjected to high temperatures and some degree of shear. Because of this, the polymer will experience some degree of degradation.

TPO materials do undergo degradation and crosslinking reactions simultaneously because they contain both polypropylene and polyethylene; polypropylene has a tendency to degrade while polyethylene prefers to crosslink in the presence of radicals. According to Bacci *et al.* [2004], crosslinking dominates if the ethylene content in the EPR rubber is high, while degradation dominates if the ethylene content is low. Since the ethylene content in the material is unknown, there is an uncertainty to whether degradation or crosslinking is the dominant reaction, and if degradation is occurring, what is the extent the degradation.

It is well known that polypropylene undergo a degradation reaction called β-scission which produces carbonyl groups that can be detectable by Fourier transform infrared spectroscopy (FT-IR). The carbonyl groups are known to exist between 1600-1800 cm^{-1}. Peak heights are proportional to the concentration of the carbonyl groups that are present in the material. As polypropylene degrades, the concentration of the carbonyl groups increases, and FT-IR can be used to track this increase in carbonyl group concentration.

The addition of clay in a polymer matrix has been shown to reduce the extent of degradation that would normally occur without the presence of clay. Studies have shown there is a shift in the degradation temperature of a polymer with the addition of 2.5 wt% clay [Pramoda *et al.*, 2003; Sinha Ray and Okamoto, 2003]. This is because the clay adds a barrier effect, which hinders the amount of heat and volatilities that diffuse in and out of the polymer. An increase in the degree of intercalation or exfoliation would enhance this barrier effect, therefore, decreasing the level of degradation. However, for materials such as polypropylene, degradation by scission reactions has a positive effect on intercalation. In degrading polypropylene, the molecular weight of the polymer is decreased. As mentioned in Section 2.5, the molecular weight affects the rate of polymer chain diffusion into the clay layers. As the chains get smaller, it is easier for these molecules to diffuse into the clay layers, therefore increasing the

degree of intercalation.

2.9 Foaming

There are many different aspects that go into studying the foamability of a polymeric material. When studying a foamed material, it is important to learn about how the cells originated, and the size, shape and distribution of the cells. This is why studying cell nucleation and cell density are important in describing the foamability of polymeric materials.

2.9.1 Chemical Blowing Agent

There are two types of blowing agents that are commonly used in a thermoplastic polymeric foaming: physical and chemical blowing agents. Physical blowing agents (PBA) involve injecting gas (usually CO_2 or N_2) into molten polymer. Chemical blowing agents (CBA) come in pelletized or powder form, and are usually mixed into the polymer before being processed. A CBA releases gas through a chemical reaction that is activated at a temperature that is higher than the melt temperature of the polymer. In this study, a chemical blowing agent that consists of citric acid and sodium bicarbonate is used, which yields sodium citrate dihydrate ($C_6H_5Na_3O_7 \bullet 2(H_2O)$), carbon dioxide ($CO_2$) and water ($H_2O$) by the following chemical equation:

$$C_6H_8O_7 + 3NaHCO_3 \rightarrow C_6H_5Na_3O_7 \bullet 2(H_2O) + 3CO_2 + H_2O$$

2.9.2 Heterogeneous Nucleation

There are two types of cell nucleation: homogeneous and heterogeneous nucleation. For heterogeneous nucleation a foreign substance is added to the system to allow bubbles to form on its surface, while for homogeneous nucleation bubbles are nucleated without the presence of a foreign substance. In a polymeric foaming system, a heterogeneous nucleating agent such as talc, clay and other particulate filler material is often used to improve the foamability of a polymer material. The surface of these nucleating agents provide low-energy wells that allow the dissolved gas in the system to form a bubble. This is why the size of the nucleating agent is important; it directly affects the surface area on which bubbles can nucleate. For instance, larger particles consist of a smaller total surface area than smaller particles making up the same total volume, meaning they have less area for bubbles to nucleate [Chen *et al.*, 2002]. For heterogeneous nucleation, nucleating agents with higher surface area are favored.

According to classical nucleation theory, the rate of heterogeneous nucleation is expressed by Equation 2.3.

$$N_1 = f_1 C_1 exp\left[\frac{-\Delta G^*_{het}}{kT}\right] \tag{2.3}$$

In Equation 2.3, N_1 is the rate of heterogeneous nucleation, f_1 is the frequency factor of the gas molecules joining the nucleus, C_1 is the concentration of heterogeneous nucleation sites, k is the Boltzmann constant, T is the temperature and G^*_{het} is the nucleation energy, which is defined in Equation 2.4.

$$\Delta G^*_{het} = \frac{16\pi\sigma^3 f(\theta)}{(3\Delta P)^2} \tag{2.4}$$

In Equation 2.4, σ is the interfacial tension, θ is the wetting angle at the interface between the polymer, the heterogeneous nucleation site and the gas, ΔP is the differ-

ence between the pressure inside and outside the bubble. f(θ) a function of θ defined by Equation 2.5.

$$f(\theta) = \frac{1}{4}(2 + cos\theta)(1 - cos\theta)^2 \tag{2.5}$$

2.9.3 Cell Density

Cell density is defined as the number of cells present in a given volume. Manufacturing high density foams is favorable because they tend to have better mechanical properties compared to low cell density foams [Williams *et al.*, 2005]. Cell density is a function of rheological properties and is sensitive to rheological changes. A decrease in viscosity due to temperature change or degradation may lead to a decrease in the overall cell density. This is primarily due to the fact that elongational viscosity is related to the viscosity of the polymeric material. Elongational viscosity is the measure of how well the material resists elongation. Elongation is experienced by the material during foaming; material along the cell wall elongates as the cell grows. If the cells are in close proximity to each other, elongational viscosity will determine how well the wall or strut between the adjacent cells resists rupture. If the material has low elongational viscosity, it would be unable to sustain the extensional forces exhibited by the growing cells, which leads to the coalescence of cells and a reduction in cell density.

The addition of filler materials has been shown to increase the cell density of foam because it provides heterogeneous nucleation sites. Clay has been shown to be a successful candidate for improving foamability because of the high aspect ratio [Zeng *et al.*, 2002; Taki *et al.*, 2004]. It produces materials with uniform cell size distribution, and also improves the cell density when compared to the virgin materials. As the clay intercalates or delaminates, the aspect ratio of the particles increases, meaning there is a greater surface area for which cells can nucleate upon. This means to achieve

optimal improvements in cell density, the clay must be exfoliated within the polymer matrix [Zeng *et al.*, 2002].

Nam *et al.* [2002]; Di Maio *et al.* [2003] have shown that the cell density increases with the addition of clay. This is because clay has been shown to increase the number of nucleation sites [Taki *et al.*, 2004] and induce strain hardening, therefore increasing the elongational viscosity of a polymer [Nam *et al.*, 2002]. However, the cell size decreases due to the increase in viscosity as well as the decreasing cell growth rate. This reduction in cell growth is attributed to the reduced diffusivity of the gas to the cell by the clay platelets that align along the cell walls [Taki *et al.*, 2004]. Cell density is also affected by the particle size and quantity. As mentioned in Section 2.9.2, the larger surface area of the filler allows for more bubbles to nucleate, and an increase in the number of particles dispersed in the polymer matrix means a greater number of nucleation sites [Chen *et al.*, 2002].

2.9.4 Injection Molding

Foamed parts produced by an injection molding process consists of a foamed layer surrounded by a skin layer, which is also known as a structural foam. The formation of the skin layer is due to bubble collapse and the fast cooling rate. Since the core has a longer cooling time than the surrounded melt layers, it remains in a melt state longer, allowing for a longer cell growth period leading to the larger cell size. For a foam injection molding process, the cell density of the foamed part depends on sampling location. The cells located at the core of the part tend to be larger than the cells located near the skin of the foam. This means that the cell density at the core of the part is lower than the cell density of the foam near the skin.

Cell size and density is affected by the operating parameters of an injection molding process. The cell density increases as the injection speed, or shear rate, is increased.

As well, an increase in the pressure drop from the nozzle to the mold can also increase the cell density [Guo *et al.*, 2004]. Packing pressure and packing volume also impact the overall cell density and cell size. Packing pressure restricts cell growth because it retains some dissolved gas in the system which limits the amount of gas that can contribute to cell growth. It also exerts more force on the cell walls, which can restrict bubble growth. Packing volume limits the overall volume expansion, therefore restricting the bubble growth of nucleated cells. Chandra *et al.* [2004] showed that shot size is the only parameter that plays a significant role in the determining the final cell density of the foam.

2.10 Flexural Modulus

Flexural modulus is the measure of ability of a material to withstand deformation under a load. This measurement is important to automotive exterior parts manufacturers because during a automobile collision the parts experience flexure. Previous studies have shown that the addition of clay improves the mechanical properties of the processed material as compared to the neat material [Ellis and D'Angelo, 2003]. However, these improvements in properties are only evident with intercalation of the clay. Addition of 4wt% clay was found to provide the greatest property enhancement [Sinha Ray *et al.*, 2003], meaning that improvements in these properties can be achieved with minimal increase in overall density of the material. Addition of more than 4wt% clay increases the brittleness of the material, therefore reducing the flexural modulus. Improvement in the flexural modulus of polymer clay nanocomposites has also been proven by other authors. Ellis and D'Angelo [2003]; McNally *et al.* [2003]; Sinha Ray *et al.* [2003] have all found significant improvements in the flexural modulus with the addition of clay into various polymeric materials.

It has been hypothesized that clay has the tendency to increase mechanical properties

because it helps assist in stress transfer [LeBaron *et al.*, 1999]. Since the aspect ratio of the clay particle is high, it provides greater reinforcement effects than other conventional fillers such as talc. Dispersing the clay particles within the polymer matrix optimizes the reinforcing effects; there are more particles to facilitate the stress transfer. This may explain why intercalated and exfoliated polymer-clay nanocomposites exhibit an improvement in mechanical properties.

Chapter 3

Experimental

3.1 Materials

Basell Hifax TPO CA387A (MRF 19g/10min), obtained from Basell Polyolefins was used to study how the addition of clay to a TPO can affect mechanical properties and the foamability of the material. This material was chosen because it is currently being used to make polymeric automotive exterior parts. Cloisite 15A from Southern Clay Products Inc. was the clay used to make the polymer clay nanocomposite. It is natural montmorillonite clay that has been modified with a dimethyl, dihydrogenated tallow, quaternary ammonium salt at a concentration of 125meq/100g clay to make it organophyllic. Polypropylene, which exists as the bulk material in TPO, lacks functional groups, which makes it difficult for compatiblization with modified clay. The most common compatibilizer used in melt blending polypropylene and clay is maleic anhydride grafted polypropylene (MAHgPP). Polybond 3200 (MFR 115g/10min) from Crompton Corporation is a MAHgPP with a MAH content of 1.0wt%. Tracel HTF-215, a powdered endothermic chemical blowing agent from Dempsey Corporation was used for foaming parts in an injection molding process.

3.2 Material Processing

3.2.1 Production of Polymer-Clay Nanocomposite

The polymer-clay nanocomposite was prepared by melt blending Hifax CA387A, 10phr (parts per hundred) of Polybond 3200 and 5phr Cloisite 15A in a Leistritz 40 L/D ZSE 27 HP co-rotating twin screw extruder. These samples containing clay will be referred to by the sample name TPOC, and samples without clay will be referred to as TPOP. The Polybond 3200 and Hifax CA387A were first tumble blended, then fed to the extruder using a K-Tron F-1 gravimetric feeder at a feed rate of 7kg/h to the feed throat. The clay was fed downstream with a Brabender Technolgie twin-screw loss-in-weight feeder at 350g/h. The temperature settings of the extruder are listed in Table 3.1 under the temperature profile of Run 1. For the first pass the extruder was set to run at 200RPM with a high shear screw configuration depicted in Figure 3.1. This screw configuration, which mainly consists of conveying and kneading elements was used to break apart clay agglomerates and uniformly distribute the compatibilizer and clay into the polymer matrix. The compounded material was then passed through the twin screw extruder for an additional nine times with a moderate shear screw configuration depicted in Figure 3.2. The moderate shear screw configuration contains distributive mixing elements along with some kneading and conveying elements. Minimizing kneading elements is thought to reduce the amount of mechanical degradation that can be experienced by the polymer and can provide some degree of shear, which might aid the intercalation process [Dennis *et al.*, 2001]. With the moderate shear screw configuraion the extruder was set to run at 75RPM, a feed rate of 7kg/h, with a temperature profile listed in Table 3.1 for Runs 2-10. The extruder exit material was pulled through a water bath at 31°C and pelletized using a Conair pelletizer.

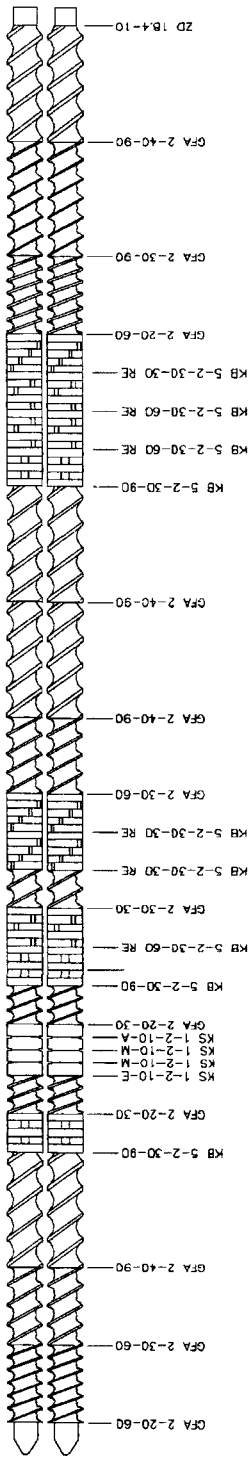

Figure 3.1: High shear screw configuration for a co-rotating twin screw extruder

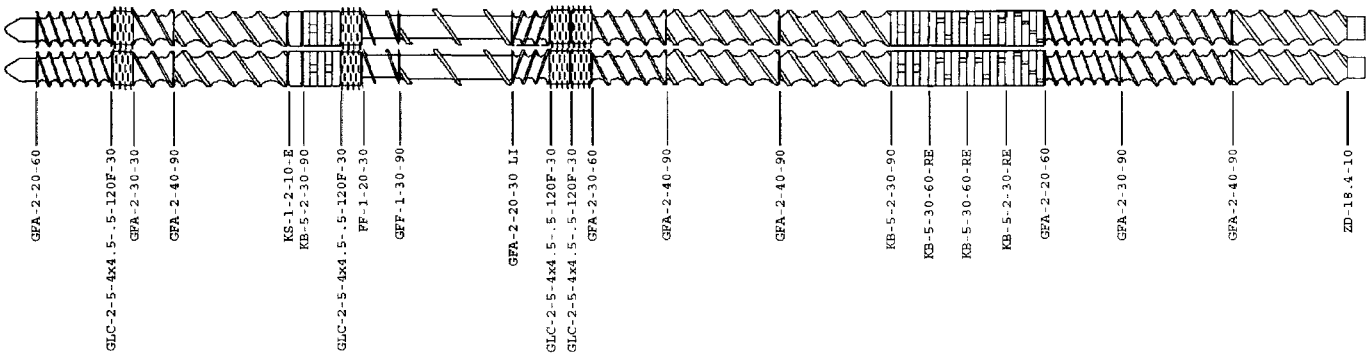

Figure 3.2: Moderate shear screw configuration for a co-rotating twin screw extruder

Table 3.1: Operating temperature of the twin screw extruder

Location	Temperature (°C) Run 1	Temperature (°C) Run 2-10
Zone1	150	190
Zone2	170	200
Zone3	180	200
Zone4	180	200
Zone5	180	200
Zone6	180	200
Zone7	180	200
Zone8	180	200
Zone9	180	200
Zone10	180	200

3.2.2 Injection Molding

Injection molding was conducted on the Arburg 55 Ton Injection Molding machine using a standard nozzle. Neat TPO (NTPO), TPOP1, TPOP4, TPOP7, TPOP10, TPOC1, TPOC4, TPOC7 and TPOC10 were injection molded into dog-bone shaped parts according to the dimensions for a Type I specimen in ASTM D638. NTPO was the only material from the group of neat TPO materials processed to be injection molded into foamed and solid parts for mechanical, density and cell density measurements as a comparison.

The parts were injection molded at an injection speed of 100ccm/s and an injection pressure of 700bar. To determine the best temperature profile and chemical blowing agent (CBA) content that would achieve the best volume reduction during a foam-

ing process, several experiments were run where these parameters were varied. The optimal operational temperature was found to be 230°C; at 240°C the injected parts showed some yellow discolouration, which is an indication of degradation. The optimal blowing agent content was found to be 4phr, which gave the foamed part a 9% volume reduction from the non-foamed part.

Each material was divided into two sample sets: one sample set was injection molded with 4phr Tracel HTF-215 endothermic CBA while the other set was injection molded without CBA. Prior to injecting foamed parts, 4phr of CBA was dry blended with the polymer pellets. A drop of mineral oil was add to help the CBA powder adhere to the surface of the polymer pellets, allowing for an even mixture of polymer pellets and CBA. Parts were injected molded at a melt temperature of 230°C with a holding time of 4s. For each sample set, 50 parts were injection molded: 20 purge parts, ten parts for flexural testing, ten parts for tensile testing, five parts for density testing, and five parts for cell density analysis.

3.3 Material Characterization

3.3.1 Melt Flow Rate (MFR)

To characterize the material, MFR measurements were obtained for NTPO, TPOP1 and TPOC1. All measurements were conducted on Kayness D-0053 Melt Flow Indexer at a capillary temperature of 230°C according to ASTM D1238. The MFR was measured using a 2.16kg weight with a sampling time of 30 seconds. Each material was sampled three times and the average of these measurements was taken. Table 3.2 show the MFR values obtained for the materials tested.

Table 3.2: MFR measurements at 2.16kg at 230°C

Material	MFR (g/10min)
NPO	19.5 ± 0.2
TPOP1	29.7 ± 0.7
TPOC1	16.2 ± 0.5

3.3.2 Ashing

An ash test was used to verify the weight percentage of clay present in the polymer clay nanocomposite. Three samples TPOC1 were weighed to find the initial polymer weight, and then placed in separate aluminum dishes. The samples were placed in a muffle furnace at 650°C for 1.25 hours to burn away the polymer and the clay surface coating, then weighed again after being removed from the furnace. Clay content was found to be 2.97wt% ± 0.09wt%.

3.3.3 Clay Aspect Ratio

The clay aspect ratio for TPOC1, TPOC4, TPOC7 and TPOC10 were measured using TEM micrographs taken at 45K magnification. For each sample, the length and width of individual clay particles were measured using digital imaging software. The aspect ratio was calculated by dividing the length by the width of the particle. In total, 112 particles were counted per material.

3.3.4 Particle Size Distribution for the Chemical Blowing Agent

Endothermic chemical blowing agent was decomposed in a muffle furnace at 600°C. It was found that there was a weight reduction in the decomposed blowing agent of 30.7%. This weight loss is attributed to the decarboxylation of citric acid and citranoate via reaction, and due to the transformation from $NaHCO_3$ to Na_2CO_3. A small amount of decomposed chemical blowing agent was placed under a Leitz optical microscope and digital photographs were taken. Using imaging software, the diameter of each particle were measured. Figure 3.3 shows the particle size distribution of the decomposed chemical blowing agent that has a median diameter of 4.17μm and the maximum diameter of 10.42μm.

3.4 Rheological Measurements

3.4.1 ARES

After each run, material was removed, and the dynamic viscosity (η^*), dynamic storage modulus (G') and dynamic loss modulus (G") were measured using the ARES Rheometrics RTE-130 parallel plate rheometer. Circular plugs 25mm in diameter and 2mm thickness were made by pressing the material in a mold with a hot melt press at 180°C for two minutes. These plugs were placed in between the parallel plates in the ARES where analysis measurements were conducted at 210°C with a plate gap of 1.5mm. For the first sample, the dynamic strain sweep test was conducted between $0.01s^{-1}$ to $100s^{-1}$ to find the viscoelastic region. For all samples, the viscoelastic region was found to be at 5% strain. For subsequent samples, the dynamic frequency sweep test was performed at a frequency range of 0.01 to 100rad/s at 5% strain rate.

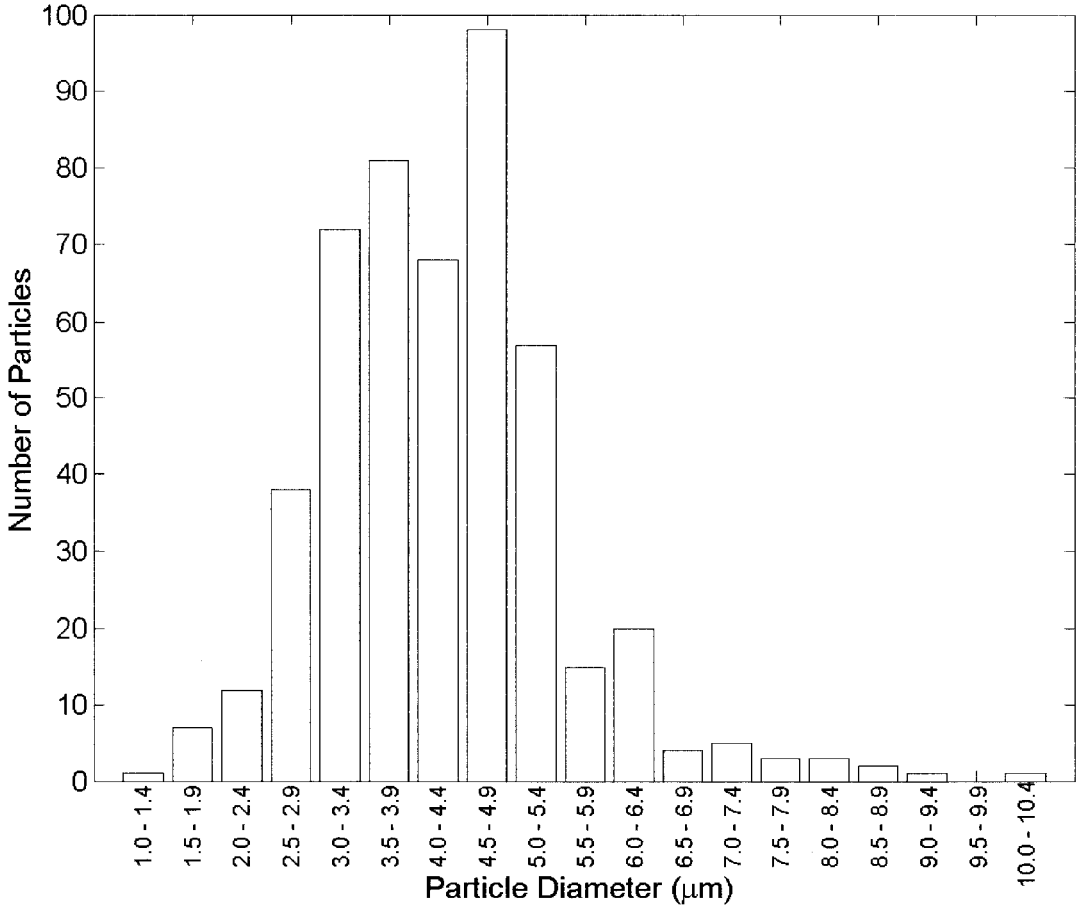

Figure 3.3: Particle size distribution of decomposed chemical blowing agent

The η^*, G' and G" were measured and plotted against the frequency.

3.4.2 ROSAND

Rheological measurements at high shear rates were conducted on the ROSAND RH7 piston driven constant speed dual barrel capillary rheometer. The capillaries have a die that had a L/D of 16 and 0.25. All viscosity values measured were Bagley and Rabinowitsch corrected. The testing was conducted using materials obtained after the first, fourth, seventh and tenth passes for TPOC, TPOP and NTPO, at a barrel temperature of 210°C with a shear rate range of $100s^{-1}$ to $5000s^{-1}$. From data obtained at these shear rates, steady shear viscosity versus shear rate was plotted.

3.5 Material Analysis

3.5.1 X-Ray Diffraction (XRD)

To determine the clay layer spacing and how it varies with increasing number of passes, XRD was conducted on Cloisite 15A, TPOP1, TPOP4, TPOP7 and TPOP10 materials. For Cloisite 15A, the powdered clay was put inside a small capillary for analysis, while the processed materials were mounted on a small brass pin, with the extrusion axis aligned along the ϕ-axis. The XRD was conducted on a Bruker D8 three circle diffractometer with a Smart6000 CCD detector using Rigaku RU-200 copper rotating anode with a cross couple parallel focusing mirror as a radiation source. The sample was exposed for 300s while being rotated along the ϕ-axis 20°.

3.5.2 Transmission Electron Microscopy (TEM)

To qualitatively view the orientation of the clay in the polymer matrix, the distribution of the clay particles and to measure the degree of intercalation, transmission electron microscopy was conducted on TPOC1, TPOC4, TPOC7 and TPOC10. Samples were prepared by a microtome yielding a specimen thickness between 60-80nm. TEMs were conducted on the Philips CM12 TEM for 45K, 60K and 125K magnifications at an excitation voltage of 120kV, and on the JEOL 2101F Field Emissions Electron Microscope for the 1M magnification at an excitation voltage of 200kV.

3.5.3 Flexural Test

In performing a flexural test on the injection molded samples, a comparison between TPOP and TPOC can be made to see if there was any improvement in flexural properties, and between TPOC samples to determine if intercalation had any effect on the flexural properties. For each tested material, ten foamed parts and ten non-foamed parts were subjected to a flexural modulus testing following ASTM-D740B using the Instron 5566. The middle portion of the dog-bone molded part was placed onto the three-point bending apparatus shown in Figure 3.4 that had a support span of 50.8mm. Testing was conducted at room temperature, at a strain rate of 0.10mm/min/min, displacement rate of 1.43mm/min and a maximum displacement of 7.0mm $\pm$ 0.008mm. The force (N) versus displacement data was automatically recorded by a computer software program. Equation 3.1 was used to calculate the tangent modulus of elasticity (E_B) in MPa, where m is the initial slope of the compression load (N) versus the compression extension (mm) (see Figure 3.5), L is the support span width (mm), b is the width of the sample and d is the depth of the sample.

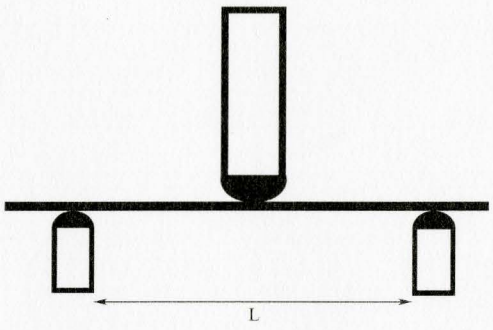

Figure 3.4: Setup for 3-point bending flexural test with a support span L

$$E_B = \frac{L^3 m}{4bd^3} \tag{3.1}$$

3.5.4 Density Test

Density measurements were conducted on a Mirage MD-200S Electronic Densimeter using the middle portion of the dog-bone injection molded part. The original injection molded parts were too big to be measured by the densimeter, so the ends of the parts were removed. Average densities for foamed and unfoamed parts are listed in Table 3.3.

Table 3.3: Average material density for unfoamed and foamed parts

Material	Unfoamed (g/cm^3)	Foamed (g/cm^3)
NTPO	0.893 ± 0.001	0.787 ± 0.007
TPOP	0.896 ± 0.002	0.799 ± 0.004
TPOC	0.914 ± 0.001	0.803 ± 0.008

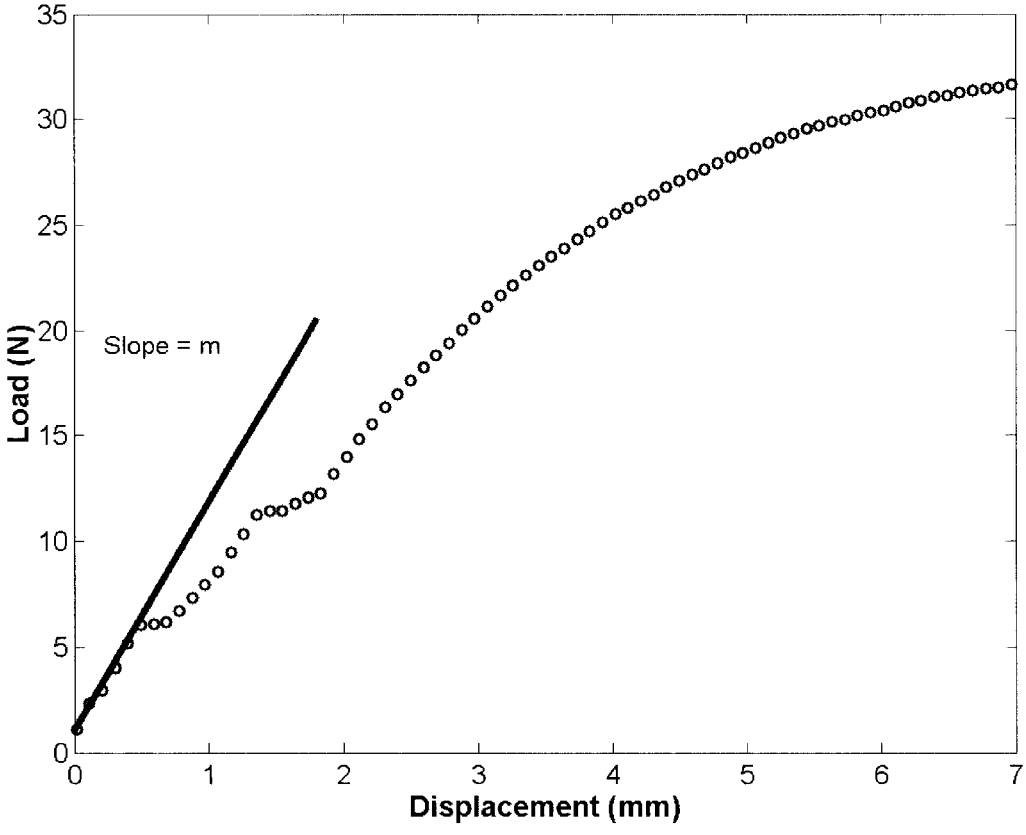

Figure 3.5: Example of compression load (N) vs. compression extension (mm) curves for TPOC4

3.5.5 Cell Density Measurements

To quantitatively and qualitatively determine how the NTPO, TPOP and TPOC materials foamed, pictures of the foamed material were taken. These photographs were used to estimate the cell density of the material. To obtain samples that were photographic-ready, a thin cross-section was taken from the middle of the dog-bone injection molded part for NTPO, TPOP1, TPOP4, TPOP7, TPOP10 and TPOC1, TPOC4, TPOC7, TPOC10 by a sharp razor blade. For each material, three dog-bone samples were chosen at random for sample preparation. One digital image per sample was taken on the edge portion of each cross-section under a Olympus SZ-CTV optical microscope with a Nikon CoolPix 995 digital camera at 6.5× magnification. The cell density was obtained by squaring off an area of the photograph and manually counting the cells included in the area. The number of cells per volume was calculated using Equation 3.2, where N is the number of cells per cubic centimeter, n is the number of cells counted in a given area, R is a unitless scaling factor, and H and W are the dimensions of the observed area.

$$N = \left[\frac{nR^2}{HW}\right]^{\frac{3}{2}} cell/cm^3 \tag{3.2}$$

Using the calculated cell densities, and the measured unfoamed and foamed densities, the average cell size was calculated using Equations 3.3 and 3.4, where ν_g is the gas volume fraction, ρ_c is the density of the polymer matrix, ρ_{fc} is the density of the foam and ρ_g is the density of the gas.

$$\nu_g = \frac{\rho_c - \rho_{fc}}{\rho_c - \rho_g} \tag{3.3}$$

$$D = 2 \times \sqrt[3]{\frac{3\nu_g}{4\pi N}} \tag{3.4}$$

In the calculations, the value of ρ_g is neglected from Equation 3.3 because it is very small compared to ρ_c and ρ_{fc}.

3.5.6 Fourier Transform Infrared Spectroscopy (FT-IR)

FT-IR was used in attempts to track the degree of degradation that occurred in the TPOP and TPOC materials after going through a multi-pass process. It is known that polypropylene exists in the material and it may produce traceable degradation products.

TPOC and TPOP samples for FT-IR analysis were prepared by pressing pelletized material in a hot melt press set at 180°C at 350bar pressure for two minutes. Each sample was analyzed in the Nicolet FTS 3000MX, with 16 scans between 400 to 4000cm^{-1} at a 2cm^{-1} resolution.

Chapter 4

Results and Discussion - Polymer Clay Nanocomposite

4.1 TEM and XRD

This section presents data obtained from TEM and XRD analysis that indicates the extent of intercalation and delamination that occurred in a TPO-clay nanocomposite through a melt blending process.

Figure 4.1 to 4.5 show results from XRD analysis on the d-spacing of clay layers for both Cloisite 15A and polymer-clay nanocomposite after multiple passes. Table 4.1 lists the 2θ values obtained from XRD analysis along with the d-spacing that was calculated using Bragg's Law. The initial clay layer spacing was found to be 3.3nm, which is comparable to the layer spacing value 3.2nm that was supplied by Southern Clay Products. This indicates that the data obtained by XRD are accurate values. These diffraction patterns will be interpreted according to Vaia *et al.* [1995]

In comparing the d-spacings, it was shown that there was no significant change in

the layer spacing between the original clay material and that of the nanocomposite after multiple passes.

Table 4.1: 2θ and clay layer spacing measured from XRD diffraction patterns

Material	2θ	Layer Spacing (nm)
Clay	2.7	3.3
TPOC1	2.6	3.3
TPOC4	2.6	3.3
TPOC7	2.7	3.3
TPOC10	2.7	3.3

Figures 4.2 to 4.5 shows a decrease in the peak intensity with each analyzed pass of the nanocomposite, which indicated that there was an increase in the number of intercalated clay tactoids with increasing residence time and shear strain [Vaia *et al.*, 1995]. This observation proves that intercalation was taking place in the system, but the method by which intercalation was occurring is still unclear. Dennis *et al.* [2001] proposed two pathways in which a clay tactoid can disperse itself into a polymer matrix during melt processing. Tactoids can either shear apart, forming more tactoids comprised of fewer platelets, or the platelets can peel away from the tactoid starting from the outer platelets. If this material system undergoes the second pathway towards intercalation, there should be an observable increase in the clay layer spacing with increasing number of passes. However, for this particular material system, based on XRD data, it appears that intercalation follows the first pathway. Figures 4.2 to 4.5 show that the breadth of the diffraction peak broadens with increasing number of passes, which indicated that the tactoid size was decreasing. This also supports the idea that the larger clay tactoids are shearing apart to form smaller tactoids.

Figure 4.6 shows examples of TEM micrographs of materials TPOC1, TPOC4, TPOC7

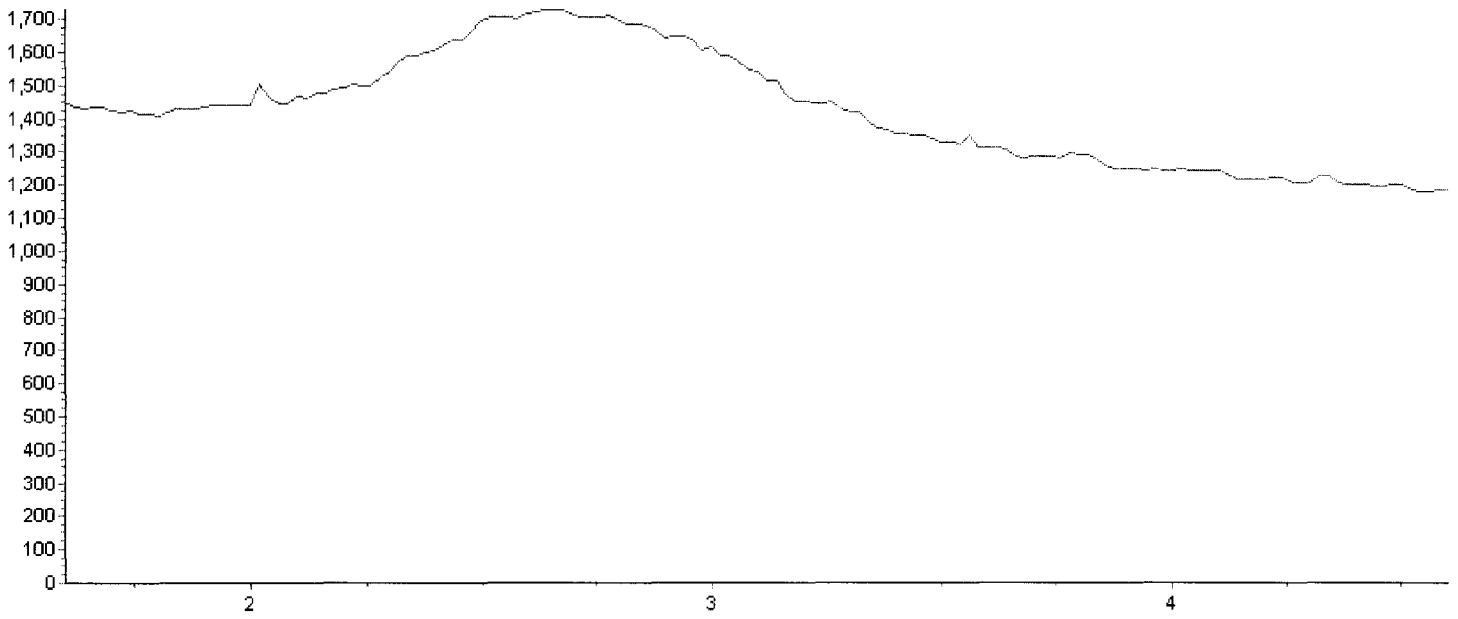

Figure 4.1: XRD diffraction pattern for Cloisite 15A (Intensity versus 2θ)

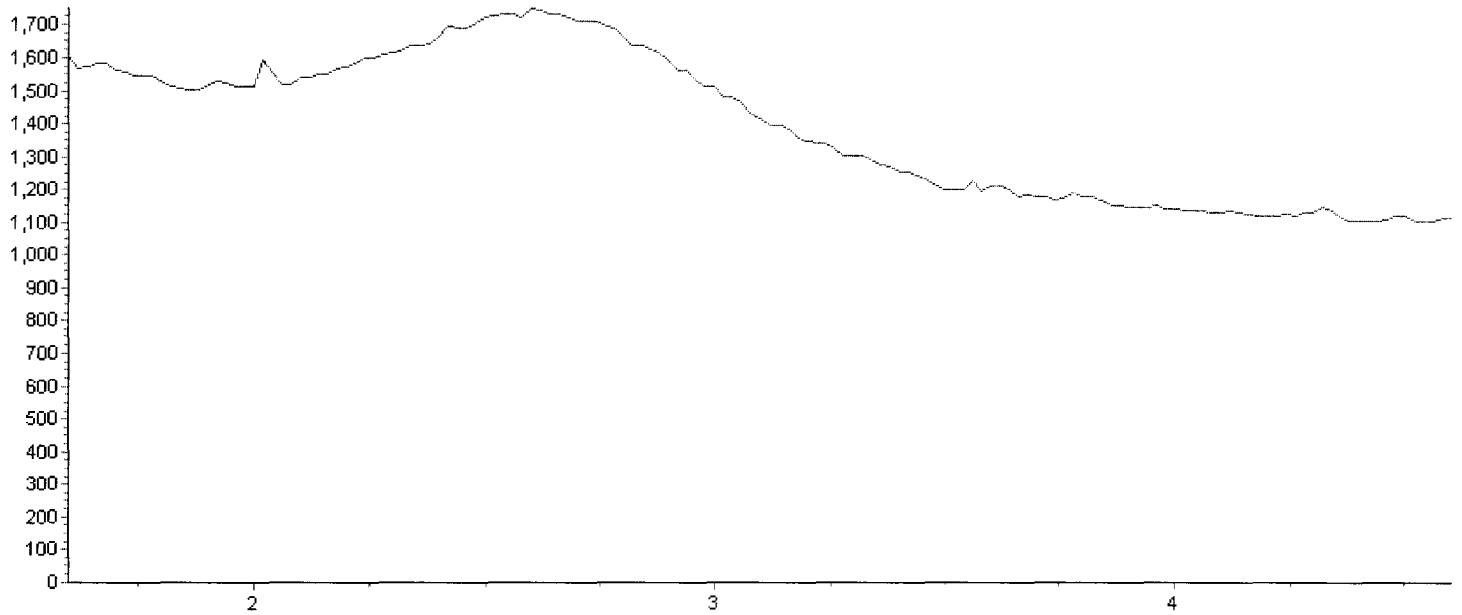

Figure 4.2: XRD diffraction pattern for TPOC1 (Intensity versus 2θ)

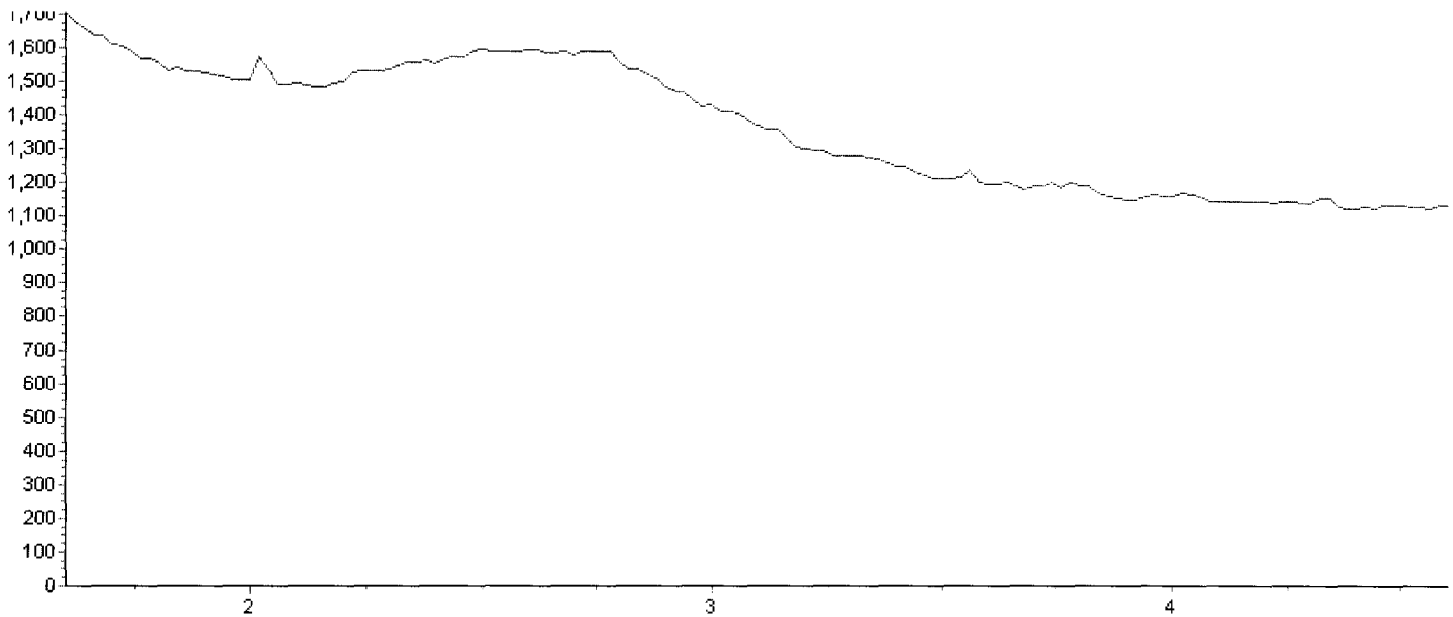

Figure 4.3: XRD diffraction pattern for TPOC4 (Intensity versus 2θ)

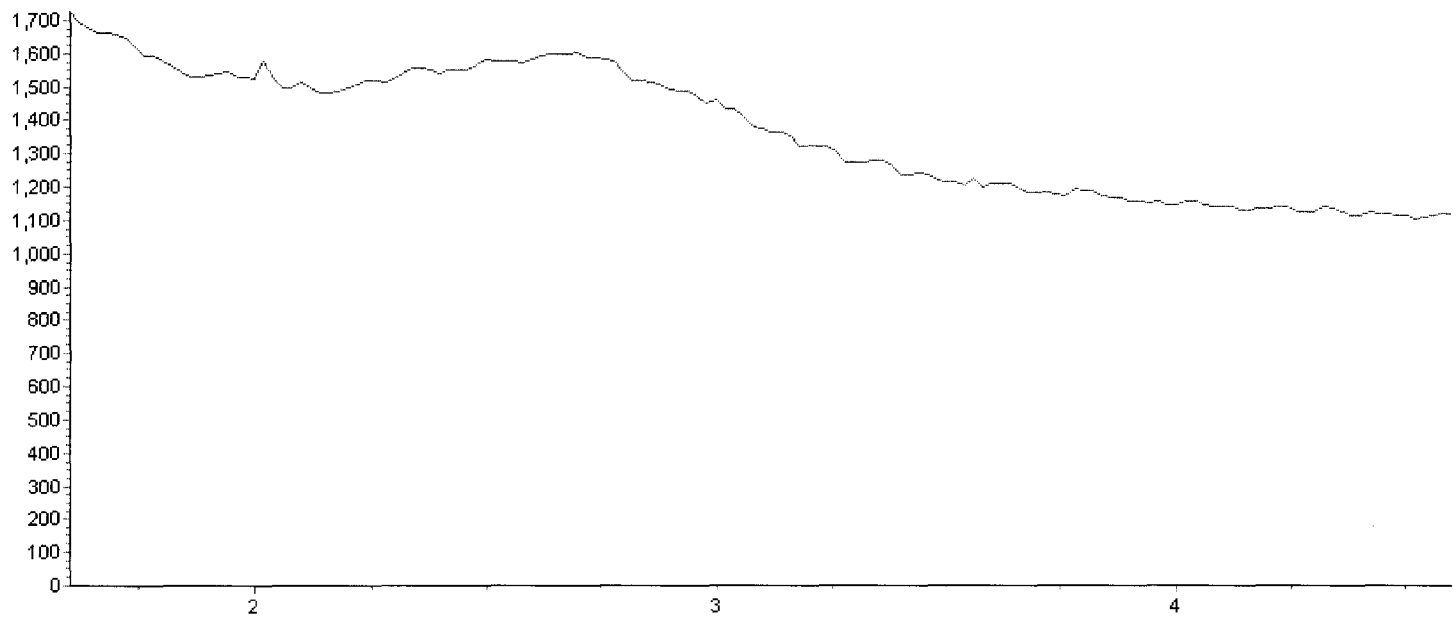

Figure 4.4: XRD diffraction pattern for TPOC7 (Intensity versus 2θ)

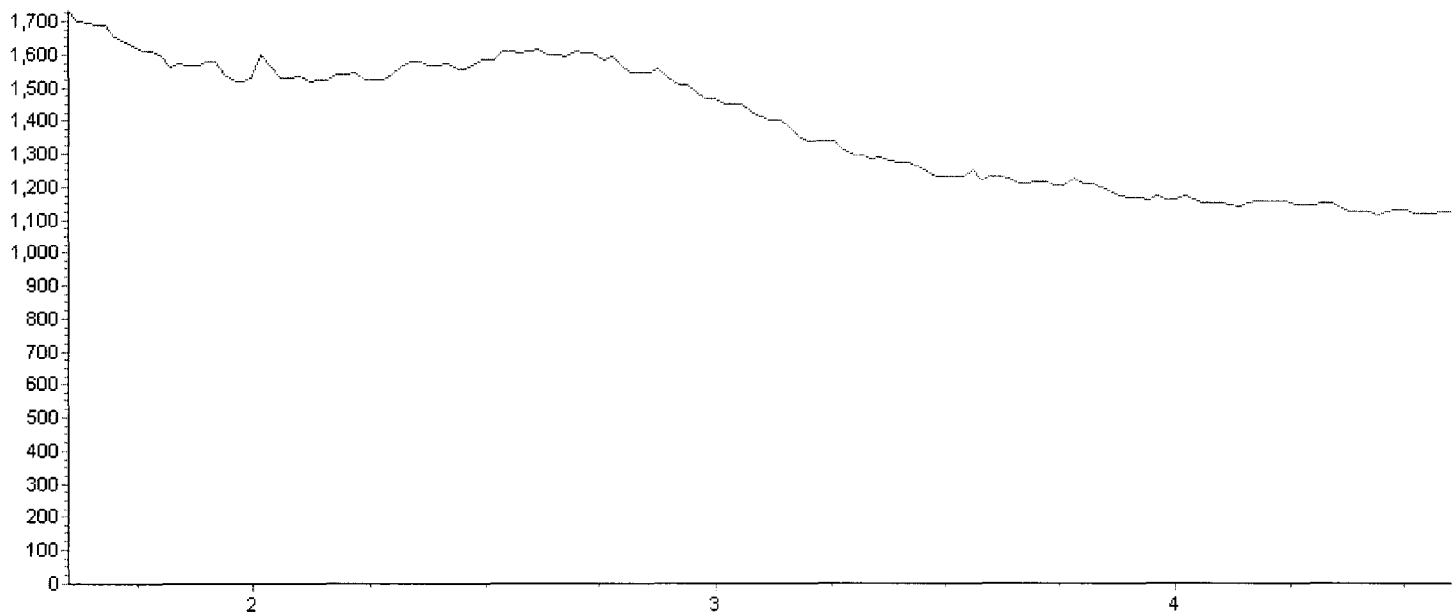

Figure 4.5: XRD diffraction pattern for TPOC10 (Intensity versus 2θ)

and TPOC10 at 1M magnification. Using digital imaging software, the spacing between the clay platelets (dark lines on the micrograph) were measured. Table 4.2 shows the average clay layer spacing measured from these micrographs. Statistically, the average distance between the clay layers for TPOC1 to TPOC7 does not differ between each material, but there appears to be an increase in the clay layer spacing for TPOC10. Figure 4.6 also shows that the tactoid in TPOC10 has a higher degree of swelling compared to the other three materials. These results are a little different than the results obtained from XRD analysis, which does not detect the increase in platelet spacing. Also, the values obtained by XRD appear to be larger than the observed clay layer spacings measured from TEM micrographs. These discrepancies can be attributed to the clay tactoid orientation for both XRD and TEM, as mentioned in Section 2.6.

Table 4.2: Average clay layer spacing measured from TEM micrographs taken at 1M magnification

Material	Spacing TEM (nm)
TPOC1	2.2 ± 0.1
TPOC4	2.3 ± 0.6
TPOC7	2.2 ± 0.2
TPOC10	2.5 ± 0.4

Figure 4.7 show micrographs of TPOC1, TPOC4, TPOC7 and TPOC10 taken at 45K magnification (see Appendix A for micrographs at 60K). Each of these micrographs show that the clay tactoids were uniformly distributed in the polymer matrix. These micrographs also show that the clay had a preferred orientation. McNally *et al.* [2003]; Okamoto *et al.* [2001] have shown that clay platelets have a preferred orientation under shear flow.

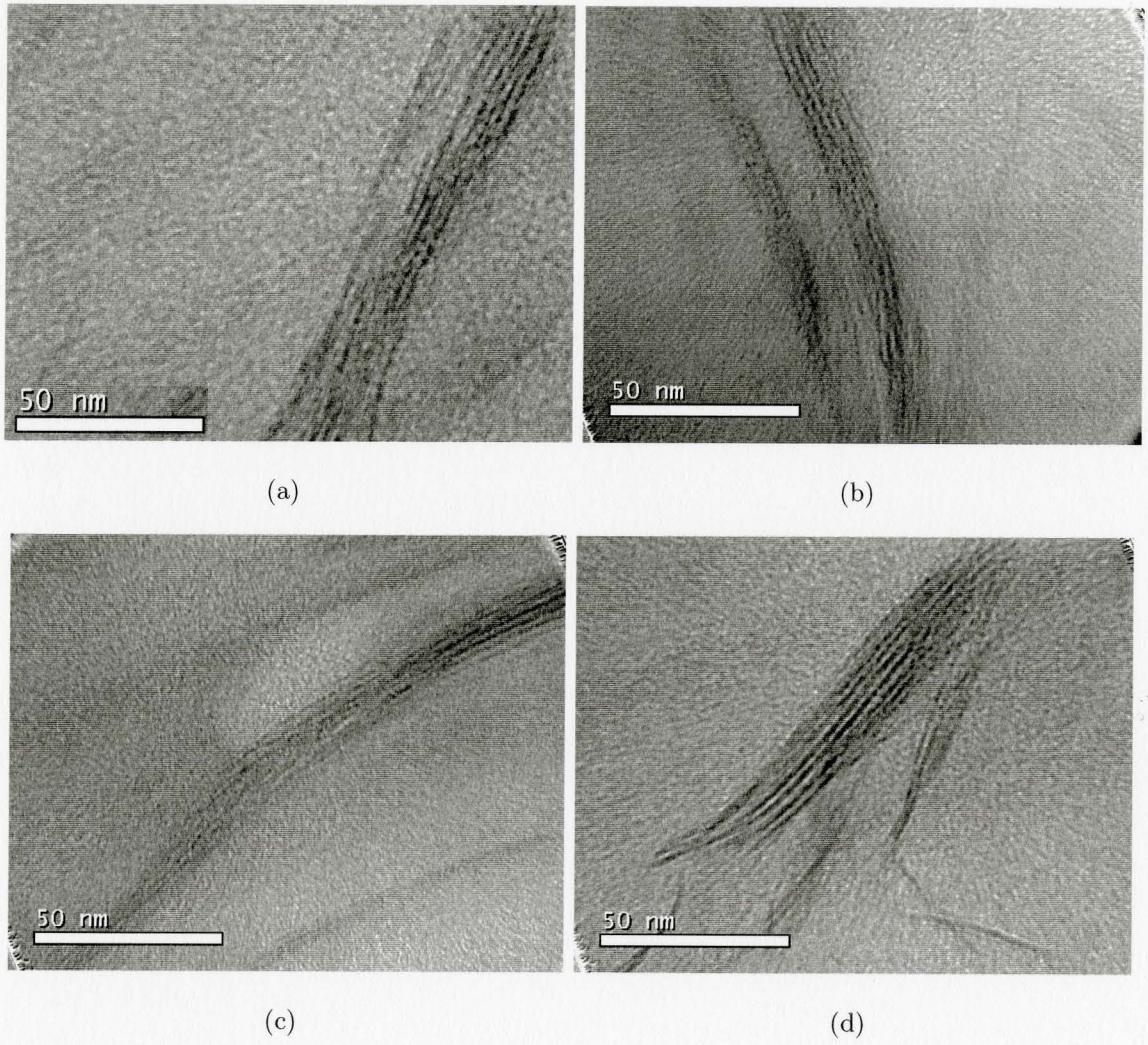

(a) (b)

(c) (d)

Figure 4.6: TEM micrographs at 1M magnification a)TPOC1 b)TPOC4 c)TPOC7 d)TPOC10

Upon closer observation and comparison of Figures 4.7, it appears that there was an increase in the amount of smaller clay tactoid structures with increasing number of passes, which is in agreement with the results obtained through XRD. To further prove this, the aspect ratio distribution of TPOC1, TPOC4, TPOC7 and TPOC10 were measured and are presented in Figure 4.8.

Figure 4.8 shows that there was a shift in the distribution towards larger aspect ratios as the number of passes through the extruder increased. Table 4.3 lists the median aspect ratio taken from the aspect ratio distributions, indicating an increase in the median aspect ratio between TPOC1 and TPOC7. Such a change in morphology can be speculated to have been caused by the mechanisms of intercalation and delamination. The micrographs shown in Figure 4.6 indicate that the ends of the clay tactoids were flaring outwards (during all passes) which supports the hypothesis of intercalation occurring in the presence of polymer chains. These findings appear to suggest the clay delaminated in a manner similar to the proposed first pathway of Dennis *et al.* [2001], where the larger clay tactoids shear apart to form smaller tactoids. Although there was a decrease in the aspect ratio median between TPOC7 and TPOC10, the shape of the distribution curve remained the same. TEM micrographs show that the gallery spacings increased, which is caused by the intercalation of the polymer matrix. This indicated that particle dispersion by delamination occurs first, followed by the swelling of clay galleries due to intercalation. This idea will be explored further in Section 4.4.

In subjecting the material to multiple pass processing, it was hoped that the degree of intercalation would be varied, which would make way for further studies on the effects of intercalation on the foamability of the TPO-clay nanocomposite. Foamability results will be discussed in Chapter 5. Based on the results obtained from XRD and TEM, the goal of varying the degree of intercalation has been achieved, although the method of which they intercalate by has yet to be answered. The method of

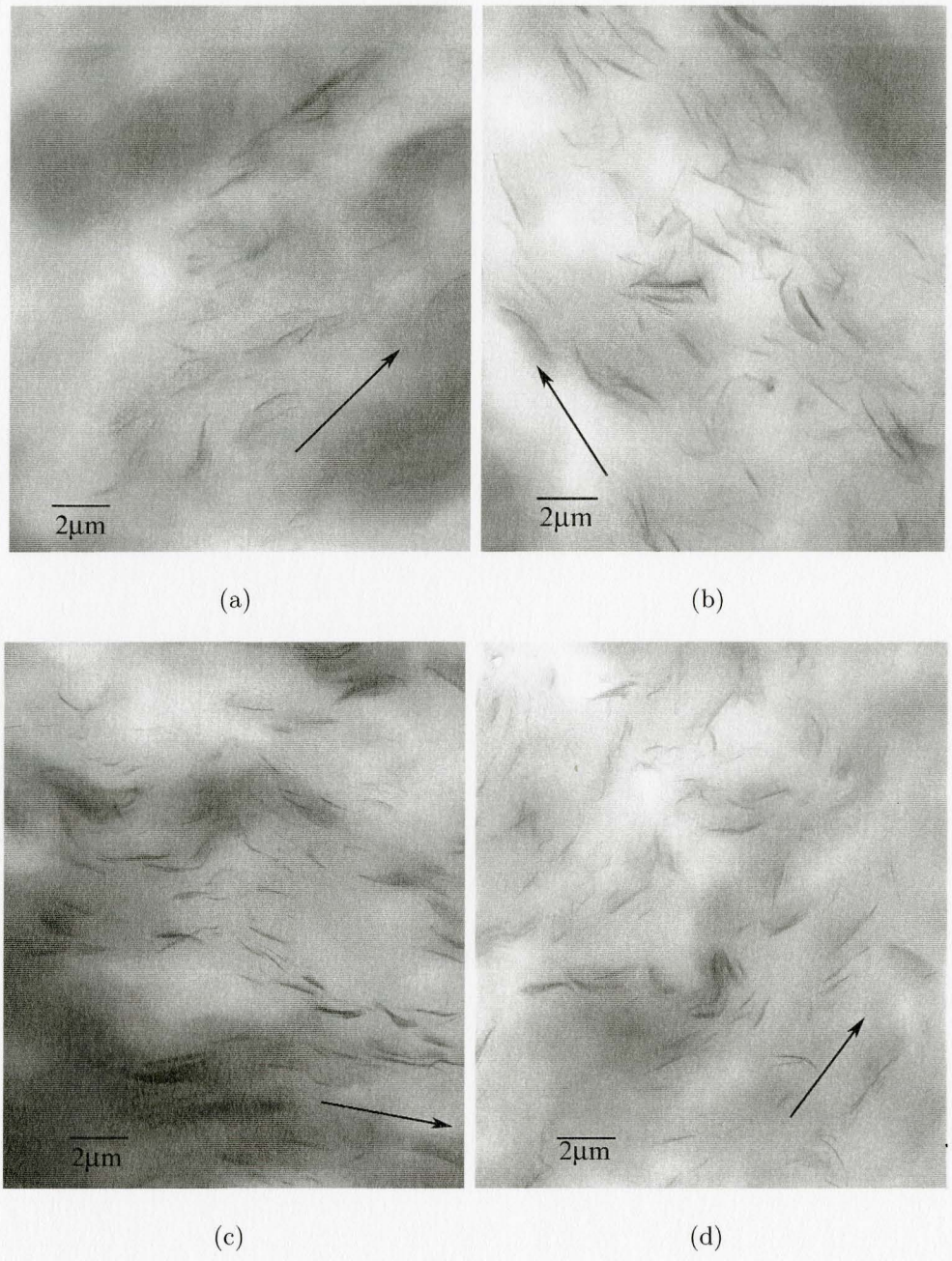

Figure 4.7: TEM micrographs at 45K magnification a)TPOC1 b)TPOC4 c)TPOC7 d)TPOC10, arrows show direction of preferred orientation

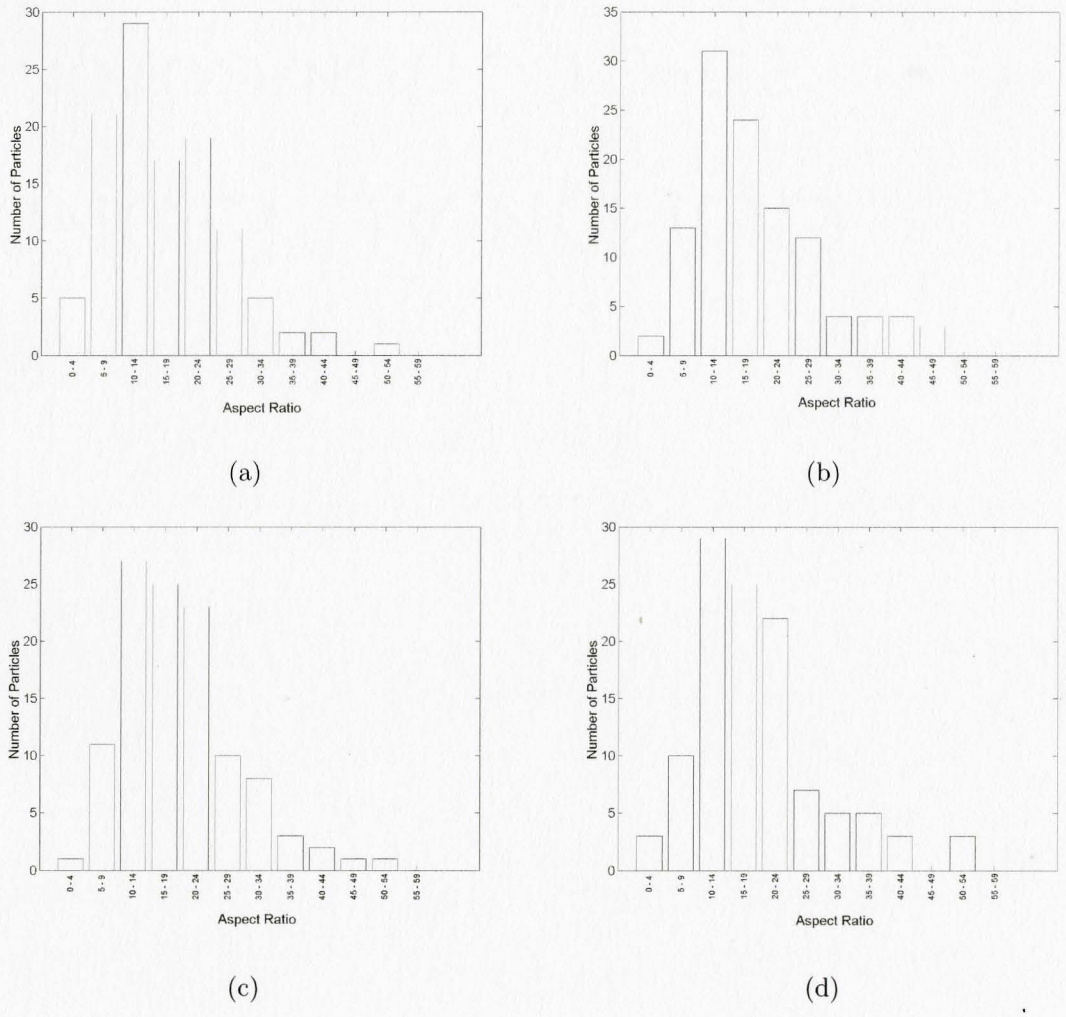

Figure 4.8: Aspect ratio distribution a)TPOC1 b)TPOC4 c)TPOC7 d)TPOC10

Table 4.3: Average clay layer spacing measured from TEM micrographs taken at 1M magnification

Material	Aspect Ratio Median
TPOC1	15
TPOC4	17
TPOC7	19
TPOC10	18

intercalation will be discussed further in Section 4.4.

4.2 Rheology

Rheology is a method that is most commonly used to track changes in the polymer structure. It is the measure of material deformation under an applied stress. In this section, results from measured dynamic viscosity (η^*), dynamic storage modulus (G') and dynamic loss modulus (G") will be presented.

Figure 4.9 shows the viscosities for NTPO, TPOP1 and TPOC1; the lower shear rate range ($0.1s^{-1}$ to $100s^{-1}$) was measured using a parallel plate rheometer, while the higher shear rate range ($100s^{-1}$ to $5000s^{-1}$) was measured using the capillary rheometer. There is an observable discrepancy between the data obtained between the two rheometers for all three materials. Viscosity measurements on immiscible polymer blends are known to be dependent on the strain amplitude [Di *et al.*, 2002]. The strain amplitude for parallel plate rheometer is lower than the strain amplitude of the capillary rheometer, which may explain the discrepancy observed for NTPO and TPOP1. For polymer-clay nanocomposites, clay platelet orientation has an effect on rheological measurements [Ren *et al.*, 2003]. If the platelets are aligned with the flow,

the platelets provide less resistance to shear, while if the platelets were unaligned, there is more resistance to shear. This means that the rheological measurements obtained for an aligned material would be lower than an unaligned material. An aligned material can be achieved by subjecting the material to high shear rates in one direction for a prolonged period of time, which is how a capillary rheometer operates. It is possible that the viscosity measured by the capillary rheometer is the viscosity of an aligned material. For the measurements pertaining to the parallel plate rheometer, because the material is subjected to oscillatory shear at low frequencies, the clay platelets may be in an unaligned state. The lack of agreement between the two rheometers is an indication that the Cox-Merz rule does not apply for TPO and TPO-clay nanocomposite materials, which complies with the findings of Di *et al.* [2002] and Ren *et al.* [2003].

For TPOP, there were notable changes in η^*, G' and G" around the low frequency end (i.e. close to $\omega = 0.1$rad/s), shown in Figures 4.10 through 4.12 respectively. It appears that all these properties decreased with increasing number of passes. These trends are more easily seen in the calculated zero-shear viscosities, calculated by fitting the viscosity data points to the Cross model. The zero-shear viscosity values are shown in Table 4.4. In the absence of organoclay, the decrease in value can be attributed to the degradation of the material. Because of the unknown make-up of the NTPO, it is difficult to determine the exact cause of degradation and the type of degradation products that were produced. Bacci *et al.* [2004] has shown that crosslinking and scission occurs simultaneously for a heterophasic EPM polymer, however, scission is more common at low ethylene content.

Maleic Anhydride (MAH) is known to cause chain scission in a polypropylene-MAH system at low concentration levels [Ho *et al.*, 1993], which is similar to the material system being used in this study. To determine whether MAH has an active role in the degradation of the TPOP, the rheological results obtained from the NTPO were

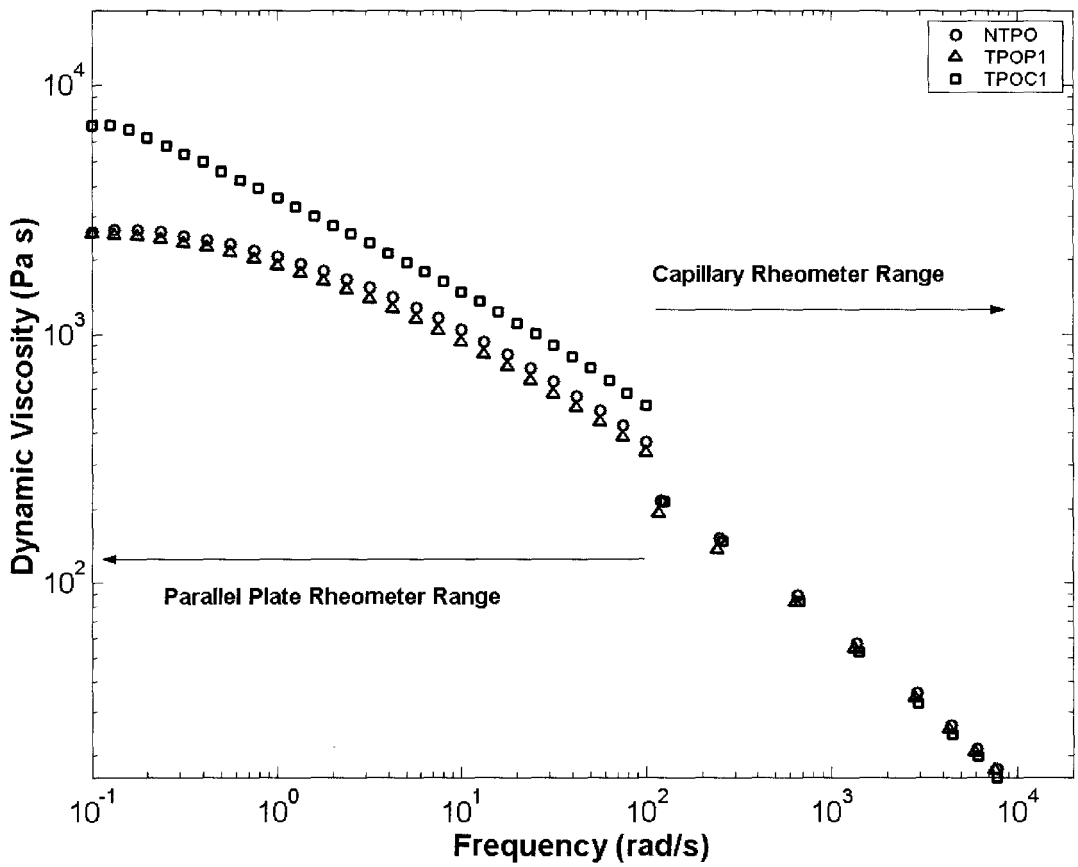

Figure 4.9: Viscosity of NTPO, TPOP1 and TPOC1 measured from parallel plate rheometer and capillary rheometer at 210°C

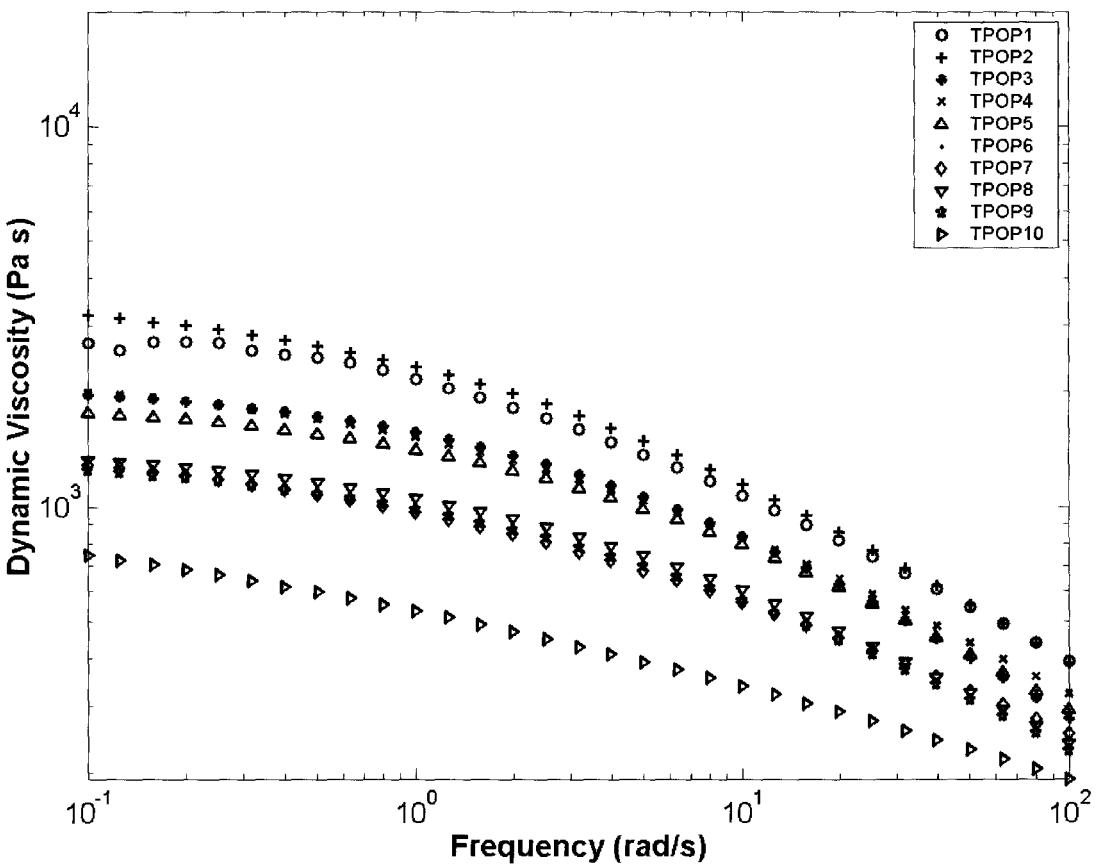

Figure 4.10: Dynamic viscosity curves for TPOP, at 210°C at 5% strain rate

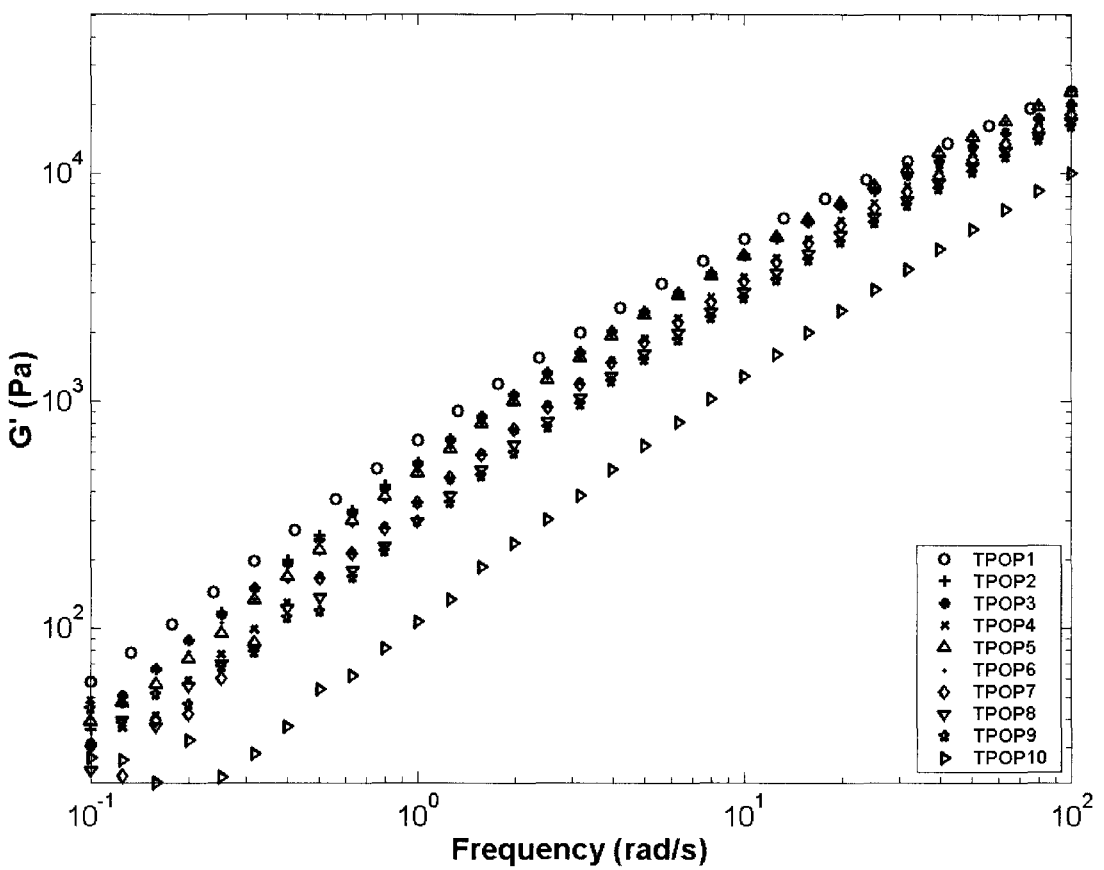

Figure 4.11: G' curves for TPOP, at 210°C at 5% strain rate

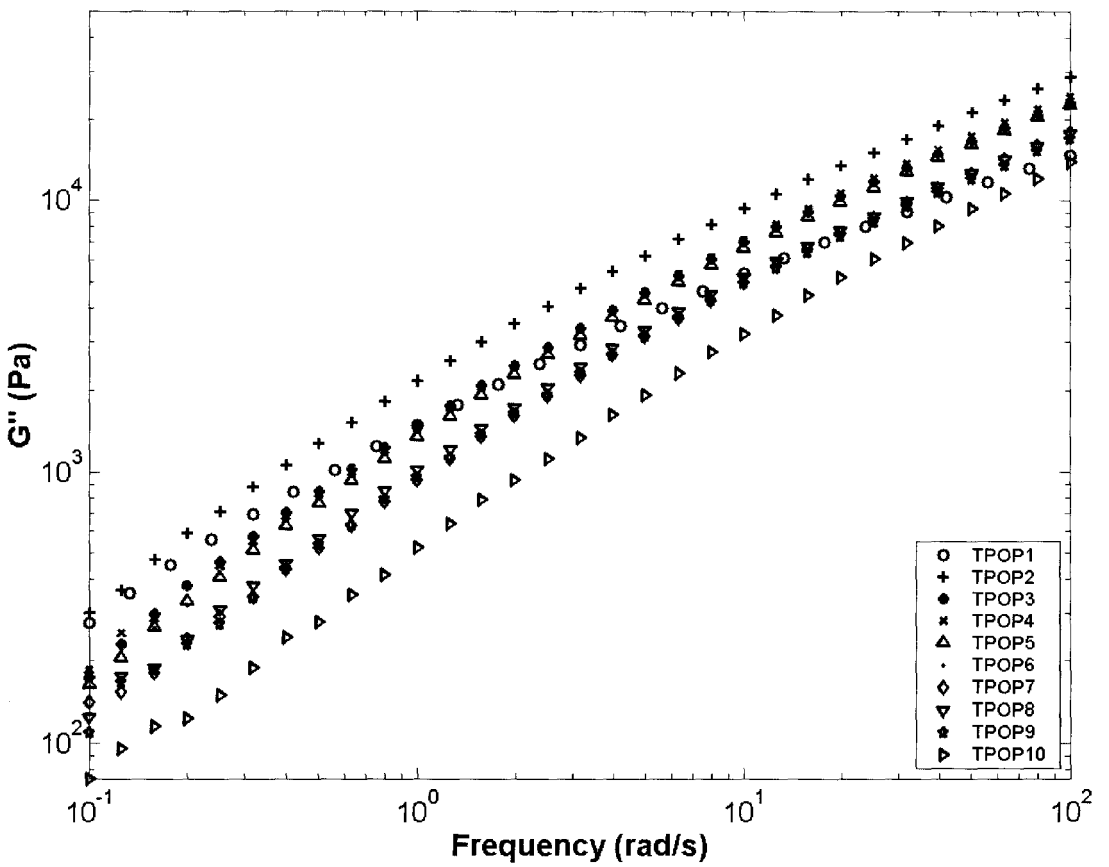

Figure 4.12: G" curves for TPOP, at 210°C at 5% strain rate

Table 4.4: Zero-shear viscosities for TPOP and TPOC after each extruder pass, at 210°C

Pass Number	TPOP (Pa s)	TPOC (Pa s)
1	3476 ± 379	12154 ± 2033
2	3670 ± 321	20811 ± 947
3	2132 ± 48	28786 ± 823
4	2285 ± 254	30786 ± 4152
5	1925 ± 58	26333 ± 4822
6	1956 ± 70	25329 ± 3944
7	1553 ± 399	18847 ± 2254
8	1478 ± 32	23243 ± 5609
9	1396 ± 193	20759 ± 2532
10	711 ± 58	19480 ± 4145

compared to the rheological results of TPOP. Figures 4.13 to 4.15 show η^*, G' and G" measurements respectively taken for NTPO, NTPO1 and NTPO10. It is shown that NTPO, NTPO1 and TPOP1 all had similar rheological properties, but NTPO10 and TPOP10 differed significantly. Viscosity, G' and G" values at all frequencies for TPOP10 appeared to be lower than NTPO10. This is an indication that MAH is a significant contributor to the extent of degradation experienced by TPOP.

Observing the crossover frequency (ω_c), which is the frequency at which G' = G" can help to verify that scission is indeed occurring in this material system. ω_c is related to the polydispersity index (PI) of the material, which is defined by Equation 4.1 where M_w and M_n are the weight average and number average molecular weights respectively.

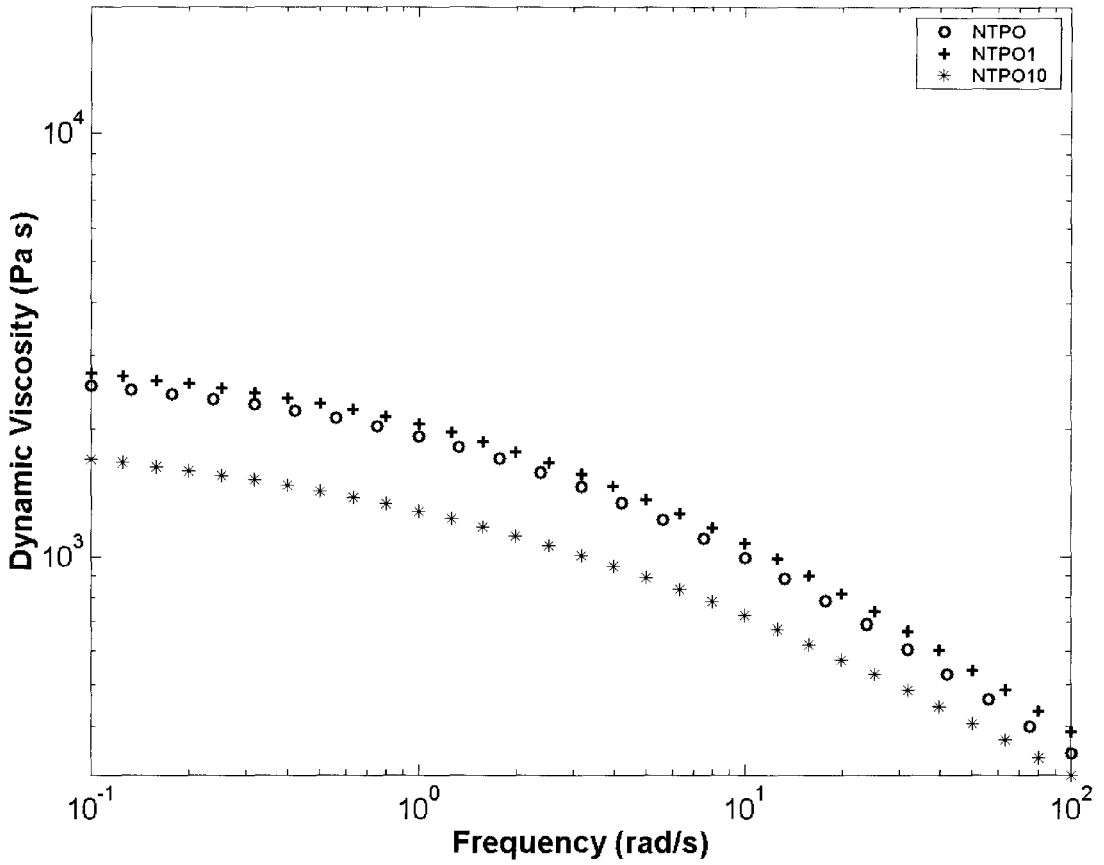

Figure 4.13: Dynamic viscosity curves for NTPO, at 210°C at 5% strain rate

$$PI = \frac{10^5(Pa)}{\omega_c} \cong \frac{M_w}{M_n} \tag{4.1}$$

In calculating the ω_c for TPOP, it was found that $\omega_c = 63$ s^{-1} for TPOP1, $\omega_c = 79$ s^{-1} for TPOP7 and $\omega_c > 100$ s^{-1} for TPOP10. The increasing values of ω_c meant that the PI was being lowered. This indicates that TPOP preferably undergo scission reactions rather than crosslinking reactions.

As mentioned in Section 2.7.1, the added clay forms a percolation network which provides resistance to flow. Therefore, an increase in η^*, G' and G" should be observed

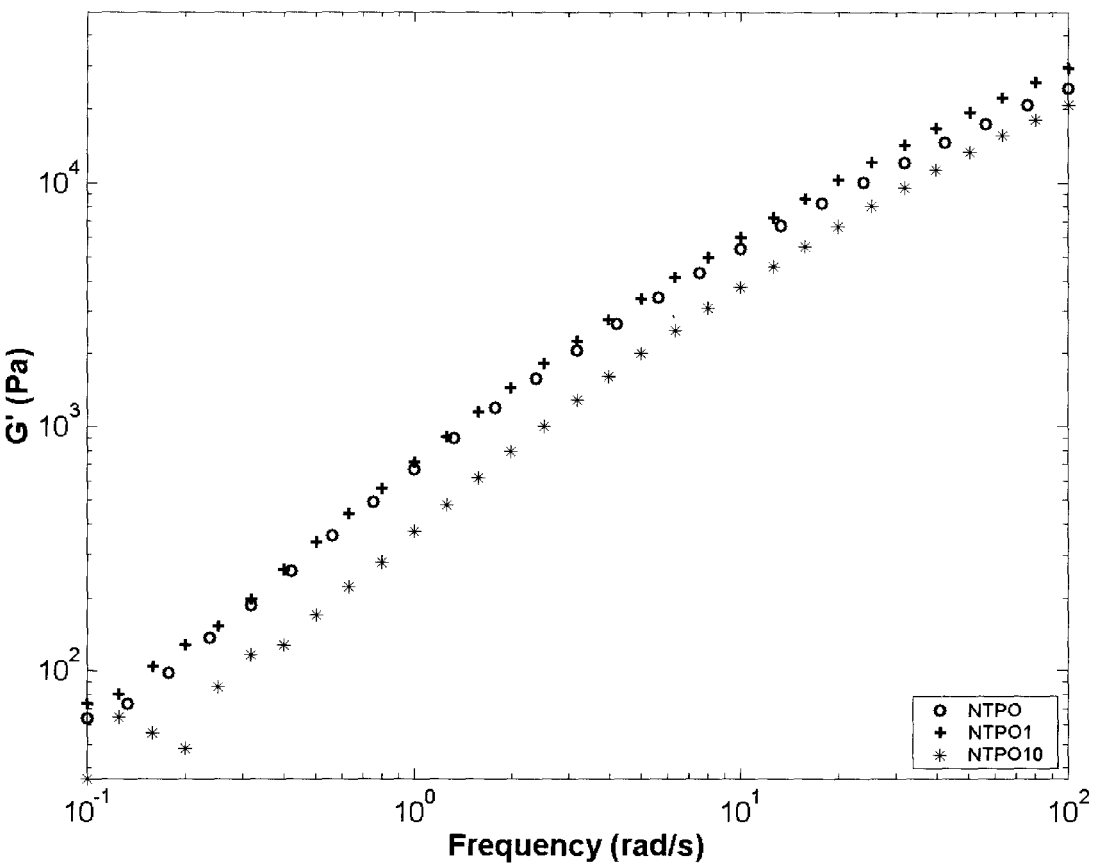

Figure 4.14: G' curves for NTPO, at 210°C at 5% strain rate

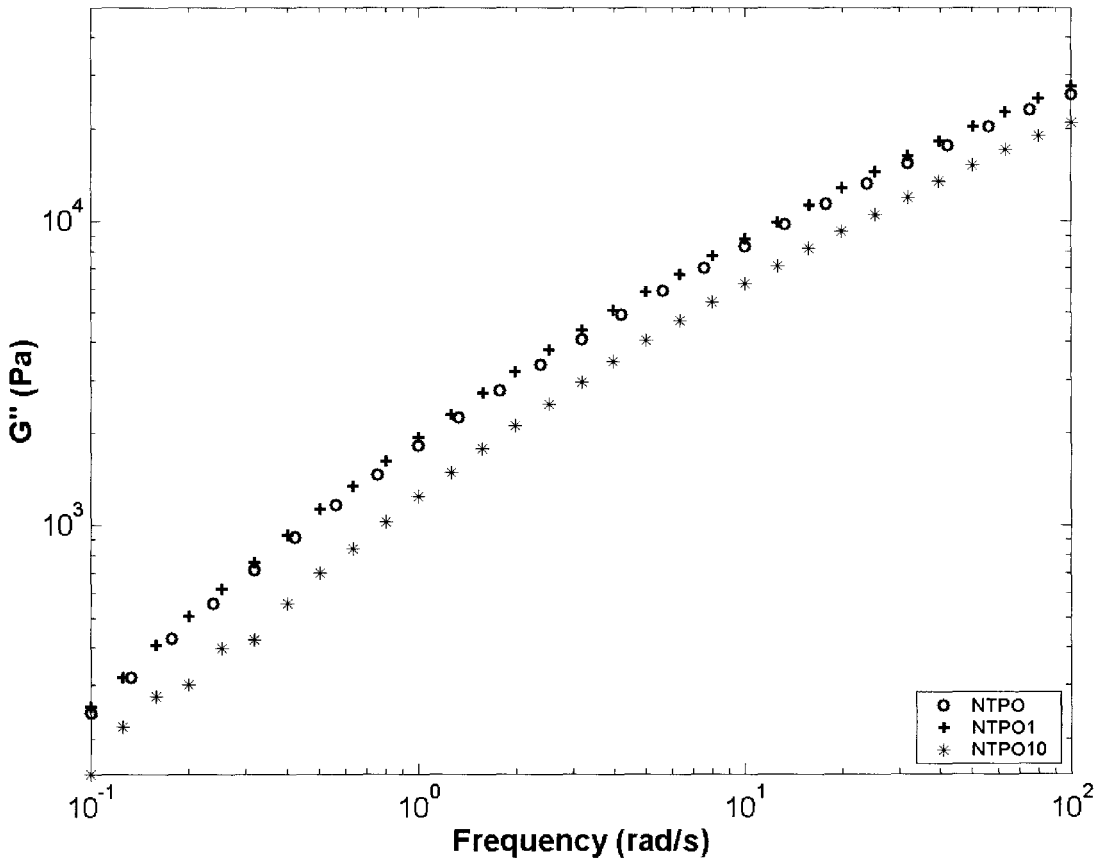

Figure 4.15: G" curves for NTPO, at 210°C at 5% strain rate

[Galgali *et al.*, 2001; Solomon *et al.*, 2001; Incarnato *et al.*, 2004]. As the degree of delamination increases, so too should these characteristic rheological parameters because more clay platelets will be introduced into the percolation network [Li *et al.*, 2003]. Table 4.4 shows that the zero-shear viscosities for TPOC were on average eleven times larger than that of TPOP, which supports the idea that viscosity increased with the addition of clay. In addition to this, it was observed that a Newtonian plateau did not exist for the viscosity of TPOC at low frequencies, shown in Figure 4.16. This was unlike the viscosity curves obtained from both TPOP and NTPO (Figures 4.10 and 4.13), which showed a Newtonian plateau. The non-Newtonian behaviour at low frequencies exhibited by TPOC is an indication that the clay platelets are restricting the movement of the polymer chains in the polymer matrix, a finding further exemplified by observing the G' and G" curves for TPOC, which are shown in Figures 4.17 and 4.18 respectively. Again, observing the low frequency region, G' and G" curves showed non-terminal behaviour, which is in agreement with literature [Solomon *et al.*, 2001; Galgali *et al.*, 2001; Li *et al.*, 2003]. Conversely, G' and G" curves for NTPO (Figures 4.14 and 4.15) and TPOP (Figures 4.11 and 4.12) show terminal behaviour. The addition of clay was responsible for the non-terminal behaviour shown by the TPOC. The clay percolation network was confining the polymer chains, thereby preventing the polymer matrix from fully relaxing [Incarnato *et al.*, 2004]. To further quantify this, the relaxation times (τ) were calculated, which is the time it takes for stress to decay to a factor of 0.37 [Vlachopoulos, 2003]. Relaxation times can be estimated by using Equation 4.2.

$$\tau = \lim_{\omega \to 0} \frac{G'}{\omega G"} \tag{4.2}$$

Calculated relaxation times are listed in Table 4.5. There are no trends that are observable for τ, especially for TPOP. Obtaining G' and G" values at low frequencies can be difficult because low frequency rheological measurements using a parallel plate

rheometer are dependent on the sensitivity of the pressure transducer present in the equipment. Because of this, these calculated τ values are not accurate estimates of the actual τ. However, Table 4.5 shows that TPOC have approximately 290% higher relaxation times compared to the TPOP, which indicates that the clay is restricting the movement of polymeric chains.

Table 4.5: Relaxation times for TPOP and TPOC

Pass Number	TPOP (s)	TPOC (s)
1	3.157 ± 0.587	6.720 ± 0.587
2	2.525 ± 0.077	9.425 ± 1.702
3	1.798 ± 0.243	10.588 ± 1.873
4	2.581 ± 0.793	10.542 ± 1.074
5	2.747 ± 0.610	11.357 ± 1.825
6	2.647 ± 1.163	9.780 ± 1.585
7	1.114 ± 0.944	8.155 ± 0.445
8	1.905 ± 0.187	9.042 ± 1.046
9	4.067 ± 1.111	9.322 ± 1.338
10	1.773 ± 1.035	9.373 ± 1.172

For the TPOC, G' and G" data, depicted in Figures 4.17 to 4.18 respectively all displayed similar trends: an increase in the properties near $\omega = 0.1$rad/s, between TPOC1 to TPOC4, then a decrease from TPOC4 to TPOC10. The zero-shear viscosities in Table 4.4 demonstrated that η^* followed the same trends. Li *et al.* [2003] has shown that rheological properties at low frequencies monotonically increased with increasing degree of intercalation. It is also known that rheological properties have a tendency to decrease with the onset of scission; shortening the chains allows the polymer chains to be more mobile, thereby decreasing η^*, G' and G". The results obtained in Section 4.1 showed that intercalation occurred in the system and the

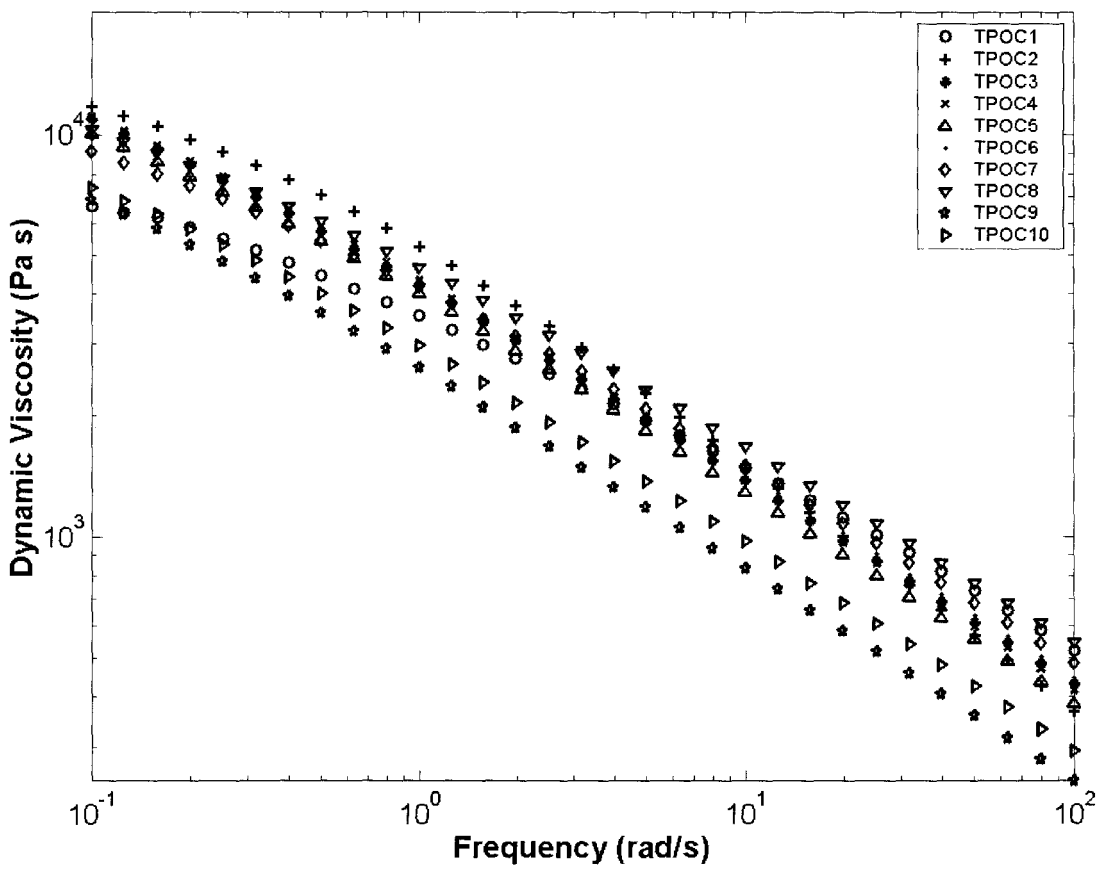

Figure 4.16: Dynamic viscosity curves for TPOC, at 210°C at 5% strain rate

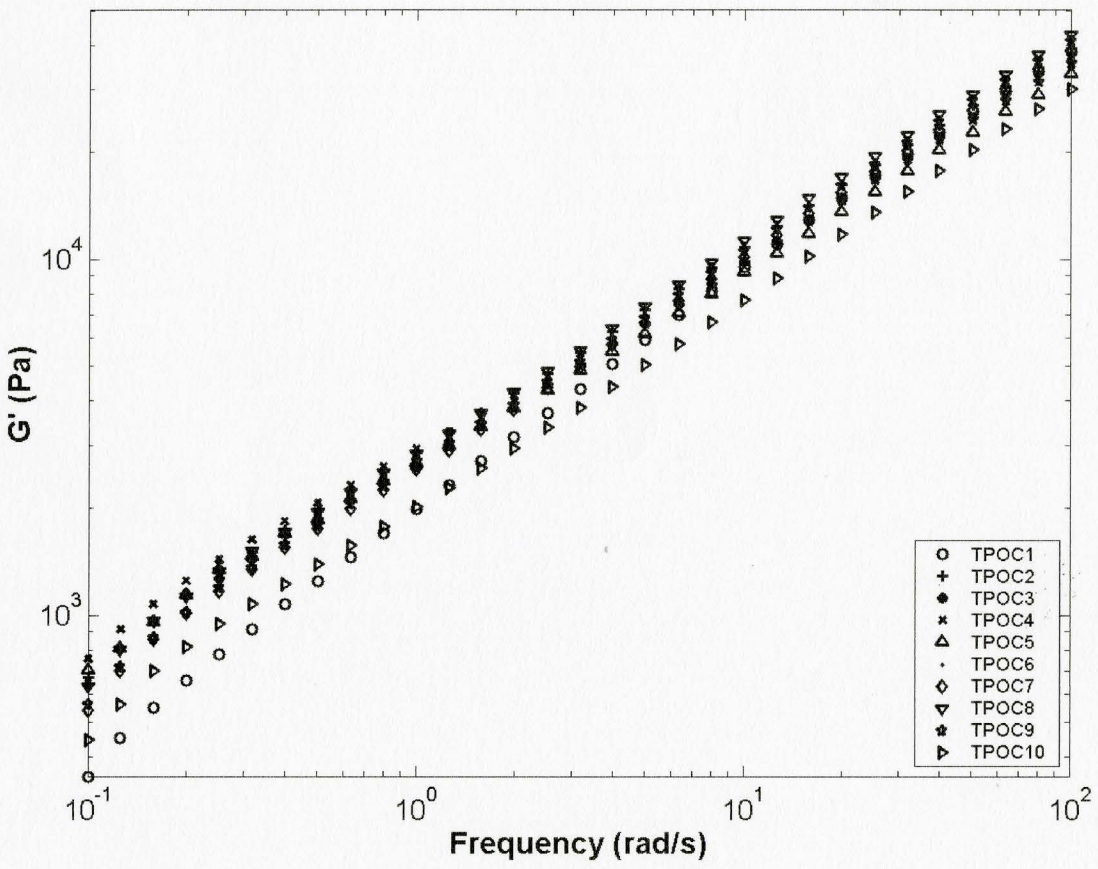

Figure 4.17: G' curves for TPOC, at 210°C at 5% strain rate

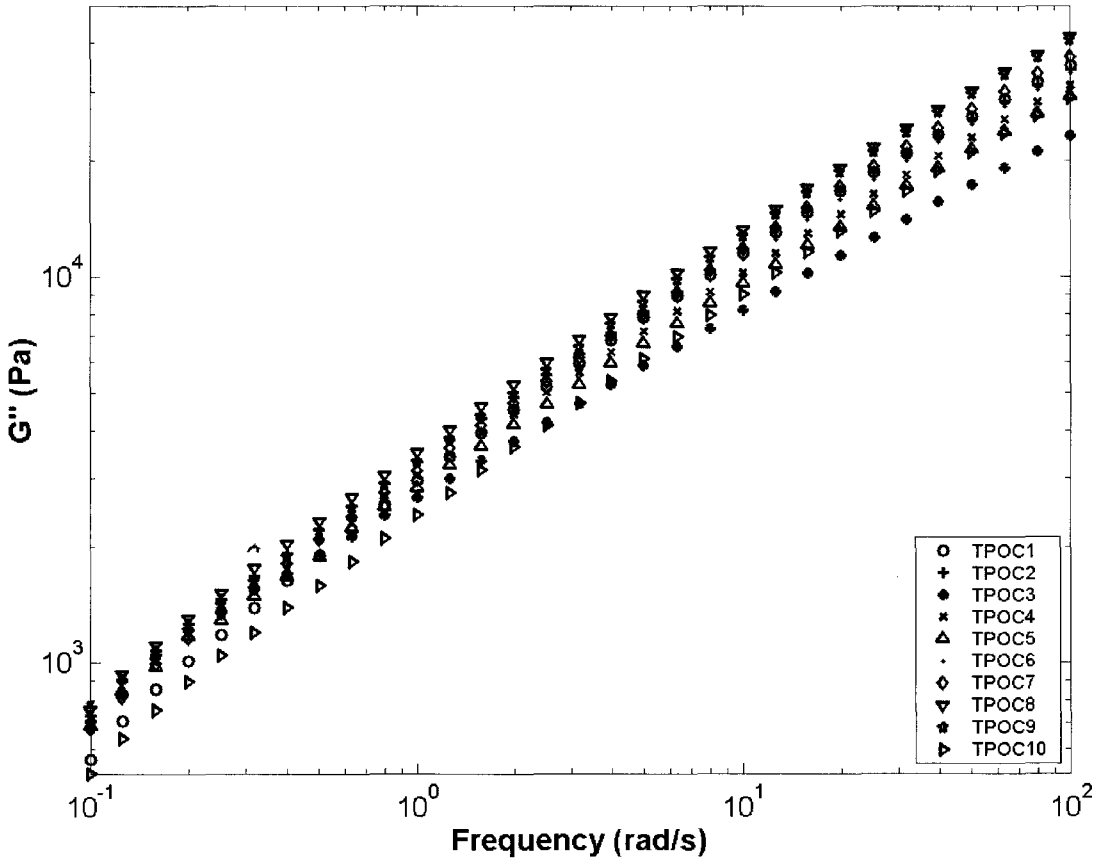

Figure 4.18: G" curves for TPOC, at 210°C at 5% strain rate

degree of intercalation increased with increasing number of passes. On the other hand, rheological data obtained for NTPO and TPOP showed that the material underwent scission reactions due to the presence of MAH. These findings lead to the conclusion that TPOC underwent intercalation and scission reactions simultaneously, where scission reactions dominated from TPOC4 to TPOC10.

4.3 Flexural Modulus

The addition of clay is known to improve the flexural properties of a polymeric material [Sinha Ray *et al.*, 2003]. Figure 4.19 shows the flexural modulus TPOP and TPOC. It was observed that the flexural modulus for TPOC was on average 44% higher than the flexural modulus for TPOP. The clay platelets formed a percolation network within the polymer matrix, which provided structural reinforcement to the nanocomposite. Also, the orientation of the clay platelets in the injection molded parts contributed to the overall flexural properties. According to Kojima *et al.* [1995], the clay platelets tend to orient themselves parallel to the surface for an injection molded bar. This means that the clay layers lie perpendicular to the direction of bending, therefore the clay has a greater area for which stress transfer can occur. This explains the dramatically higher flexural modulus in the clay materials.

There are also observable trends with increasing number of passes for both materials. For TPOP, there was approximately a 20% decrease in the flexural modulus between TPOP1 to TPOP10. Referring back to Section 4.2, the trends in the flexural modulus mirror the trends observed in rheological properties. This suggests that the decrease in the flexural modulus was due to degradation of the material. For TPOC the flexural modulus appeared to remain constant from TPOC1 to TPOC4, and then decreased with subsequent passes. Although TEM analysis and rheology showed that the degree of intercalation did increase between TPOC1 to TPOC4, the

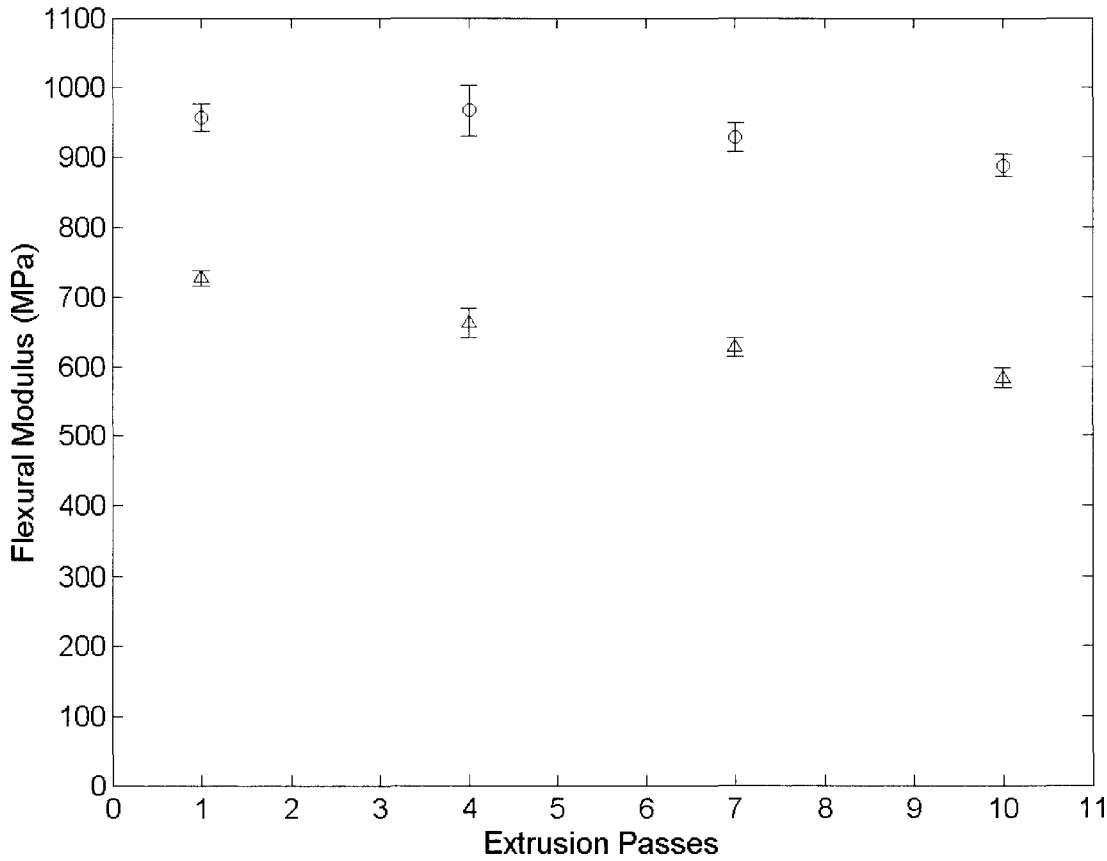

Figure 4.19: Average flexural modulus for TPOP and TPOC after multiple extrusions (△ - TPOP, ◯ - TPOC)

flexural modulus between TPOC1 to TPOC4 showed minimal change. Theoretically, intercalated and exfoliated structures would increase the flexural modulus because it would introduce more clay particles that can participate in the percolation network, although there are no current studies that supports the idea the fully exfoliated structures improve flexural properties. It is possible that the degradation of the material was offsetting the increase in the flexural modulus that may have been attributed to the increase in delamination due to intercalation, therefore a minimal change was observed. The decrease in flexural properties between TPOC4 to TPOC10 reiterates the idea expressed in Section 4.2 that scission reactions were dominant in this processing window. Overall, the flexural modulus for TPOC saw approximately a 7% decrease in flexural properties from TPOC1 to TPOC10.

4.4 FT-IR

Degradation of polypropylene is known to yield products that contain carbonyl groups. Since carbonyl groups exists in MAH and antioxidants, which is present in the current material systems, the change in concentration of carbonyl groups was tracked using FT-IR to monitor the extent of degradation. Figure 4.20 show FT-IR scans of TPOP, TPOC and NTPO. The figures show that there was no observable peaks between 1600cm^{-1} to 1700cm^{-1}, which corresponds to the stretching mode vibration bands for carbonyl groups. According to FT-IR results, there is no evidence that thermo-oxidative degradation occurred, however, rheology shows that scission occurs in the system. It is possible that the concentration of these carbonyl groups were below the detection capabilities of the instrument. Small changes to the chain structure (such as chain scission and long chain branching) is known to alter the flow characteristics of the polymer, making rheological measurements more sensitive to small changes in the molecular structure to the chain [La Mantia *et al.*, 1989].

An observable peak at 1742cm^{-1} which corresponds to an ester group appeared to be diminishing with increasing number of passes for TPOP. This ester group relates to the antioxidant that is present in the material system put in by the material manufacturer to minimize degradation effects. The ester peak was observed for TPOC, but a lower intensity peak was observed for TPOC1 compared to TPOP1. A study conducted by Hu *et al.* [1994] on the effects of antioxidants on a talc filler showed that antioxidants, or stabilizers, adsorb to the surface of the talc particles, which can explain why there was a decrease in the concentration of the antioxidant with the introduction of clay into the material. The reduction of the antioxidants leaves the system more vulnerable to degradation reactions. This would suggest that TPOC experienced higher levels of degradation compared to NTPO and TPOP based on the notion that the nanoclay does not provide thermal stability to the polymer matrix [Tidjani *et al.*, 2003].

Peaks that are associated with maleic anhydride grafted material were also present in the FT-IR spectra. These peaks included maleic anhydride (1780cm^{-1}), succinyl anhydride (1792cm^{-1}) and cyclopentanone (1772cm^{-1}). The most notable change was in the cyclopentanone peak, which appeared unchanged for TPOP, but diminishes for TPOC. It is noted that there was a change in the peak height between TPOP and TPOC1, indicating that the presence of clay had an effect on the compatibilizer. The difference between the peaks for TPOP materials and TPOC1 was an indication that the compatibilizer species was the first to participate in intercalation due to its polar nature; it is more attracted to the clay layer surface [Li *et al.*, 2001]. Since IR is based on the detection of the vibrational movement of molecules, the decrease can be attributed to the restrictions of these movements vibrations upon the knowledge that the molecule is not being modified in any way. Based on the assumption that the polymer matrix in the TPOC materials behave in the same manner as TPOP during melt processing, the maleic anhydride groups should remain present in the system according to the FT-IR data obtained from TPOP, therefore, the decrease in

the cyclopentanone peak can be attributed to the intercalation of the compatibilizer into the clay layers.

FT-IR data, coupled with the data obtained from the TEM micrographs and rheological measurements can give insight into how intercalation progressed in this material system. As mentioned in Section 4.1, there are two intercalation stages that are occurring during processing. The first stage involves the intercalation of compatibilizer and polypropylene scission products. FT-IR of TPOC have shown that the compatibilizer intercalated into the system after the first pass and the antioxidant was being adsorbed onto the surface of the clay platelets. Intercalation of the compatibilizer actually aids the intercalation process by weakening the interactions between the clay platelets, allowing for easier intercalation of polymer species. This may have occurred during the first four passes, which explains the increase in aspect ratio median between TPOC1 and TPOC4, which led to the increase in the rheological properties. Between TPOC4 to TPOC7, majority of the antioxidant species had been adsorbed, meaning more degradation products were present in the material system. Degradation products include aldehydes and ketones, which are polar and participate in the intercalation process in the same manner as the compatibilizer. This means the interaction between the clay layers was further weakened, which explains the further shift in the aspect ratio median between TPOC4 and TPOC7. By TPOC7, the interactions between the clay platelets become so weak it allowed for polymer chains to intercalate into the clay layers, which explains the gallery expansion for TPOC10 materials from the TEM micrographs.

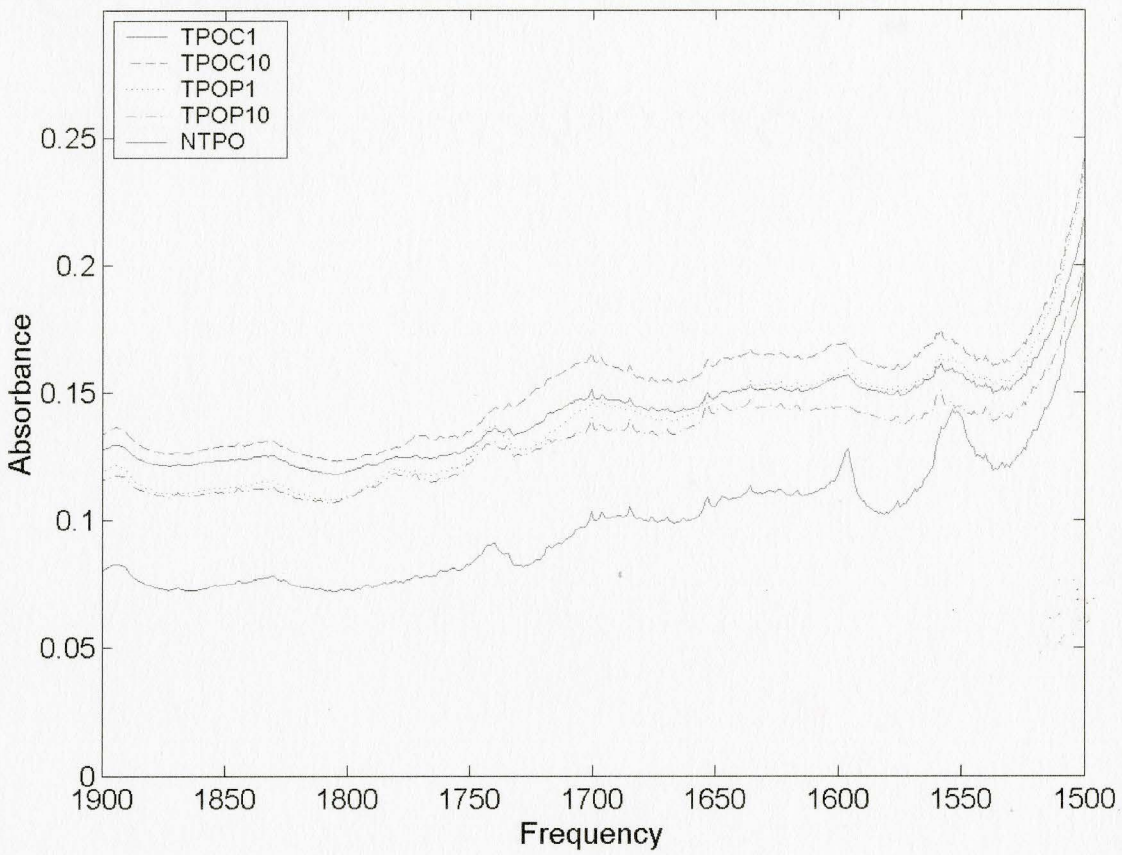

Figure 4.20: FT-IR scan on TPOP, TPOC and NTPO between 1500cm^{-1} to 1900cm^{-1}, 16 scans at 2cm^{-1} resolution

Chapter 5

Results and Discussion - Foaming

Foaming in an injection molding process causes a density reduction, which was experienced by NTPO, TPOP1, TPOP4, TPOP7, TPOP10, TPOC1, TPOC4, TPOC7 and TPOC10 (Table 3.3). There was an approximate 10.9% density reduction for TPOP foamed parts and 12.1% density reduction for TPOC foamed parts.

5.1 Effects of Clay on Foaming

Quantifying the foamability of a material usually involves either measuring the cell density and/or cell size of a foamed part. Cell density is the measure of the number of cells in a given volume, and it tends to be a more accurate analysis of a foam based on observations of its cross-section. Cell size measurement, on the other hand, is dependent on where the cross section is taken, for example, if the cross section is taken near the top of the bubble, the measured cell will be smaller than its actual size. For this case, the cell size will be calculated based on a mass balance using the cell density, and unfoamed and foam material density. Cell density was determined using cross-section digital images of TPOP and TPOC foamed parts shown in Figures 5.1

Table 5.1: Calculated average cell size

	Cell Size (mm)	
Extrusion Pass	TPOP	TPOC
1	0.109	0.118
4	0.117	0.109
7	0.133	0.095
10	0.171	0.121

and 5.2 respectively. Figure 5.3 shows a diagram of the location at which these digital images were taken. The calculated average cell size was subsequently determined for select samples and listed in Table 5.1. The trends will be discussed below as the cell density data is analyzed.

For NTPO and TPOP, the decomposed CBA acted as a foam nucleating agent. TPOC offers a more complicated scenario in that the system contains both decomposed CBA and clay particles, both of which can act as foam nucleating agents. Not only can the clay act as a nucleating agent, but it can also provide structural reinforcement for the cell [Nam *et al.*, 2002]. There are three cases that must be considered when determining the role of the clay in a foaming process; in all three cases, the CBA acted as a foam nucleating agent. Firstly, the clay platelets merely provided structural support for the growing cell by aligning along the cell wall [Nam *et al.*, 2002]. Secondly, the clay platelets could be acting as a foam nucleating agent. Alternatively, the nanoclay can be acting as both foam nucleating agent and a structural reinforcement. To determine which is the case, observations will be made from cell density, viscosity effects and cell size.

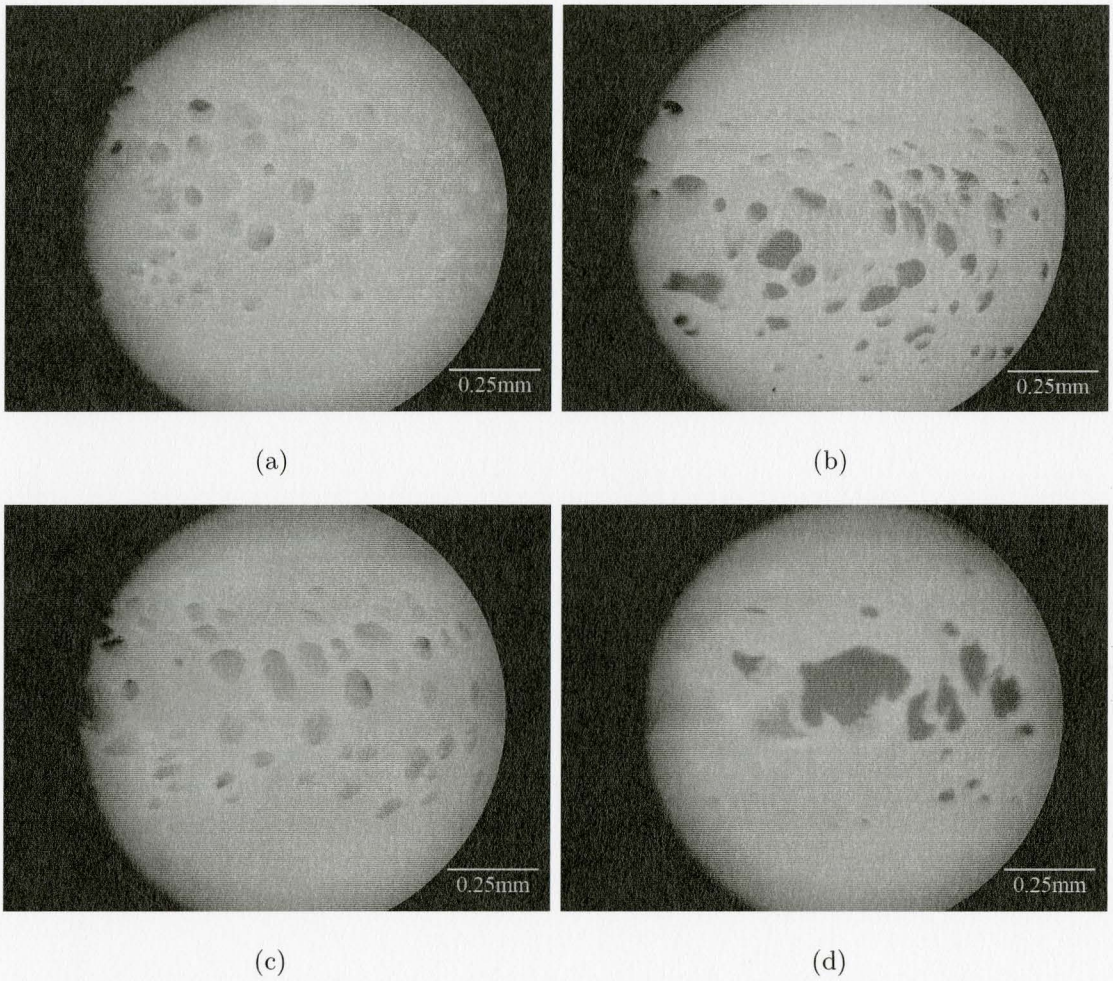

Figure 5.1: Cross-section of injection molded foamed parts taken at the edge of the sample a)TPOP1 b)TPOP4 c)TPOP7 d)TPOP10

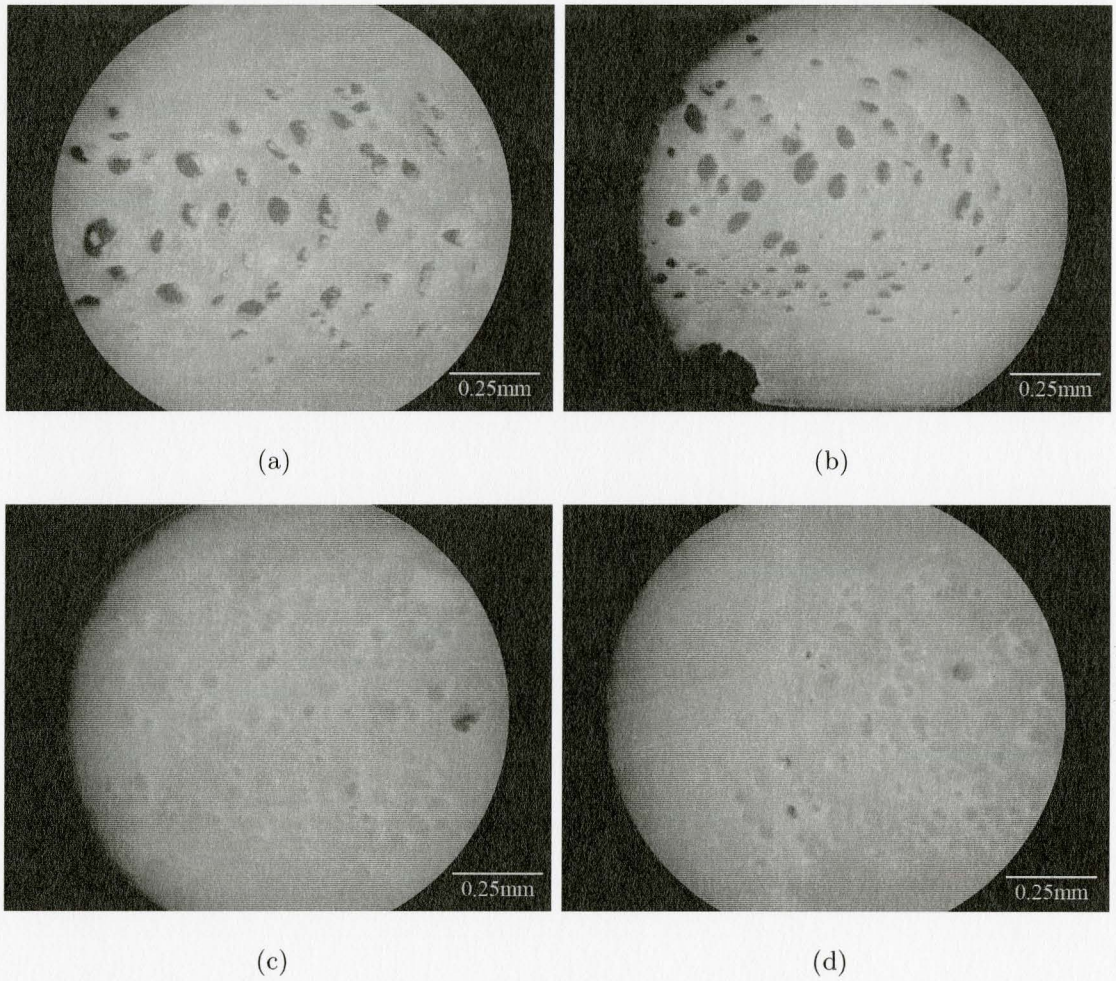

Figure 5.2: Cross-section of injection molded foamed parts taken at the edge of the sample a)TPOC1 b)TPOC4 c)TPOC7 d)TPOC10

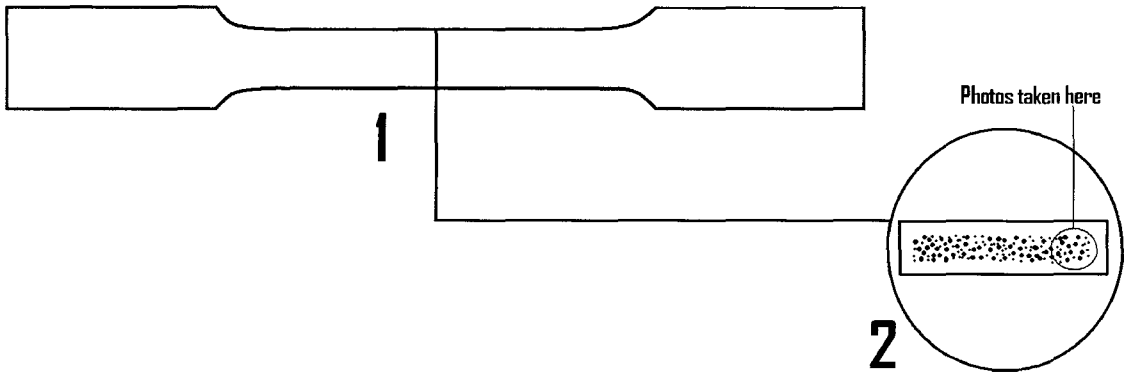

Figure 5.3: Cell density images: 1. Location where cross-section was obtained, 2. Small circle represents the area the digital images were taken

5.1.1 Cell Density

Figure 5.4 shows the average cell density for NTPO, TPOP1, TPOP4, TPOP7, TPOP10, TPOC1, TPOC4, TPOC7 and TPOC10 measured from digital images taken in the location specified by Figure 5.3. Assuming cell growth occurs only after the material has been injected into the mold, observing the zero-shear viscosities can explain the trends observed in the cell density. Extensional viscosity is proportional to the viscosity of the material. For TPOP, the decrease in zero-shear viscosity with increasing number of passes showed a decrease in the extensional viscosity. Figure 5.4 shows that the cell density decreases for TPOP as the number of passes increases, which follows the same trend as the zero-shear viscosity. This trend will be further discussed in Section 5.3.

TPOC showed a different trend in cell density to that of TPOP, with it increasing from TPOC1 to TPOC7, then decreasing for TPOC10. As mentioned in Section 2.9.2, the surface area of a heterogeneous foam nucleating agent (HFNA) is important. If the total surface area of the HFNA upon which a cell can nucleate is increased, so should the number of cells being formed, therefore increasing the cell density. Current

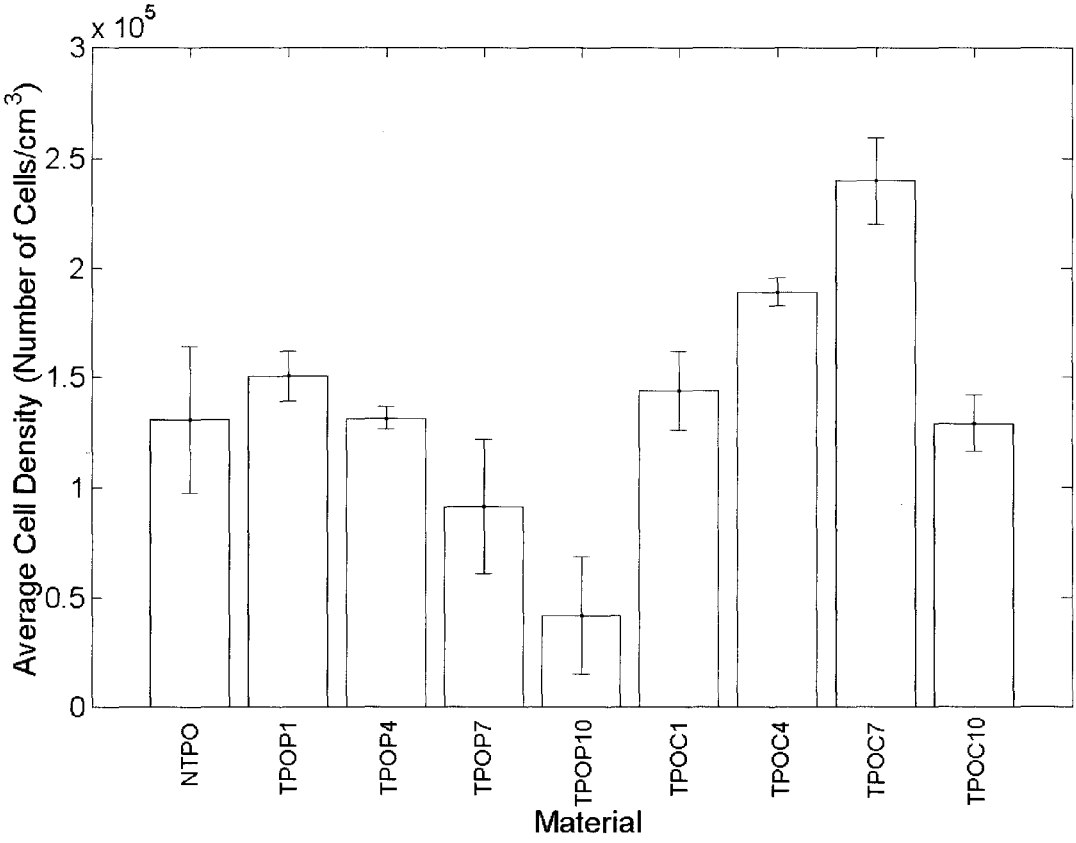

Figure 5.4: Cell density for NTPO, TPOP and TPOC

analytical techniques make it virtually impossible to obtain an accurate measurement of the total surface area of clay tactoids and platelets in a given volume. However, in this case, a rough estimate is only needed to determine whether the surface area has increased. From the TEM micrographs, the average width of a tactoid and the number of tactoids presented in a given area were calculated and counted for the TPOC material from four different passes. Also, the average tactoid length for all TPOC samples was calculated. Assuming that the length of the tactoid was constant, the tactoid depth was 1μm, and the shape of the tactoid was a rectangular prism, the total surface area for a given volume was calculated (assuming the depth of the given volume is 1μm). Based on these calculations (see Appendix B), it was found that the clay surface area increased 20% between TPOC1 to TPOC4, which brought upon a cell density increase of 31%, and surface area increase by 19% between TPOC4 to TPOC7, which brought a 27% increase in the cell density. The general trend was that the total surface area gradually increased as the number of passes increased. Since the CBA content is constant for all materials, this increase in total surface area may have contributed to the increase in the cell density attributed by the intercalation of clay. Also, the clay does not affect the solubility of CO_2 in the polymer matrix [Taki *et al.*, 2004], meaning the gas concentration in all injection molded foamed samples is assumed to be same. This indicates that the increase in the cell density can be attributed to the addition of clay into the polymer. However, it does not yet prove that the clay was only acting as a heterogeneous nucleating agent.

Unlike TPOP, the cell density trend for TPOC does not follow that of the zero-shear viscosity. The difference in trends lies between TPOC4 to TPOC7, where the zero-shear slightly decreased yet the cell density increased. Based on aspect ratio data, TPOC7 contains more tactoid particles than TPOC4. It is possible that the platelets are aligning along the cell walls, which form a barrier around the cell and provides structural reinforcement [Nam *et al.*, 2002]. This suggests the clay is preventing the cell from coalescing or collapsing, allowing it to maintain a high cell density.

5.1.2 Viscosity Effects

Viscosity of the material also affects the cell density both during nucleation and cell growth. For the injection molding processing conditions used in this study, the injection speed remained constant for all samples. Materials with high viscosity requires more pressure to inject at a set injection speed compared to a material with a lower viscosity, leading to a higher pressure drop (ΔP) from the injection nozzle to the mold. According to Equations 2.3 and 2.4, high ΔP relates to higher heterogeneous nucleation rates, leading to higher cell densities. The ΔP for each injection molded part was calculated by finding the approximate wall shear rate the material experienced during injection using Equation 5.1, where $\dot{\gamma}$ is the shear rate, Q is the volumetric flowrate and R is the radius of the mold runner. The viscosity of the material at the calculated shear rate was found using the viscosity data obtained from experimentation, then calculating the ΔP using Equation 5.2, where L is the length of the mold runner. Refer to Appendix C for sample calculations.

$$\dot{\gamma} = \frac{4Q}{\pi R^3} \tag{5.1}$$

$$\Delta P = \frac{-\eta 8QL}{\pi R^4} \tag{5.2}$$

Based on the results, TPOP and TPOC materials display similar pressure drops due to the similar viscosities in the shear thinning region. Nanocomposites have been shown in literature to exhibit similar shear thinning behaviour to their unfilled counterparts due to alignment of clay particles during shear flow [Lim *et al.*, 2002]. From this, it can be assumed that the difference in cell density does not arise from differences in viscosity at the onset of nucleation. However, viscous behaviour in the shear thinning region is only relevant to nucleation, while zero-shear viscosity or extensional viscosity tend to be more important to cell growth.

5.1.3 Cell Size

Increase in cell size or non-spherical/non-elliptical shaped cells can be attributed to coalescence. Compared to TPOP foamed parts, the cells of the TPOC foamed parts appeared to have smaller cell sizes and a lower degree of coalescence as determined by the lower presence of irregular shaped cells, even after undergoing multiple passes. The rheological analysis of the nanocomposites had already shown that a percolating network structure of clay exists at low deformation similar to the conditions of cell growth. This network of clay acts as reinforcement for the cell structure.

To summarize, in determining the role of the clay in a TPO-clay nanocomposite foaming process, there were three scenarios that were considered: the clay was acting as a foam nucleating agent, as structural reinforcement or a combination of the two first cases. It was found that the clay acted as a foam nucleating agent by discovering that the increase in cell density was due to the increase in the clay tactoid surface area and not due to viscosity effects. It has also been shown that the percolation network formed by the clay tactoids prevents the collapse and coalescence of cells, thus providing structural reinforcement. Therefore, the data showed that the clay acted as both a foam nucleating agent and structural reinforcement.

5.2 Skin Thickness

The foamed parts produced by injection molding have a sandwich structure consisting of a foam layer (core) surrounded by layers of non-foamed material. This is known as an intergral structural foam, and provides higher mechanical properties compared to foamed parts with no skin. The foam core provides compression properties while the skin layers provides tensile properties, which makes structural foams more appealing to automotive interior/exterior part manufacturers. The flexural properties of a

structural foam (a combination of compressive and tensile properties) are dependent on the skin thickness; flexural properties of parts with a larger skin thickness tend to be similar to the flexural properties of a non-foamed part [Blanchet and Rodrigue, 2004].

The skin thickness for NTPO foamed parts was found to be 0.72 ± 0.04mm, while the skin thickness for TPOP and TPOC parts are listed in Table 5.2. The notedly large standard error given with the data is due to the irregularity of the skin-core interface, which makes it difficult to differentiate the definite border between the foamed and non-foamed layers. It appears that the skin layer thickness was lower for TPOC foamed parts compared to TPOP foamed parts. This may be an indication that the material near the skin layer of TPOC samples remains in a melt state longer, providing more time for the nucleated cells to grow. This is based on the assumption that nucleated cells are uniformly dispersed in the molten material entering into the mold cavity. The material must somehow be retaining or generating heat during cell growth to maintain the temperature high enough for cell growth. Again, there are three scenarios that must be explored. Firstly, the rate at which the part is being cooled may have been affected by the addition of clay. Introducing clay into the polymer matrix might reduce the bulk thermal conductivity of the polymer-clay nanocomposite material. The thermal conductivity (k) for clay is lower than the k value for polymers. By adding clay and dispersing clay into the polymer matrix, the k for a polymer-clay nanocomposite should theoretically decrease, which can slow down the rate of cooling. Secondly, high viscosity materials undergo higher levels of frictional heat generation, or viscous dissipation. The temperature change due to viscous dissipation is defined in Equation 5.3, where T_{max} is the temperature including viscous dissipation, T_i is the bulk melt temperature and v is the flow velocity.

$$T_{max} = T_i + \frac{\eta}{8k} v^2 \tag{5.3}$$

It is possible that this increase in temperature is able to sustain the temperature high enough for cell growth closer to the mold wall. Lastly, the temperature retention can be due to both the increase in k and viscous dissipation.

Table 5.2: Skin layer thickness for TPOP and TPOC injection molded foamed parts

Material	Skin Layer Thickness (mm)	Material	Skin Layer Thickness (mm)
TPOP1	0.689 ± 0.044	TPOC1	0.678 ± 0.055
TPOP4	0.690 ± 0.030	TPOC4	0.619 ± 0.015
TPOP7	0.723 ± 0.073	TPOC7	0.576 ± 0.066
TPOP10	0.764 ± 0.124	TPOC10	0.583 ± 0.049

To determine the effects of the addition of clay on the cooling rate, the time it takes for the core of the injection molded part to reach the crystallization temperature was estimated using Heisler charts (see Appendix D for calculations). k of the polymer-clay nanocomposite was estimated by a weighted k value using volume fractions; the heat capacity (c_p) was estimated in the same manner. The volume fraction of clay in TPOC was found to be 1.5vol%, which is minute compared to the volume fraction of the polymer matrix. The k and c_p values for TPOC were similar to that of TPOP, suggesting that heat transfer rate was not significantly affected by the addition of clay; cooling times should have been similar for TPOP and TPOC.

Using Equation 5.3, the temperature difference due to viscous dissipation was calculated. To estimate the viscosity of the material as it enters the mold, it was assumed that system was a pressure driven flow between two plates; the width and thickness of the plate was equivalent to the center of the dog-bone part. Through calculations, it was found that the shear rates of both TPOP and TPOC greater than $1500s^{-1}$, where the viscosities for TPOP and TPOC are similar (see Appendix E for calculations).

Since the velocity and thermal conductivity of the materials are almost the same, the temperature change due to viscous dissipation would be similar for both materials. Therefore, the change in skin thickness can not be due to viscous dissipation. The data collected above suggests that the decrease in the skin thickness for TPOC may not be due to the retention and/or generation of heat.

The decrease in the skin thickness may be attributed to gas diffusion effects. In an injection molding process, gas diffuses into the center of the part because it remains in a molten state longer than the areas closest to the mold wall. The presence of clay particles makes diffusion into the core of the molded part difficult; the clay creates a torturous path for the gas molecules to travel through [Yano *et al.*, 1993]. Because of this, it is easier for the gas to diffuse into the already nucleated cells located near the edge of the mold than to remain localized, which leads to the decrease in skin thickness.

Referring back to Section 4.1, it was shown that there was an increase in the number of clay tactoids in the polymer matrix with increasing number of passes. Yano *et al.* [1993] has shown that gas permeability decreases with increasing clay content, therefore, increasing the number of tactoids effectively decreases the gas permeability. This suggests that gas permeability decreased with increasing number of passes, which may have led to the decreasing skin thickness with increasing number of passes.

It was hypothesized that the decrease in the skin thickness was due to the changes in the thermal conductivity of the material with the addition of clay, increase in mold temperature due to viscous dissipation which allowed for a larger window for cell growth, or due to gas diffusion effects. Based on rough calculations, changes in thermal conductivity and viscous dissipation were found to be the same between TPOP and TPOC materials. This means that the decrease in skin thickness may have been attributed to gas diffusion effects.

5.3 Degradation

Polypropylene is known to undergo degradation reactions via β-scission. Scission reactions lower the melt strength, which leads to the inability of the material to sustain the extensional forces exerted by an expanding cell wall during cell growth. This causes the cell to either collapse or to coalesce with surrounding cells [Park and Cheung, 1997]. Coalescence can occur when the melt strength or elongational viscosity of a polymer is decreased, which can be brought about through degradation. The results from Sections 4.2 and 4.3 indicate that the level of scission increased with increasing number of passes for TPOP. Figure 5.4 shows as the number of passes increased, the cell density of the TPOP decreased despite the fact that the gas and foam nucleating agent concentration were constant. Therefore, observing the cell density along with the cell size and shape, similar to rheological measurements, can provide indirect evidence of whether degradation occurred, at least on a comparative basis. This is based on the assumption that the system undergoes instantaneous nucleation of bubbles (which is feasible for the high dP/dt rate experienced in injection molding) and that the rate of diffusion of gas remained the same for each bubble. With the assumption that the number of nucleation sites in TPOP remained the same for all passes and knowledge that there was no pressure drop difference between the injection molded foamed samples, the decrease in the cell density and the increase in cell size was attributed to possible reduced viscosity and/or cell coalescence. Figure 5.1 showed that there was evidence of coalescence for TPOP foamed parts. In observing the cell shape, it appeared that TPOP1 exhibited a more spherical bubble shape compared to the other three TPOP materials. The non-spherical shape of the bubbles produced from materials TPOP4, TPOP7 and TPOP10 would indicate coalescence of the bubbles.

As mentioned in Section 5.1, TPOC foamed parts have a higher cell density than TPOP foamed parts, which was brought upon by the increase in the elongational

viscosity (which is related though the viscosity). Majority of the TPOC foamed cells remained in a spherical or elliptical shape, meaning there was less evidence of coalescence compared to TPOP. Unlike TPOP, the cell density for TPOC samples did not exactly follow the trends obtained from the viscosity data. Between TPOC4 to TPOC7, rheology showed that the viscosity decreased yet the cell density increased. This indicates that the addition of clay has the ability to reduce the effects of degradation on a foaming process.

Between TPOC7 and TPOC10 there was a dramatic decrease in the cell density and increase in cell size, indicating that the reduction in the effects of degradation in a foaming process was limited. This means that this material has a limit to the number of times it can be recycled before the foamability of the material decreases.

5.4 Flexural Modulus

The flexural modulus was determined for TPOP1, TPOP4, TPOP7, TPOP10, TPOC1, TPOC4, TPOC7 and TPOC10 on both foamed and non-foamed parts to quantify the change between foamed and non-foamed parts, as well as to determine whether the addition of clay improved the flexural modulus.

When a material is foamed, it has a tendency to decrease in overall flexural modulus. Comparing Figure 4.19 to Figure 5.5 shows that this trend was observed for TPOP1, where the flexural modulus for the foamed part was slightly lower than the unfoamed part. From TPOP4 to TPOP10 the flexural moduli for the foamed parts were statistically the same as the unfoamed parts due to the increase in skin thickness and presence of filler (Na_2CO_3) in foamed specimens. Unlike tensile modulus, which tends to be a bulk value, the flexural modulus for foamed injection molded bars is strongly dependent on the skin thickness and the elasticity of the material in the skin; parts

with a large skin thickness had a similar flexural modulus to that of a non-foamed part [Blanchet and Rodrigue, 2004]. The non-foamed skin contributes more towards the overall flexural modulus. Looking back at Table 5.2, TPOP parts exhibited an increase in skin thickness with increasing number of passes. Although the skin thickness slightly increased as the number of passes increased, the flexural modulus for TPOP foamed parts decreased with increasing number of passes. Theoretically, the flexural modulus should increase with increasing skin thickness, but in this case, the material underwent degradation, which has a negative effect on flexure.

The flexural modulus for TPOC foamed parts was found to be on average 16% lower than the unfoamed parts. Although we see a decrease in the flexural modulus for foamed parts, foamed TPOC parts display on average a 23% higher flexural moduli than TPOP foamed parts. The enhancement in the TPOC foamed parts is due to the rigidity the clay platelets and Na_2CO_3 imparted to both the skin layer and the actual foam cell wall. The reinforcing nature of the clay platelets in the skin layer was similar to that experienced by unfoamed TPOC parts stated in Section 4.3. As mentioned in Section 5.1 the clay platelets align along the cell wall. The clay platelets can be larger than the minimum strut dimensions, which may allow the clay to act as structural reinforcement. The platelets will minimize the deformation of a cell when the part is introduced to flexural stress. In comparing the skin thicknesses, the TPOC foamed parts showed an opposite trend to TPOP foamed parts, where the skin thickness decreased with increasing number of passes. The decrease in skin thickness can be contributing to the decreasing trend of the flexural modulus, along with degradation effects stated in Section 4.3.

It was found that the specific flexural modulus TPOP materials was 8% higher for the foamed parts compared to the unfoamed parts. On the other hand, TPOC materials exhibit 7% higher specific flexural modulus for non-foamed parts compared to foamed parts. Like the non-foamed parts, the specific flexural modulus decreased with in-

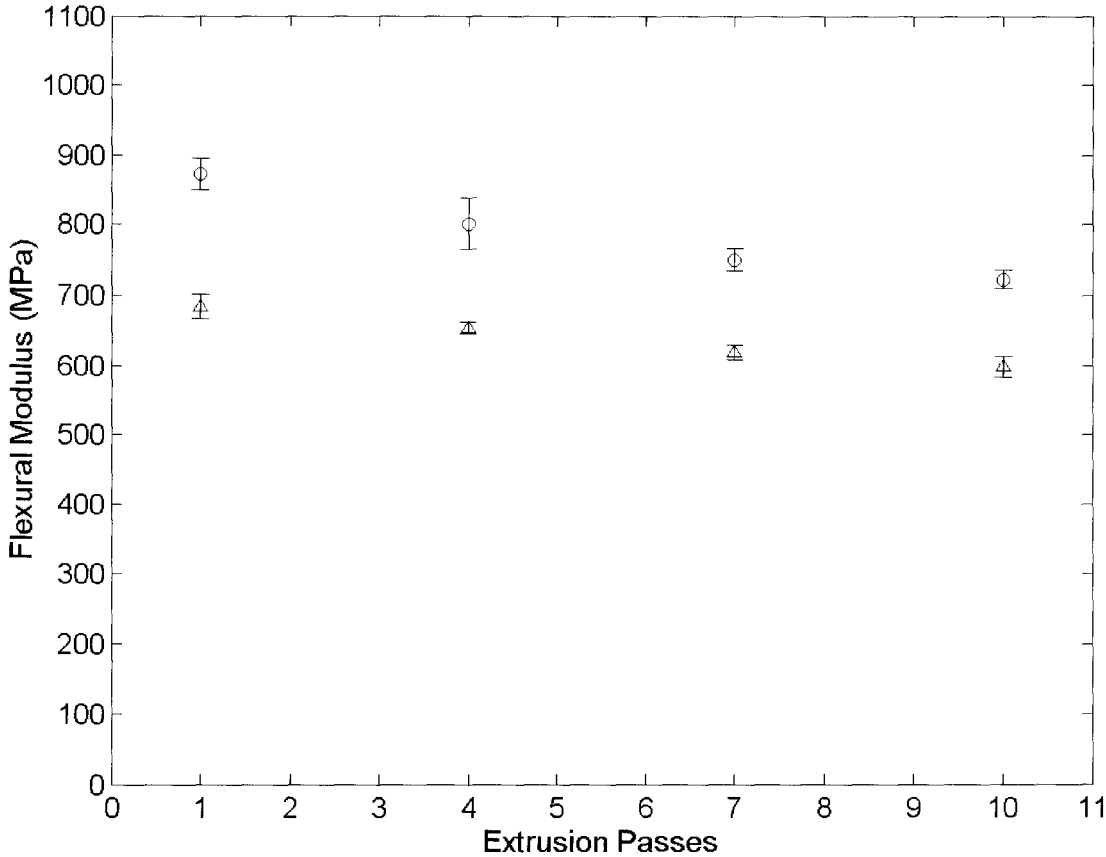

Figure 5.5: Average flexural modulus for foamed TPOP and TPOC materials after multiple extrusions (△ - TPOP, ◯ - TPOC)

creasing number of passes. The calculated values of the specific flexural modulus for foamed and unfoamed parts for TPOP and TPOC materials are depicted in Figures 5.6 and 5.7 respectively. Although these properties for TPOC were lower than the non-foamed parts, they are still higher than the TPOP materials. This demonstrates the reinforcement behaviour of the nanoclay.

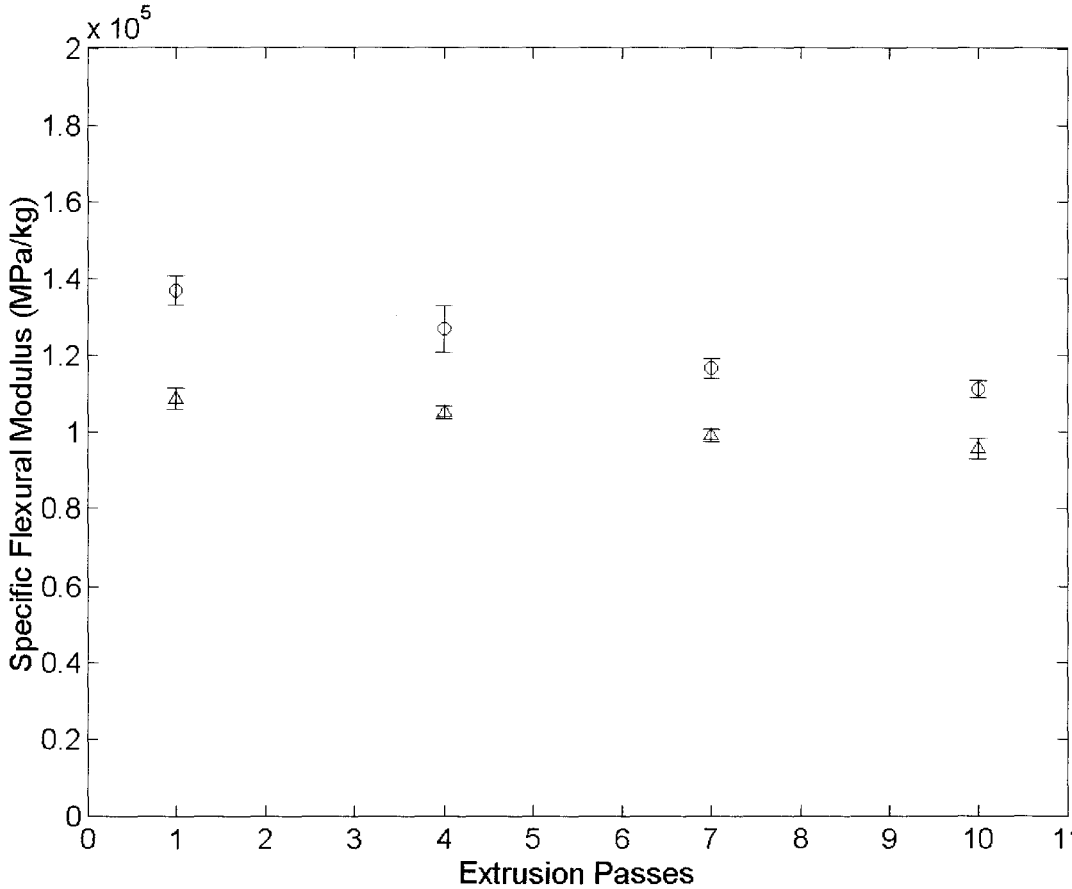

Figure 5.6: Average specific flexural modulus per weight for foamed TPOP and TPOC materials after multiple extrusions (△ - TPOP, ◯ - TPOC)

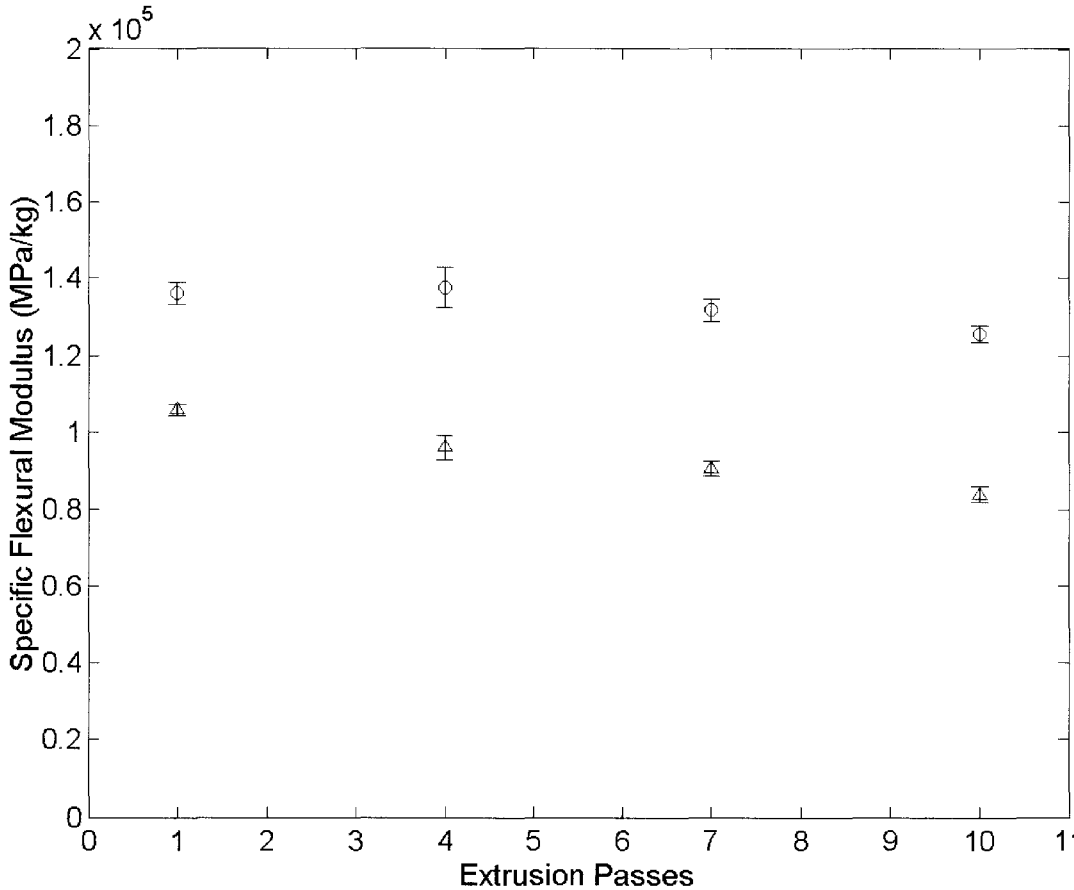

Figure 5.7: Average specific flexural modulus for TPOP and TPOC materials after multiple extrusions (△ - TPOP, ◯ - TPOC)

Chapter 6

Conclusions and Future Work

6.1 Conclusions

A study of automotive grade TPO in a multi-pass extrusion process and the effects on mechanical properties and foamability of a TPO-clay nanocomposite material was presented.

It has been shown that the degree of intercalation increased with increasing number of passes. TEM and XRD data revealed that the clay layer spacing did not change from TPOC1 to TPOC7, but there was an increase between TPOC7 to TPOC10. However, based on the aspect ratio distribution data, the number of clay tactoids increased with increasing number of passes. This suggests that the degree of intercalation was varied not by increasing the d-spacing, but is the result of larger clay tactoids shearing apart to form smaller tactoids.

Rheology showed that TPOP underwent β-scission reactions based on the decreasing rheological properties with increase number of passes as well as observing the increasing trend in crossover frequency ω_c. Rheological measurements for TPOC

showed that intercalation and β-scission occurred simultaneously, where β-scission reactions are dominant from TPOC4 to TPOC10. It was found that MAH was the main contributor to the degradation reactions.

Coupling FT-IR data with TEM, XRD and rheological data gave insight to the method of intercalation. It is believed that there are two intercalation stages. The first stage, TPOC1 to TPOC7, involved the intercalation of antioxidants and MAH, which all contained functional groups. This was based on the diminishing peak intensities observed for the antioxidant ester group ($1742cm^{-1}$) and cyclopentanone groups ($1772cm^{-1}$). Intercalation of β-scission reaction products, which contain aldehyde and ketone functional groups, also occurred. This weakened the interactions between the clay platelets, which allowed for easier intercalation and delamination. This explains the increase in the number of tactoids with increasing number of passes from TPOC1 to TPOC7. This brings about the second stage of intercalation, where the interactions between the clay platelets are weak enough to allow polymer chains to intercalate into the clay layers, which causes an increase in the d-spacing, which was shown in the TEM data.

TPOC exhibited improved foamability compared to TPOP. It was found that the cell density increased with the addition of clay up to TPOC7. This cell density increase was attributed to the increase in the total surface area upon which the cells could nucleate, and not due to the changes in rheology during the injection molding process. The change in total surface area was the result of an increase in the degree of intercalation. The structural foam skin thickness for TPOC was found to be thinner than TPOP foamed parts, which may be due to gas diffusion effects. As well, due to degradation effects, TPOC has a limit to the number of times it can be recycled before the foamability of the material decreases.

Addition of clay has shown to improve flexural properties of TPO for both unfoamed and foamed parts. TPOC experienced on average a 44% increase in flexural modulus

for unfoamed parts and 23% increase for foamed parts compared to TPOP unfoamed and foamed parts respectively. In general, the flexural modulus for unfoamed and foamed TPOP and TPOC parts decreased with increasing number of passes, which was caused by the degradation of the material.

6.2 Future Work

Possible future work on TPO-clay nancomposites is as follows:

- Conduct foaming experiments using physical foaming agents. This will help in the study of the foamability of TPOC minus the effects of the decomposed CBA.
- Study the thermal stability of TPOC, which can provide insight on how the addition of clay affects the extent of degradation.
- Measure the crystallinity of the materials and determine whether it affects the foamability of TPOC.

List of References

Bacci, D., Marchini, R., and Scrivani, M. (2004). Peroxide crosslinking of ziegler-natta thermoplastic polyolefins. *Polym. Eng. Sci.*, **44**(1), 131–140.

Blanchet, J. and Rodrigue, D. (2004). The effect of skin thickness on the mechanical properties of structural foams. *Cell. Polym.*, **23**(4), 193–210.

Canevarolo, S. and Babetto, A. (2002). Effect of screw element type in degradation of polypropylene upon mulitple extrusions. *Adv. Polym. Tech.*, **21**(4), 243–429.

Chandra, A., Gong, S., Turng, L., and Gramann, P. (2004). Cell development in microcellular injection molded polyamide-6 nanocomposite and neat resin. *ANTEC 2004-Proceedings of the 62th Annual Technical Conference & Exhibition, Chicago, IL, Society of Plastics Engineers*, , 540–544.

Chen, L., Blizard, K., Straff, R., and Wang, X. (2002). Effect of filler size on cell nucleation during foaming process. *Journal of Cellular Plastics*, **38**, 139–148.

Chien, R., Chen, S., Lee, P., and Huang, J. (2004). Study on the molding characteristics and mechanical properties of injection-molded foaming polypropylene parts. *J. Reinf. Plast. Compos.*, **23**(4), 429–444.

DE GOEDE, S., BRLL, R., PASCH, H., AND MARSHALL, N. (2003). Monitoring thermo-oxidative degradation of polypropylene by crystaf and sec-ftir. *Macromol. Symp.*, **193**, 35–43.

DENNIS, H., HUNTER, D., CHANG, D., KIM, S., WHITE, J., CHO, J., AND PAUL, D. (2001). Effect of melt processing conditions on the extent of exfoliation in organoclay-based nanocomposites. *Polymer*, **42**, 9513–9522.

DI, Y., IANNACE, S., AND NICOLAIS, L. (2002). Thermal behaviour and morphological and rheological properties of polypropylene and novel elastomeric ethylene copolymer blends. *J. Appl. Polym. Sci.*, **86**, 3430–3439.

DI MAIO, E., IANNACE, S., DI, Y., DEL GIACOMO, E., AND NICOLAIS, L. (2003). Heterogeneous bubble nucleation in plc/clay nanocomposite foams. *Plast. Rubb. Comp.*, **32**(7), 313–317.

ECKEL, D., BALOGH, M., FASULO, P., AND RODGERS, W. (2004). Assessing organo-clay dispersion in polymer nanocomposites. *J. Appl. Polym. Sci.*, **93**, 1110–1117.

ELLIS, T. AND D'ANGELO, J. (2003). Thermal and mechanical properties of a polypropylene nanocomposite. *J. Appl. Polym. Sci.*, **90**, 1639–1647.

FUKUSHIMA, Y., OKADA, A., KAWASUMI, M., KURAUCHI, T., AND KAMIGAITO, O. (1988). Swelling behaviour of montmorillonite by poly-6-amide. *Clay Miner.*, **23**, 27–34.

GALGALI, G., RAMESH, C., AND LELE, A. (2001). A rheological study on the kinetics of hybrid formation in polypropylene nanocomposites. *Macromolecules*, **34**, 852–858.

GENDRON, R. AND VACHON, C. (2003). Effect of viscosity on low density foaming of poly(ehtylene-co-octene) resins. *Journal of Cellular Plastics*, **39**, 117–132.

GIJSMAN, P. AND DOZEMAN, A. (1996). Comparison of the uv-degradation chemistry of unstabilized and hals-stabilized polyethylene and polypropylene. *Polym. Degrad. Stab.*, **53**, 45–50.

GUO, Q., WANG, J., PARK, C., AND OHSHIMA, M. (2004). Design of a foaming simulation system with a high pressure drop rate. *ANTEC 2004-Proceedings of the 62th Annual Technical Conference & Exhibition, Chicago, IL, Society of Plastics Engineers*, , 2615–2619.

HAN, X., ZENG, C., LEE, L., KOELLING, K., AND TOMASKO, D. (2003). Extrusion of polystyrene nanocomposite foams with supercritical co_2. *Polym. Eng. Sci.*, **43**(6), 1261–1275.

HASEGAWA, N., OKAMOTO, H., AND USUKI, A. (2004). Preparation and properties of ehtylene polypropylene rubber (epr)-clay nanocomposites based on maleic anhydride-modified epr and organophilic clay. *J. Appl. Polym. Sci.*, **93**, 758–764.

HO, R., SU, A., AND WU, C. (1993). Functionalization of polypropylene via melt mixing. *Polymer*, **34**(15), 3264–3269.

HOBBIE, E., WANG, H., KIM, H., AND LIN-GIBSON, S. (2003). Orientation of carbon nanotubes in a sheared polymer melt. *Phys. Fluids*, **15**(5), 1196–1202.

HU, X., XU, H., AND ZHANG, Z. (1994). Influence of fillers on the effectiveness of stabilizers. *Polym. Degrad. Stab.*, **43**, 225–228.

INCARNATO, L., SCARFATO, P., SCATTEIA, L., AND ACIERNO, D. (2004). Rheological behaviour of new melt compounded copolyamide nanocomposites. *Polymer*, **45**, 3487–3496.

KATO, M. AND USUKI, A. (2000). Polymer-Clay Nanocomposites. In Pinnavaia, T. and Beall, G. (Eds.), *Polymer-Clay Nanocomposites*, pp. 97–109. John Wiley & Sons, Ltd.

KIM, J., KOO, C., CHOI, Y., WANG, K., AND CHUNG, I. (2004). Preparation and characterization of polypropylene/layered silicate nanocomposites using an antioxidant. *Polymer*, **45**, 7719–7727.

KODGIRE, P., KALGAONKAR, R., HAMBIR, S., BULAKH, N., AND JOG, J. (2001). Pp/clay nanocomposites: Effect of clay treatment on morphology and dynamic mechanical properties. *J. Appl. Polym. Sci.*, **81**(7), 1786–1792.

KOJIMA, Y., USUKI, A., KAWASUMI, M., OKADA, A., AND KURAUCHI, T. (1995). Novel preferred orientation in injection-molded nylon 6-clay hybrid. *J. Polym. Sci., Part B: Polymer Physics*, **33**, 1039–1045.

KRISHNAMOORTI, R. AND SILVA, A. (2000). Rheological Properties of Polymer-Layered Silicate Nanocomposites. In Pinnavaia, T. and Beall, G. (Eds.), *Polymer-Clay Nanocomposites*, pp. 315–343. John Wiley & Sons, Ltd.

KRISHNAMOORTI, R., VAIA, R., AND GIANNELIS, E. (1996). Structure and dynamics of polymer-layered silicate nanocomposites. *Chem. Mater.*, **8**, 1728–1734.

LA MANTIA, F., CITTA, V., AND VALENZA, A. (1989). Influence of low extents of degradation on the processing behaviour of high density polyethylene. *Polym. Degrad. Stab.*, **23**, 109–119.

LEBARON, P., WANG, Z., AND PINNAVAIA, T. (1999). Polymer-layered silicate nanocomposites: an overview. *Appl. Clay Sci.*, **15**, 11–29.

LEE, S. AND KIM, J. (2004). Surface modification of clay and its effect on the intercalation behaviour of the polymer/clay nanocomposites. *J. Polym. Sci., Part B: Polymer Physics*, **42**, 2367–2372.

LEW, C., MURPHY, W., AND MCNALLY, G. (2004a). Recyclability of polymer-clay nanocomposites: Part 1. the influence of multiple-extrusions on structure and

mechanical properties. *ANTEC 2004-Proceedings of the 62th Annual Technical Conference & Exhibition, Chicago, IL, Society of Plastics Engineers*, , 299–303.

LEW, C., MURPHY, W., AND MCNALLY, G. (2004b). Recyclability of polymer-clay nanocomposites: Part 2. the influence of multiple-extrusions on thermal and rheological properties. *ANTEC 2004-Proceedings of the 62th Annual Technical Conference & Exhibition, Chicago, IL, Society of Plastics Engineers*, , 304–308.

LI, J., ZHOU, C., WANG, G., AND ZHAO, D. (2003). Study of kinetics of polymer melt intercalation by a rheological approach. *J. Appl. Polym. Sci.*, **89**, 318–323.

LI, X., KANG, T., CHO, W., LEE, J., AND HA, C. (2001). Preparation and characterization of poly(butyleneterephthalate)/organoclay nanocomposites. *Macromol. Rapid Commun.*, **22**, 1306–1312.

LIM, S., KIM, J., CHIN, I., AND CHOI, H. (2002). Rheological properties of a new rubbery nanocomposite: Polyepichlorohydrin/organoclay nanocomposites. *J. Appl. Polym. Sci.*, **86**(14), 3735–3739.

LIN, H. AND JERMAIN, W. (2002). The effects of cell content on the mechanical characteristics of structural foams. *Journal of Cellular Plastics*, **27**, 295–319.

MA, J., ZHANG, S., QI, Z., AND HU, Y. (2002). Crystallization behaviors of polypropylene/montmorillonite nanocomposites. *J. Appl. Polym. Sci.*, **83**, 1978–1985.

MCNALLY, T., MURPHY, W., LEW, C., TURNER, R., AND BRENNAN, G. (2003). Polyamide-12 layered silicate nanocomposites by melt blending. *Polymer*, **44**, 2761–2772.

NAM, P., MAITI, P., OKAMOTO, M., KOTAKA, T., HASEGAWA, N., AND USUKI, A. (2001). A hierarchical structure and properties of intercalated polypropylene/clay nanocomposites. *Polymer*, **42**, 9633–9640.

NAM, P., MAITI, P., OKAMOTO, M., KOTAKA, T., NAKAYAMA, T., TAKADA, M., AND OHSHIMA, M. (2002). Foam processing and cellular structure of polypropylene/clay nanocomposites. *Polym. Eng. Sci.*, **42**(9), 1907–1918.

OKAMOTO, M., NAM, P., MAITI, P., KOTAKA, T., HASEGAWA, N., AND USUKI, A. (2001). A house of cards structure in polypropylene/clay nanocomposites under elongational flow. *Nano Letters*, **1**(6), 295–298.

PARK, C. AND CHEUNG, L. (1997). A study of cell nucleation in the extrusion of polypropylene foams. *Polym. Eng. Sci.*, **37**(1), 1–10.

PINNAVAIA, T. AND BEALL, G. (2000). *Polymer-Clay Nanocomposites.* John Wiley & Sons, Ltd.

PINTER, G., HAAGER, M., WOLF, C., AND LANG, R. (2004). Thermo-oxidative degradation during creep crack growth of pe-hd grades as assessed by ft-ir spectroscopy. *Macromol. Symp.*, **217**, 307–316.

PONTIFF, T. (2000). Foaming Agents for Foam Extrusion. In Lee, S. (Ed.), *Principles of Thermoplastic Foam Extrusion*, pp. 251–262. Technomic Publishing Company Inc.

POSPISIL, L., JANCAR, J., AND RYBNIKAR, F. (1990). Activated heterogeneous nucleation of isotatic polypropylene. *J. Mater. Sci. Lett.*, **9**(4), 495–496.

PRAMODA, K., LIU, T., LIU, Z., HE, C., AND SUE, H. (2003). Thermal degradation behaviour of polyamide 6/clay nanocomposites. *Polym. Degrad. Stab.*, **81**, 47–56.

QIN, H., ZHAO, C., ZHANG, S., CHEN, G., AND YANG, M. (2003). Photo-oxidative degradation of polyethylene/montmorillonite nanocomposite. *Polym. Degrad. Stab.*, **81**, 497–500.

REN, J., CASANUVEA, B., MITCHELL, C., AND KRISHNAMOORTI, R. (2003). Disoriented kinetics of aligned polymer layered silicate nanocomposites. *Macromolecules*, **36**, 4188–4194.

SINHA RAY, S. AND OKAMOTO, M. (2003). Polymer/layered silicate nanocomposites: a review from preparation to processing. *Prog. Polym. Sci*, **28**, 1539–1641.

SINHA RAY, S., YAMADA, K., OKAMOTO, M., AND UEDA, K. (2003). New polyactide-layered silicate nanocomposites. 2. concurrent improvements of material properties, biodegradability and melt rheology. *Polymer*, **44**, 857–866.

SOLOMON, M., ALMUSALLAM, A., SEEFELDT, K., SOMWANGTHANAROJ, A., AND VARADAN, P. (2001). Rheology of polypropylene/clay hybrid materials. *Macromolecules*, **34**, 1864–1872.

TAKI, K., YANAGIMOTO, T., FUNAMI, E., OKAMOTO, M., AND OHSHIMA, M. (2004). Visual observation of co^2 foaming of polypropylene-clay nanocomposites. *Polym. Eng. Sci.*, **44**(6), 1004–1011.

THOMPSON, M. R., TZOGANAKIS, C., AND REMPEL, G. (1997). Functionalization of terminal double bonds in polypropylene. *ANTEC 1997-Proceedings of the 55th Annual Technical Conference & Exhibition, Toronto, Ont, Society of Plastics Engineers*, , 2981–2985.

TIDJANI, A. (2005). Polypropylene-graft-maleic anhydride-nanocomposites: Ii - fire behaviour of nanocomposites produced under nitrogen and in air. *Prog. Polym. Sci*, **87**, 43–49.

TIDJANI, A., WALD, O., POHL, M., HENTSCHEL, M., AND SCHARTEL, B. (2003). Polypropylene-graft-maleic anhydride-nanocomposites: I - characterization and thermal stability of nanocomposites produced under nitrogen and in air. *Polym. Degrad. Stab.*, **82**, 133–140.

VAIA, R., JANDT, K., KRAMER, E., AND GIANNELIS, E. (1995). Kinetics of polymer melt intercalation. *Macromolecules*, **28**, 8080–8085.

VAIA, R., JANDT, K., KRAMER, E., AND GIANNELIS, E. (1996). Microstructural evolution of melt intercalated polymer-organically layered silicates nanocomposites. *Chem. Mater.*, **8**, 2628–2635.

VAIA, R., PRICE, G., RUTH, P., NGUYEN, H., AND LICHTENHAN, J. (1999). Polymer/layered silicate nanocomposites as high performance ablative materials. *Appl. Clay Sci.*, **15**, 67–92.

VLACHOPOULOS, J. (2003). Introduction to plastics processing. Lecture Notes, Dept. of Chem. Eng., McMaster University, Canada.

WANG, K., LIANG, S., DU, R., ZHANG, Q., AND FU, Q. (2004). The interplay of thermodynamics and shear on the dispersion on polymer nanocomposite. *Polymer*, **45**, 7953–7960.

WANG, Z., NAKAJIMA, H., MANIAS, E., AND CHUNG, T. (2003). Exfoliated pp/clay nanocomposites using ammonium-terminated pp as the organic modification for montmorillonite. *Macromolecules*, **36**, 8919–8922.

WILLIAMS, M., WEISER, E., FESMIRE, J., GRIMSLEY, B., SMITH, T., BRENNER, J., AND NELSON, G. (2005). Effects of cell structure and density on the properties of high performance polyimide foams. *Polym. Adv. Technol.*, **16**, 167–174.

WONG, S. AND CHEN, L. (2002). Mechanical and fracture properties of nanoclay-filled polypropylene. *ANTEC 2002-Proceedings of the 60th Annual Technical Conference & Exhibition, San Francisco, CA, Society of Plastics Engineers*, , 1–4.

XU, J. AND KISHBAUGH, L. (2003). Simple modeling of the mechanical properties with part weight reduction for microcellular foam plastic. *Journal of Cellular Plastics*, **39**, 29–47.

YANO, K., USUKI, A., OKADA, A., KURAUCHI, T., AND KAMIGAITO, O. (1993). Synthesis and properties of polyimide-clay hybrid. *J. Polym. Sci., Part A: Polymer Chemistry*, **31**, 2493–2498.

ZANETTI, M., BRACCO, P., AND COSTA, L. (2004). Thermal degradation behaviour of pe/clay nanocomposites. *Polym. Degrad. Stab.*, **85**, 657–665.

ZENG, C., HAN, X., LEE, L., KOELLING, K., AND TOMASKO, D. (2002). Structure of nanocomposite foams. *ANTEC 2002-Proceedings of the 60th Annual Technical Conference & Exhibition, San Francisco, CA, Society of Plastics Engineers*, , 1–5.

ZENG, C., HAN, X., LEE, L., KOELLING, K., AND TOMASKO, D. (2003). Polymer-clay nanocomposite foams prepared using carbon dioxide. *Adv. Mater.*, **15**(20), 1743–1747.

Appendix A

TEM Micrographs

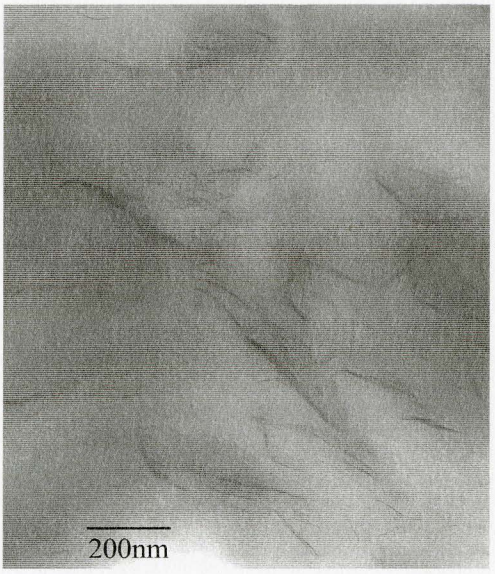

Figure A.1: TEM micrograph of TPOC1 at 60K magnification

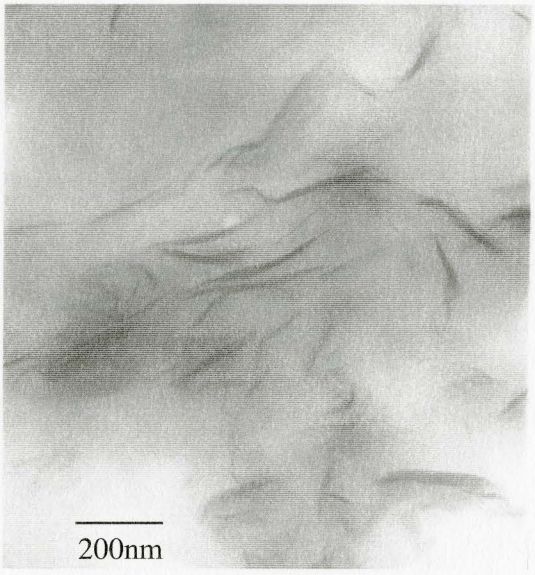

Figure A.2: TEM micrograph of TPOC4 at 60K magnification

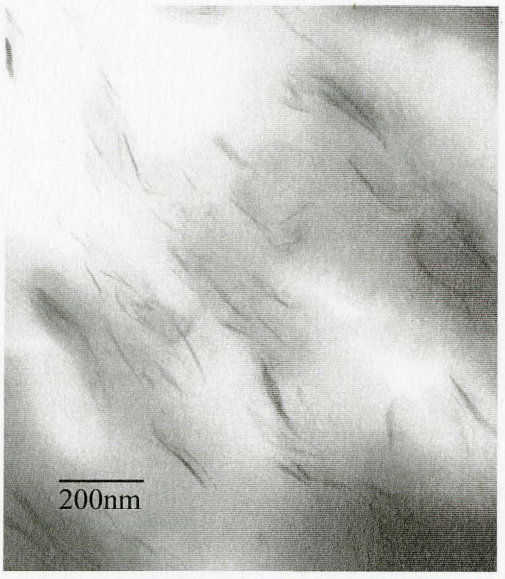

Figure A.3: TEM micrograph of TPOC71 at 60K magnification

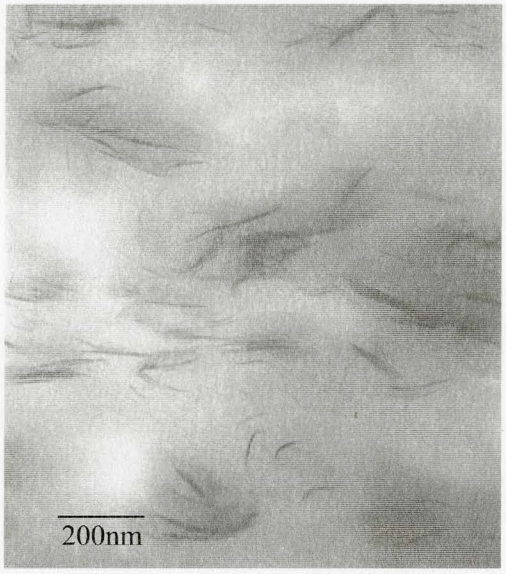

Figure A.4: TEM micrograph of TPOC10 at 60K magnification

Appendix B

Sample Calculations: Clay Surface Area

Assumptions:

- Length of all tactoids are the same; L = 106nm
- In-plane depth of all tactoids are the same; d = 1nm
- Sample cross sectional volume has a depth of 1nm

For TPOC1, the number of tactoids calculated in a 60mm x 60mm area from Figure 4.7(a) is 115.

The average width of the tactoid for TPOC1 is 8.6nm.

The surface area for one tactoid = 2(106x8.6)+2(106)+2(8.6) = 2052.4 nm^2

The total surface area of the tactoids for TPOC1 at the given volume = 2052.4 x 115 = 236026nm^2

Table B.1 shows the calculated surface areas for TPOC1, TPOC4, TPOC7 and TPOC10.

Table B.1: Total surface area of clay tactoids in 60nm x 60nm x 1nm volume

Material	Average Width (nm)	Number of Tactoids	Surface Area (nm^2)
TPOC1	8.6	115	236026
TPOC4	7.3	141	250162
TPOC7	5.7	183	262019
TPOC10	5.9	194	286072

Appendix C

Sample Calculations: Pressure Drop

From Equation 5.1, and assuming R = 0.32 cm, Q = 100 cm/s

$\dot{\gamma} = (4)(100)/(\pi)(0.32)^3 = 3885\ s^{-1} \approx 4000\ s^{-1}$

From the Rosand data shown in Figure C.1, the viscosity η was found for each sample for $\dot{\gamma} = 500\ s^{-1}$. Using Equation 5.2, ΔP was calculated, shown in Table C.1.

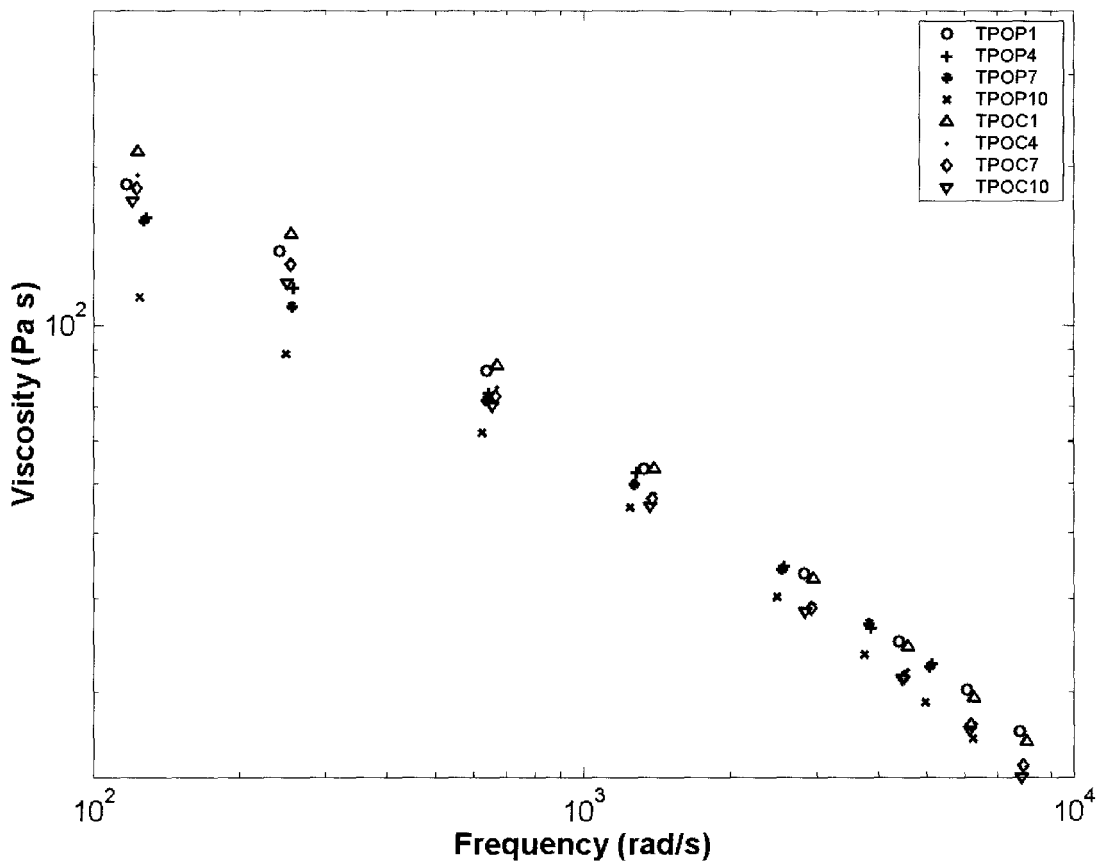

Figure C.1: Shear viscosity measurements for TPOP and TPOC

Table C.1: Estimated pressure drop during injection molding

Material	η (Pa s)	ΔP (Pa)
TPOC1	26	631413
TPOC4	17	412847
TPOC7	17	412847
TPOC10	16	388562
TPOP1	22	534277
TPOP4	22	534277
TPOP7	22	534277
TPOP10	20	485702

Appendix D

Sample Calculations: Heat Transfer

Heisler charts are used to find the time it takes for the center of an injection molded part to reach the crystallization temperature of polypropylene.

Assumptions:

- Material consists of polypropylene and clay only
- Thermal conductivity coefficient (k) and heat capacity (c_p) are weighted values calculated using volume fraction
- Transient heat transfer
- h = 2000 W/m^{2}K
- L = 1.5 mm
- Thermal conductivity coefficient of polypropylene $k_{PP} = 0.12$ W/mK
- Thermal conductivity coefficient of clay $k_c = 0.25$ W/mK

- Heat capacity of polypropylene c_{pPP} = 1925 J/molK
- Heat capacity of clay c_{pc} = 920 J/molK

Volume fractions: 1.58vol% clay; 98.42vol% Polypropylene

Initial and Boundary Conditions:

At t = 0, T = T_i; t = t_o, T = T_o

T_∞ = Temperature of the mold = 30°C

T_i = Initial temperature of the part = 230°C

T_o = Final temperature of the part = 115°C

Calculations:

Thermal conductivity of nanocomposite = k_{PCN}

k_{PCN} = 0.0158(0.25) + 0.9843(0.12) = 0.122 W/mK

Heat capacity of nanocomposite = c_{pPCN}

c_{pPCN} = 0.0158(920) + 0.9843(1925) = 1909 J/molK

To use the Heisler charts, values for thermal diffusivity (α), θ_o and θ_i need to be calculated. These are defined in Equations D.1 to D.3.

$$\alpha = \frac{k}{\rho c_p} \tag{D.1}$$

$$\theta_i = T_i - T_\infty \tag{D.2}$$

$$\theta_o = T_o - T_\infty \tag{D.3}$$

$\alpha = (0.122)/(910)(1909) = 7.023 \times 10^{-8}$ m^2/s

θ_i = 230 - 30 = 200°C

θ_o = 115 - 30 = 95°C

$\theta_o/\theta_i = 95/200 = 0.45$

k/hL = (0.122)/(2000)(0.0015) = 0.0406

From the Heisler charts, αt/L = 0.03

t = 9.61 s

Appendix E

Sample Calculations: Viscous Dissipation

Assumptions:

- Pressure driven flow between two plates
- W = width of narrow portion of the dogbone part = 1.2 cm
- b = half the thickness of the dogbone part = 0.15 cm
- Q = volumetric flowrate = 100 cm^3/s

Calculations:

To find the viscosity of the material flowing into the mold, the shear rate at the wall of the mold is calculated using Equation E.1.

$$\dot{\gamma} = \frac{2n+1}{n}\frac{2Q}{4Wb^2} \tag{E.1}$$

Table E.1 shows the values of $\dot{\gamma}$ calculated. n was obtained by fitting the viscosity data to the Cross model.

Table E.1: Shear rate in the mold during injection molding

Material	n	Shear rate (s^{-1})
TPOC1	0.5	1851
TPOC4	0.54	1783
TPOC7	0.51	1833
TPOC10	0.54	1783
TPOP1	0.60	1697
TPOP4	0.54	1783
TPOP7	0.64	1649
TPOP10	0.30	2469

The shear rate calculated are similar, and they fall under the shear thinning region in the viscosity curve. The viscosity for all the materials is approximately 45Pa s. Since the viscosities are similar, the difference in the temperature change due to viscous dissipation between TPOP and TPOC is insignificant.